ESTIMATION OF THE UNIAXIAL COMPRESSIVE STRENGTH OF TRONA AND INTERBURDEN ROCKS USING THE POINT LOAD TEST RESULTS AND NUMERICAL MODELING

A THESIS SUBMITTED TO
THE GRADUATE SCHOOL OF APPLIED AND NATURAL SCIENCES
OF
MIDDLE EAST TECHNICAL UNIVERSITY

BY

MEHMET ALTINPINAR

IN PARTIAL FULFILLMENT OF THE REQUIREMENTS
FOR
THE DEGREE OF MASTER OF SCIENCE
IN
MINING ENGINEERING

MAY 2016

Approval of the thesis:

ESTIMATION OF THE UNIAXIAL COMPRESSIVE STRENGTH OF TRONA AND INTERBURDEN ROCKS USING THE POINT LOAD TEST RESULTS AND NUMERICAL MODELING

submitted by **MEHMET ALTINPINAR** in partial fulfillment of the requirements for the degree of **Master of Science in Mining Engineering Department, Middle East Technical University** by,

Prof. Dr. Gülbin Dural Ünver _____
Dean, Graduate School of **Natural and Applied Sciences**

Prof. Dr. Celal Karpuz _____
Head of Department, **Mining Engineering**

Assoc. Prof. Dr. Hasan Öztürk _____
Supervisor, **Mining Engineering Dept., METU**

Examining Committee Members:
Prof. Dr. Celal Karpuz _____
Mining Engineering Dept., METU

Assoc. Prof. Dr. Hasan Öztürk _____
Mining Engineering Dept., METU

Prof. Dr. Levend Tutluoğlu _____
Mining Engineering Dept., METU

Assoc. Prof. Dr. H. Aydın Bilgin _____
Mining Engineering Dept., METU

Asst. Prof. Dr. İ. Ferid Öge _____
Mining Engineering Dept.,
Muğla Sıtkı Koçman University

Date: 26.05.2016

I hereby declare that all information in this document has been obtained and presented in accordance with academic rules and ethical conduct. I also declare that, as required by these rules and conduct, I have fully cited and referenced all material and results that are not original to this work.

Name, Last name: Mehmet ALTINPINAR

Signature:

ABSTRACT

ESTIMATION OF THE UNIAXIAL COMPRESSIVE STRENGTH OF TRONA AND INTERBURDEN ROCKS USING THE POINT LOAD TEST RESULTS AND NUMERICAL MODELING

ALTINPINAR, Mehmet

M.Sc., Department of Mining Engineering

Supervisor: Assoc. Prof. Dr. Hasan Öztürk

May 2016, 165 pages

Point load (PL) test is used as an index for rock strength classification. It is generally used for estimation of uniaxial compressive strength (UCS) because of its economic advantages and simplicity in testing. If the PL index of a specimen is known, the UCS can be estimated according to some conversion factors. Several conversion factors have been proposed by different researchers and are dependent upon the rock type. In the literature, conversion factors on different sedimentary, igneous and metamorphic rocks can be found, but no study exists on trona. In this study, an extensive literature review was carried out and then laboratory UCS and field PL tests were carried out on trona and interburden rocks. PL to UCS conversion factors of the trona and interburden rocks were proposed. The tests were modeled numerically throughout the rigorous simulations using a code called Particle Flow Code (PFC) based on Discrete Element Modeling (DEM) in an attempt to guide researchers having different kinds of modeling problems (excavation, slope stability etc.) of the abovementioned rock types. A calibration coefficient both for UCS and

PL testing between macro and micro properties of PFC was calculated. It was observed that PFC overestimates the tensile strength of the rocks by a factor that ranges from 19 to 750.

Keywords: UCS, point load, Discrete Element Method (DEM), Particle Flow Code 2D (PFC2D), trona (natural soda).

ÖZ

NOKTA YÜKLEME DENEYİ SONUÇLARI KULLANILARAK TRONA VE ARA KESME KAYAÇLARIN TEK EKSENLİ BASMA DAYANIMLARININ KESTİRİMİ VE SAYISAL MODELLEME

ALTINPINAR, Mehmet

Yüksek Lisans, Maden Mühendisliği Bölümü

Tez Yöneticisi: Doçent Doktor Hasan Öztürk

Mayıs 2016, 165 sayfa

Nokta yükleme (NY) deneyi, kaya dayanımı sınıflandırmasına yönelik bir indis olarak kullanılmaktadır. Bu deneyin genel kullanım amacı tek eksenli basma dayanımını (TEBD) belirlemektir. Bunun nedeni hem ekonomik olarak daha avantajlı olması hem de deney prosedürünün kolaylığıdır. Eğer bir numunenin NY indisi biliniyorsa, bazı dönüşüm katsayıları kullanılarak TEBD belirlenebilir. Araştırmacılar tarafından farklı dönüşüm katsayıları önerilmiştir ve bu dönüşüm katsayıları kayanın cinsine bağlıdır. Literatürde farklı tortul, volkanik ve başkalaşım kayaları için farklı dönüşüm katsayıları bulunmaktadır fakat trona için herhangi bir çalışma mevcut değildir. Bu çalışmada, geniş bir literatür araştırması yapıldıktan sonra, trona ve ara kesme kayaç numuneleri için laboratuvarda TEBD ve arazide NY deneyleri yapılmıştır. Trona ve ara kesme kayaçlar için NY'den TEBD'na geçişe yönelik dönüşüm katsayıları önerilmiştir. Deneyler, yukarıda bahsedilen kayaç türlerine ilişkin farklı modelleme problemleri (kazı, şev duraylılığı vs.) ile karşılaşan araştırmacılara rehberlik etmesi amacıyla, Ayrık Elemanlar Yöntemine (AEY)

dayanan Parçacık Akış Kodu (Particle Flow Code - PFC) adlı bir kod kullanılarak, titizlikle yürütülen simülasyonlar aracılığıyla sayısal olarak modellenmiştir. Hem TEBD hem de NY deneyleri için PFC'nin makro ve mikro özellikleri arasında bir kalibrasyon parametresi hesaplanmıştır. PFC'nin, kayaçların çekme dayanımını 19 ila 750 arasında değişen bir oranda yüksek tahmin ettiği gözlemlenmiştir.

Anahtar Kelimeler: TEBD, nokta yükleme, Ayrık Elemanlar Yöntemi (AEY), Particle Flow Code 2D (PFC2D), trona (doğal soda).

To My Wife

For her everlasting support and encouragement

ACKNOWLEDGEMENTS

I would like to express my deep and sincere appreciation to my supervisor Assoc. Prof. Dr. Hasan Öztürk for his guidance, support and encouragement, thanks to which this study has been completed successfully.

I owe my special thanks to the examining committee members, Prof. Dr. Celal Karpuz, Prof. Dr. Levend Tutluoğlu, Assoc. Prof. Dr. H. Aydın Bilgin and Asst. Prof. Dr. İ. Ferid Öge for their comments and suggestions and for serving on the M. Sc. thesis committee.

I would like to thank research assistant Doğukan Güner for his support and helps as well as valuable contributions to this study.

I would also like to thank Mr. Güray Çakmakçı, Mine Manager of Kazan Soda of Ciner, for sharing the available data and supplying the test samples.

I also wish to express my sincere gratitude to my parents and sister, who always encouraged me during the course of this study, and also to Mr. İbrahim Ata Ferhatoğlu, Country Manager of Kenz Mining Co., for his unconditional support.

Finally, I would like to express my sincere appreciation to my wife for her moral and material support throughout this process and I am grateful to her for her encouragement.

This research was supported by METU Scientific Research Projects Coordination Center (BAP-03-05-2013-002).

TABLE OF CONTENTS

ABSTRACT v

ÖZ vii

ACKNOWLEDGEMENTS x

TABLE OF CONTENTS xi

LIST OF TABLES xv

LIST OF FIGURES xviii

CHAPTERS

1 INTRODUCTION 1

1.1 General Remarks 1

1.2 Problem Statement 3

1.3 Objectives of Study 3

1.4 Research Methodology 4

2 LITERATURE SURVEY 5

2.1 Literature Review 5

2.2 Correlations between PL Index and UCS for Various Rock Types 6

3 POINT LOAD AND UNIAXIAL COMPRESSIVE STRENGTH TESTS 9

3.1 The Mine Site and the Geology 9

3.2 Point Load (PL) Tests 10

3.3 Uniaxial Compressive Strength (UCS) Tests 21

3.4 Matching Drillhole Intervals Used in PL and UCS Tests 27

3.5 Outlier Detection 28

3.6 Analyzing PL and UCS Tests....34
3.6.1 Analysis of Claystone....35
3.6.2 Analysis of Bituminous Shale....36
3.6.3 Common Analysis of Claystone and Bituminous Shale....37
3.6.4 Analysis of Upper Trona....38
3.6.5 Analysis of Lower Trona....39
3.6.6 Common Analysis of Upper and Lower Trona....40
3.7 Material Properties Obtained by Analyzing the PL and UCS Tests....40
4 NUMERICAL MODELING....43
4.1 Discrete Element Method (DEM)....43
4.2 Determining Model Input Parameters....48
4.2.1 Particle Radius....48
4.2.2 The Rest of the Input Parameters for PFC....52
4.3 Modeling UCS Tests....54
4.3.1 Numerical Modeling of UCS Tests for Claystone Specimens....55
4.3.1.1 Numerical Modeling of UCS Test for CS GT1-904....56
4.3.1.2 Numerical Modeling of UCS Test for CS GT1-908....58
4.3.1.3 Numerical Modeling of UCS Test for CS GT2-698....60
4.3.1.4 Numerical Modeling of UCS Test for CS GT2-712....63
4.3.2 Numerical Modeling of UCS Tests for Bituminous Shale Specimens....65
4.3.2.1 Numerical Modeling of UCS Test for BS GT1-855....66
4.3.2.2 Numerical Modeling of UCS Test for BS GT1-860....68
4.3.2.3 Numerical Modeling of UCS Test for BS GT2-657....70
4.3.2.4 Numerical Modeling of UCS Test for BS GT2-659....72
4.3.3 Numerical Modeling of UCS Tests for Upper Trona Specimens....74
4.3.3.1 Numerical Modeling of UCS Test for UT GT1-874....74

4.3.3.2 Numerical Modeling of UCS Test for UT GT1-875 77
4.3.3.3 Numerical Modeling of UCS Test for UT GT2-674 79
4.3.3.4 Numerical Modeling of UCS Test for UT GT2-679 81
4.3.4 Numerical Modeling of UCS Tests for Lower Trona Specimens 83
4.3.4.1 Numerical Modeling of UCS Test for LT GT2-708 84
4.3.4.2 Numerical Modeling of UCS Test for LT GT2-719 86
4.3.4.3 Numerical Modeling of UCS Test for LT GT2-723 88
4.3.4.4 Numerical Modeling of UCS Test for LT GT2-733 90
4.3.5 Material Properties Obtained from Iterations for UCS Tests 92
4.4 Modeling PL Index Tests 94
4.4.1 Numerical Modeling of PL Tests for Claystone Specimens 96
4.4.1.1 Numerical Modeling of PL Test for CS GT1-61 96
4.4.1.2 Numerical Modeling of PL Test for CS GT1-63 99
4.4.1.3 Numerical Modeling of PL Test for CS GT2-58 102
4.4.1.4 Numerical Modeling of PL Test for CS GT2-79 105
4.4.2 Numerical Modeling of PL Tests for Bituminous Shale Specimens 108
4.4.2.1 Numerical Modeling of PL Test for BS GT1-8 109
4.4.2.2 Numerical Modeling of PL Test for BS GT1-14 112
4.4.2.3 Numerical Modeling of PL Test for BS GT2-14 115
4.4.2.4 Numerical Modeling of PL Test for BS GT2-16 118
4.4.3 Numerical Modeling of PL Tests for Upper Trona Specimens 121
4.4.3.1 Numerical Modeling of PL Test for UT GT1-27 121
4.4.3.2 Numerical Modeling of PL Test for UT GT1-28 124
4.4.3.3 Numerical Modeling of PL Test for UT GT2-36 127
4.4.3.4 Numerical Modeling of PL Test for UT GT2-39 130
4.4.4 Numerical Modeling of PL Tests for Lower Trona Specimens 133

4.4.4.1 Numerical Modeling of PL Test for LT GT2-84 134
4.4.4.2 Numerical Modeling of PL Test for LT GT2-92 137
4.4.4.3 Numerical Modeling of PL Test for LT GT2-100 140
4.4.4.4 Numerical Modeling of PL Test for LT GT2-114 143
4.4.5 Material Properties Obtained From Iterations for PL Tests 146
4.5 Interpretation for Numerical Modeling of UCS and PL Tests 150
4.6 Comparison of PL and UCS Tests Modeled in PFC 150
5 CONCLUSIONS AND RECOMMENDATIONS 155
REFERENCES 161

LIST OF TABLES

TABLES

Table 2-1 Correlation between PL Strength Index and UCS for Various Rock Types6
Table 3-1 Generalized Index to Strength Conversion Factor (K)....16
Table 3-2 PL Tests – Claystone....16
Table 3-3 PL Tests – Bituminous Shale....18
Table 3-4 PL Tests – Trona (Upper and Lower)....18
Table 3-5 I_{S50} and CoV Values of Different Units....20
Table 3-6 UCS Tests – Claystone....24
Table 3-7 UCS Tests – Bituminous Shale....24
Table 3-8 UCS Tests – Trona (Upper and Lower)....25
Table 3-9 UCS and CoV Values of Different Units....26
Table 3-10 Outlier Detection for PL Tests....29
Table 3-11 Outlier Detection for UCS Tests....29
Table 3-12 PL and UCS Test Results for Claystone....30
Table 3-13 PL and UCS Test Results for Bituminous Shale....31
Table 3-14 PL and UCS Test Results for Claystone and Bituminous Shale....31
Table 3-15 PL and UCS Test Results for Upper Trona....32
Table 3-16 PL and UCS Test Results for Lower Trona....32
Table 3-17 PL and UCS Test Results for Trona (Upper and Lower)....33
Table 3-18 Lithological Unit Classifications....35
Table 3-19 Conversion Factors and Correlation Coefficients....41
Table 4-1 Particle Radius Determination of UCS Tests....51
Table 4-2 Parameters Used For Numerical Modeling Studies of UCS Tests....55
Table 4-3 Parameters of CS GT1-904....56
Table 4-4 Parameters of CS GT1-908....58
Table 4-5 Parameters of CS GT2-698....61
Table 4-6 Parameters of CS GT2-712....63
Table 4-7 Parameters of BS GT1-855....66

Table 4-8 Parameters of BS GT1-860 68
Table 4-9 Parameters of BS GT2-657 70
Table 4-10 Parameters of BS GT2-659 72
Table 4-11 Parameters of UT GT1-874 75
Table 4-12 Parameters of UT GT1-875 77
Table 4-13 Parameters of UT GT2-674 79
Table 4-14 Parameters of UT GT2-679 81
Table 4-15 Parameters of LT GT2-708 84
Table 4-16 Parameters of LT GT2-719 86
Table 4-17 Parameters of LT GT2-723 88
Table 4-18 Parameters of LT GT2-733 90
Table 4-19 Material Properties Obtained from Iterations for UCS Tests 93
Table 4-20 Parameters Used For Numerical Modeling Studies of PL Tests 95
Table 4-21 Parameters of CS GT1-61 97
Table 4-22 Field PL Model vs. UCS Calibrated PL Model - CS GT1-61 99
Table 4-23 Parameters of CS GT1-63 100
Table 4-24 Field PL Model vs. UCS Calibrated PL Model - CS GT1-63 102
Table 4-25 Parameters of CS GT2-58 103
Table 4-26 Field PL Model vs. UCS Calibrated PL Model - CS GT2-58 105
Table 4-27 Parameters of CS GT2-79 106
Table 4-28 Field PL Model vs. UCS Calibrated PL Model - CS GT2-79 108
Table 4-29 Parameters of BS GT1-8 109
Table 4-30 Field PL Model vs. UCS Calibrated PL Model - BS GT1-8 111
Table 4-31 Parameters of BS GT1-14 112
Table 4-32 Field PL Model vs. UCS Calibrated PL Model - BS GT1-14 114
Table 4-33 Parameters of BS GT2-14 115
Table 4-34 Field PL Model vs. UCS Calibrated PL Model - BS GT2-14 117
Table 4-35 Parameters of BS GT2-16 118
Table 4-36 Field PL Model vs. UCS Calibrated PL Model - BS GT2-16 120
Table 4-37 Parameters of UT GT1-27 122
Table 4-38 Field PL Model vs. UCS Calibrated PL Model - UT GT1-27 124
Table 4-39 Parameters of UT GT1-28 125

Table 4-40 Field PL Model vs. UCS Calibrated PL Model - UT GT1-28 127
Table 4-41 Parameters of UT GT2-36 128
Table 4-42 Field PL Model vs. UCS Calibrated PL Model - UT GT2-36 130
Table 4-43 Parameters of UT GT2-39 131
Table 4-44 Field PL Model vs. UCS Calibrated PL Model - UT GT2-39 133
Table 4-45 Parameters of LT GT2-84 134
Table 4-46 Field PL Model vs. UCS Calibrated PL Model - LT GT2-84 136
Table 4-47 Parameters of LT GT2-92 137
Table 4-48 Field PL Model vs. UCS Calibrated PL Model - LT GT2-92 139
Table 4-49 Parameters of LT GT2-100 140
Table 4-50 Field PL Model vs. UCS Calibrated PL Model - LT GT2-100 142
Table 4-51 Parameters of LT GT2-114 143
Table 4-52 Field PL Model vs. UCS Calibrated PL Model - LT GT2-114 145
Table 4-53 Material Properties Obtained From Iterations of UCS Calibrated PL Models 147
Table 4-54 Material Properties Obtained From Iterations of Field PL Models 149
Table 4-55 Comparison of UCS and PL Modeling Results in Terms of Parallel Bond 152
Table 4-56 Comparison of Conversion Factors from Modeling and Test Results 154

LIST OF FIGURES

FIGURES

Figure 3-1 Typical PL Test Equipment 10
Figure 3-2 Conical platens 11
Figure 3-3 Load Configurations and Specimen Shape Requirement.....12
Figure 3-4 Typical Modes of Failure for Valid and Invalid PL Strength Index Tests 13
Figure 3-5 Graph for Size Correction Factor 14
Figure 3-6 Correlation between PL Strength Index and UCS 15
Figure 3-7 Histogram Showing Distribution of I_{S50} Values of Lithological Units....21
Figure 3-8 Typical UCS Test Equipment 22
Figure 3-9 Histogram Showing Distribution of UCS Values of Lithological Units..27
Figure 3-10 PL vs. UCS Graph for Claystone 35
Figure 3-11 PL vs. UCS Graph for Bituminous Shale.....36
Figure 3-12 PL vs. UCS Graph for Claystone and Bituminous Shale.....37
Figure 3-13 PL vs. UCS Graph for Upper Trona.....38
Figure 3-14 PL vs. UCS Graph for Lower Trona 39
Figure 3-15 PL vs. UCS Graph for Upper and Lower Trona 40
Figure 4-1 Illustration of Bond Models Provided in PFC.....45
Figure 4-2 Calculation Cycle in PFC.....47
Figure 4-3 Microscopic View for Claystone 49
Figure 4-4 Microscopic View for Bituminous Shale.....50
Figure 4-5 Microscopic View for Upper Trona.....50
Figure 4-6 Typical Model Geometry in PFC for UCS Test.....54
Figure 4-7 Numerically Modeled CS GT1-904 56
Figure 4-8 PFC Model of CS GT1-904 and Fractures Developed 57
Figure 4-9 Stress-Strain Curves of Lab. Test vs. Modeled Test for CS GT1-904.....58
Figure 4-10 Numerically Modeled CS GT1-908 59
Figure 4-11 PFC Model of CS GT1-908 and Fractures Developed 59

Figure 4-12 Stress-Strain Curves of Lab. Test vs. Modeled Test for CS GT1-908...60
Figure 4-13 Numerically Modeled CS GT2-698.....61
Figure 4-14 PFC Model of CS GT2-698 and Fractures Developed.....62
Figure 4-15 Stress-Strain Curves of Lab. Test vs. Modeled Test for CS GT2-698...63
Figure 4-16 Numerically Modeled CS GT2-712.....64
Figure 4-17 PFC Model of CS GT2-712 and Fractures Developed.....64
Figure 4-18 Stress-Strain Curves of Lab. Test vs. Modeled Test for CS GT2-712...65
Figure 4-19 Numerically Modeled BS GT1-855.....66
Figure 4-20 PFC Model of BS GT1-855 and Fractures Developed.....67
Figure 4-21 Stress-Strain Curves of Lab. Test vs. Modeled Test for BS GT1-855...68
Figure 4-22 Numerically Modeled BS GT1-860.....69
Figure 4-23 PFC Model of BS GT1-860 and Fractures Developed.....69
Figure 4-24 Stress-Strain Curves of Lab. Test vs. Modeled Test for BS GT1-860...70
Figure 4-25 PFC Model of BS GT2-657 and Fractures Developed.....71
Figure 4-26 Stress-Strain Curves of Lab. Test vs. Modeled Test for BS GT2-657...72
Figure 4-27 PFC Model of BS GT2-659 and Fractures Developed.....73
Figure 4-28 Stress-Strain Curves of Lab. Test vs. Modeled Test for BS GT2-659...74
Figure 4-29 Numerically Modeled UT GT1-874.....75
Figure 4-30 PFC Model of UT GT1-874 and Fractures Developed.....76
Figure 4-31 Stress-Strain Curves of Lab. Test vs. Modeled Test for UT GT1-874..77
Figure 4-32 Numerically Modeled UT GT1-875.....78
Figure 4-33 PFC Model of UT GT1-875 and Fractures Developed.....78
Figure 4-34 Stress-Strain Curves of Lab. Test vs. Modeled Test for UT GT1-875..79
Figure 4-35 Numerically Modeled UT GT2-674.....80
Figure 4-36 PFC Model of UT GT2-674 and Fractures Developed.....80
Figure 4-37 Stress-Strain Curves of Lab. Test vs. Modeled Test for UT GT2-674..81
Figure 4-38 Numerically Modeled UT GT2-679.....82
Figure 4-39 PFC Model of UT GT2-679 and Fractures Developed.....82
Figure 4-40 Stress-Strain Curves of Lab. Test vs. Modeled Test for UT GT2-679..83
Figure 4-41 Numerically Modeled LT GT2-708.....84
Figure 4-42 PFC Model of LT GT2-708 and Fractures Developed.....85
Figure 4-43 Stress-Strain Curves of Lab. Test vs. Modeled Test for LT GT2-708...86

Figure 4-44 Numerically Modeled LT GT2-719 87
Figure 4-45 PFC Model of LT GT2-719 and Fractures Developed 87
Figure 4-46 Stress-Strain Curves of Lab. Test vs. Modeled Test for LT GT2-719...88
Figure 4-47 Numerically Modeled LT GT2-723 89
Figure 4-48 PFC Model of LT GT2-723 and Fractures Developed 89
Figure 4-49 Stress-Strain Curves of Lab. Test vs. Modeled Test for LT GT2-723...90
Figure 4-50 Numerically Modeled LT GT2-733 91
Figure 4-51 PFC Model of LT GT2-733 and Fractures Developed 91
Figure 4-52 Stress-Strain Curves of Lab. Test vs. Modeled Test for LT GT2-733...92
Figure 4-53 Typical Model Geometry in PFC for PL Test.....94
Figure 4-54 UCS Calibrated PL Model of CS GT1-61 97
Figure 4-55 Field PL Model of CS GT1-61.....98
Figure 4-56 UCS Calibrated PL Model of CS GT1-63 100
Figure 4-57 Field PL Model of CS GT1-63.....101
Figure 4-58 UCS Calibrated PL Model of CS GT2-58 103
Figure 4-59 Field PL Model of CS GT2-58.....104
Figure 4-60 UCS Calibrated PL Model of CS GT2-79 106
Figure 4-61 Field PL Model of CS GT2-79.....107
Figure 4-62 UCS Calibrated PL Model of BS GT1-8 110
Figure 4-63 Field PL Model of BS GT1-8.....111
Figure 4-64 UCS Calibrated PL Model of BS GT1-14 113
Figure 4-65 Field PL Model of BS GT1-14.....114
Figure 4-66 UCS Calibrated PL Model of BS GT2-14 116
Figure 4-67 Field PL Model of BS GT2-14.....117
Figure 4-68 UCS Calibrated PL Model of BS GT2-16 119
Figure 4-69 Field PL Model of BS GT2-16.....120
Figure 4-70 UCS Calibrated PL Model of UT GT1-27 122
Figure 4-71 Field PL Model of UT GT1-27 123
Figure 4-72 UCS Calibrated PL Model of UT GT1-28 125
Figure 4-73 Field PL Model of UT GT1-28 126
Figure 4-74 UCS Calibrated PL Model of UT GT2-36 128
Figure 4-75 Field PL Model of UT GT2-36 129

Figure 4-76 UCS Calibrated PL Model of UT GT2-39 131
Figure 4-77 Field PL Model of UT GT2-39 132
Figure 4-78 UCS Calibrated PL Model of LT GT2-84 135
Figure 4-79 Field PL Model of LT GT2-84 136
Figure 4-80 UCS Calibrated PL Model of LT GT2-92 138
Figure 4-81 Field PL Model of LT GT2-92 139
Figure 4-82 UCS Calibrated PL Model of LT GT2-100 141
Figure 4-83 Field PL Model of LT GT2-100 142
Figure 4-84 UCS Calibrated PL Model of LT GT2-114 144
Figure 4-85 Field PL Model of LT GT2-114 145

CHAPTER 1

INTRODUCTION

Humankind has used materials produced from mining activities since prehistoric ages. Mining activities were developed for stone products and metal commodities together with the civilization. People first utilized and processed minerals at the surface and shallow depths and in the course of time they have improved mining methods with the help of inventions. At the present time, thanks to state-of-the-art equipment they can have continuous operations at mines without being interrupted by climatic, geographic or geological issues.

Due to increasing demand for materials from mining activities and changes in economic conditions, underground mining had become a necessity and numerous feasible underground mining projects had been developed all around the world. When it comes to underground mining, the first factor to be considered is safety. Support system is the most important factor with respect to underground mine safety. For underground mining that have been performed for centuries, several support systems have been developed and different support systems have been utilized at different mines.

1.1 General Remarks

Support systems are one of the most important factors for underground mining projects. Calculations to choose appropriate support system, which would ensure a safe environment for an underground operation, should be carried out with utmost care and with the least margin of error. There are numerous types of tests and determining parameters for underground safety. Uniaxial Compressive Strength (UCS) test is one of

the primary tests to be applied during the process of selecting appropriate support system. This test, however, is applied in laboratory environment and it is not possible to apply this test under field conditions. For this reason, point load (PL) strength test, which is a more practical and economic method, is applied under field conditions in order to classify rock strength within a short period of time during the course of drilling campaign.

PL is an index test and is intended to be used to classify rock strength. This index test is performed by subjecting a rock specimen to an increasingly concentrated load until failure occurs by splitting the specimen. The concentrated load is applied through coaxial, truncated conical platens. The failure load is used to calculate the point load strength index (ASTM D5731–08, 2008).

The PL strength index can be used to classify the rocks. Specimens in the form of rock cores, blocks or irregular lumps are used. This test method can be performed in either the field or laboratory (ASTM D5731–08, 2008). Details of PL test program should be determined before applying the test and, if possible, before samples are taken. While determining the said details, the factors such as budget and purpose of use of data to be obtained at the end of the tests should be identified.

Since test equipment is portable and specimens can easily be prepared for testing after being taken, PL test method can be applied under field conditions.

UCS test is used to determine compressive strengths of rock specimens. This method is more time consuming and expensive as compared to PL test. When a test, which can be applied with a preliminary or basic preparation, is required and when data is needed to be obtained on site within a short period of time, PL test is the best choice as it saves time and it is economic. Especially, during exploration phase, use of this method enables more appropriate and effective decisions to be taken and also produces results at low costs.

Advantages of PL strength tests can be summarized as follows:

- It is an inexpensive test
- It quickly yields results
- It can be applied under field conditions

PL test results should not be used for design or analytical purposes (ASTM D5731–08, 2008). The objective of this test is to classify rocks based on their strength indices. Comparison of UCS and PL tests is achieved by performing regression analyses.

PL test equipment consists of a loading set-up, loading pump, gauges, two conical platens and a scale that measures distance between two conical platens. First, an uncorrected PL strength (I_S) is found by using specimen dimensions and failure load that is obtained at the end of test. Test can be performed on specimens with different equivalent diameter and thus uncorrected PL strength index varies. Therefore uncorrected PL strength index is corrected by applying a size correction in order to obtain a unique PL strength index for the rock specimen.

1.2 Problem Statement

It is possible to estimate UCS of rock specimens by utilizing PL tests, which are more economic and practical and also applicable under field conditions on the specimens. As given in detail in the Literature Survey chapter, researchers have suggested correlations and conversion factors for different rock types. However, there is no study for trona.

Discontinuum modeling of structures in rock or soil requires calibration of the micro mechanical properties of the materials by using UCS tests as well as direction tension tests. In the literature, such calibration does not exist for the abovementioned rock types.

1.3 Objectives of Study

The first objective of this study is to determine conversion factors to be used to estimate UCS of trona and interburden rocks (claystone, bituminous shale) by utilizing the

results of the PL tests applied on the drill core specimens in the field and UCS tests carried out in the laboratory.

The second objective of this study is to numerically model both laboratory UCS tests and field PL tests by using 2-dimensional Particle Flow Code (PFC2D, ItascaTM, 2008). An attempt is made to guide researchers having different kinds of modeling problems (excavation, slope stability etc.). Calibration coefficients are proposed for the abovementioned rock types throughout the rigorous PFC simulations.

1.4 Research Methodology

The methodology outlined below was followed in this study:

1- Literature was reviewed,
2- All drillhole database and the results of the PL tests performed at the field were obtained from the company that performed the drilling,
3- Lithological units were collected under “claystone”, “bituminous shale” and “trona” headings,
4- PL tests on the untested intervals were performed in the laboratory,
5- UCS tests were conducted on the specimens obtained from the company,
6- UCS and PL intervals that were close to each other were matched (if there were more than one PL test interval matching with one UCS interval, average of those PL tests were used),
7- Regression graphs were constructed by using PL and UCS test results
8- Conversion factors were obtained from those graphs,
9- 16 PL tests and 16 UCS tests were numerically modeled by using PFC,
10- Results of the laboratory tests were compared to those of numerical models,
11- PFC calibration coefficients between macro and micro mechanical properties for both UCS and PL tests were proposed.

CHAPTER 2

LITERATURE SURVEY

Literature was comprehensively reviewed within the scope of this study and the details are given in this chapter.

2.1 Literature Review

PL strength index (I_{S50}) obtained from PL test is used to indirectly determine uniaxial compressive and tensile strengths of rocks (Broch & Franklin, 1972; Bieniawski, 1975; Al-Jassar & Hawkins, 1979; Norbury, 1986; Wljk, 1980), to classify rocks in terms of material properties and according to their strengths (Guidicini et al., 1973; Bieniawski, 1975), to determine rock anisotropy (Greminger, 1982; Broch, 1983), to make RMR rock mass classification (Bieniawski, 1989), to estimate rate of tunnel boring machine (McFeat & Tarkoy, 1979), to classify rocks in terms of excavatability (Pettifer & Fookes, 1994) and to determine rock strengths against external effects (Fookes et al., 1988; Rodrigues & Jeremias, 1990).

PL test is generally suggested for rocks but it was also applied on concrete specimens. This method is also used for geotechnical core logging (BSI, 1981; Hawkins, 1986). PL test can be performed axially or diametrically on rock cores and blocks prepared in laboratory environment or on irregular lumps by taking specimen dimensions into consideration. This test was suggested by Broch and Franklin (1972) for the first time and then ISRM (1972) and Anon (1972) also acknowledged it. It was commonly used in subsequent studies and has eventually become an international method at present (ISRM, 1985).

In the literature, the researchers (Bearman, 1999; Gunsallus and Kulhawy, 1984) suggested linear equations for the rapid estimation of mode I fracture toughness.

2.2 Correlations between PL Index and UCS for Various Rock Types

Correlations between PL strength index and UCS for various types of rocks were suggested in numerous studies carried out by researchers. Table 2-1 shows such correlations from 6 different studies. While some of the equations in Table 2-1 are original equations obtained as a result of the tests performed within the scope of the corresponding studies, some of them were forced to pass through the origin. Passing through the origin means that when PL strength index of a specimen is zero, UCS of that specimen should also be zero. In other words, the trendline of such a correlation needs to pass through the origin. Exponential relationships were also suggested (Kahraman, 2014).

Table 2-1 Correlation between PL Strength Index and UCS for Various Rock Types

No	Author	Rock Type	Correlation between PL and UCS	Correlation Coeff. (R^2)
1	Vallejo et al., 1989	1) Shale	$UCS = 12.5I_{S50}$	*0.62*
		2) Sandstone	$UCS = 17.4I_{S50}$	*0.38*
2	Kahraman, 2001	1) 22 different rock types	$UCS = 8.41I_{S50} + 9.51$	*0.72*
		2) Coal measure rocks	$UCS = 23.62I_{S50} - 2.69$	*0.86*
3	Mishra & Basu, 2013	1) Granite	$UCS = 10.9I_{S50} + 49.03$	0.80
		2) Schist	$UCS = 11.21I_{S50} + 4.008$	0.84
		3) Sandstone	$UCS = 12.95I_{S50} - 5.19$	0.84
		4) All tested rocks	$UCS = 14.63I_{S50}$	0.88
4	Kahraman & Günaydın, 2009	1) 52 different rock types	$UCS = 10.92I_S + 24.24$	0.56
		2) Igneous rocks	$UCS = 8.20I_S + 36.43$	0.68
		3) Metamorphic rocks	$UCS = 18.45I_S - 13.63$	0.77
		4) Sedimentary rocks	$UCS = 29.77I_S - 51.49$	0.78

Table 2-1 Correlation between PL Strength Index and UCS for Various Rock Types (continued)

5	Rusnak & Mark, 2000	1) Coal measure rocks	UCS = $17.6I_{S50}$ + 1970$^{(*)}$	0.68
6	Read et al., 1980	1) Sedimentary rocks	UCS = $16I_{S50}$	-
		2) Basalts	UCS = $20I_{S50}$	-
7	Singh et al., 2012	Rock salt	UCS = $16.1I_{S50}$	0.71
8	Kahraman, 2014	Different soft rocks	UCS = $2.68e^{0.93Is}$	0.93

$^{(*)}$ In terms of psi

In the literature the conversion factor is changing between 11.8 and 50 depending on the rock type. ISRM (1985) suggested that on average, UCS was 20-25 times I_S although it was stated that in tests of many different rock types the range varied between 15 and 50, especially for anisotropic rocks. Commonly used conversion factor is 24.

CHAPTER 3

POINT LOAD AND UNIAXIAL COMPRESSIVE STRENGTH TESTS

In this chapter, two types of testing methodologies are presented. In the first section, PL tests that were carried out under field conditions will be discussed in detail and in the second section details about UCS tests that were performed in the laboratory environment will be given.

Consequently, conversion factors to be used to estimate UCS of trona as well as interburden rocks (claystone and bituminous shale) by utilizing the results of the PL tests applied on drill core specimens were determined.

Note: For simplicity, the following abbreviations were used for lithological units in this study:

1- CS : Claystone
2- BS : Bituminous Shale
3- UT : Upper Trona
4- LT : Lower Trona
5- T : Trona

3.1 The Mine Site and the Geology

Beypazarı Trona mine is located 20 km northwest of Beypazarı Town in Ankara. Solution mining method is used for exploitation. In solution mining method a trona (natural soda) leaching cavern is generated by the well pairs, which are connected to

each other by means of directional drilling. The solvent is sent through one of the wells (the injection well) to the underground (cavern) thus dissolving the ore.

The trona field is characterized by the Pliocene and Miocene aged formations consisting of sedimentary and volcano-sedimentary lithological units deposited in the lake facies and the alluvium (Helvacı et al., 1989).

The site contains different quality of trona veins and the company names them as upper and lower trona.

3.2 Point Load (PL) Tests

In this section, the majority of the information with respect to PL tests is quoted from ASTM (D5731–08, 2008) standard. PL strength test is an index test that is used to classify strengths of rock materials. Test results are not used for design or analytical purposes but they can be used to estimate the design parameter called UCS strength. Typical PL test equipment is comprised of the components depicted in Figure 3-1.

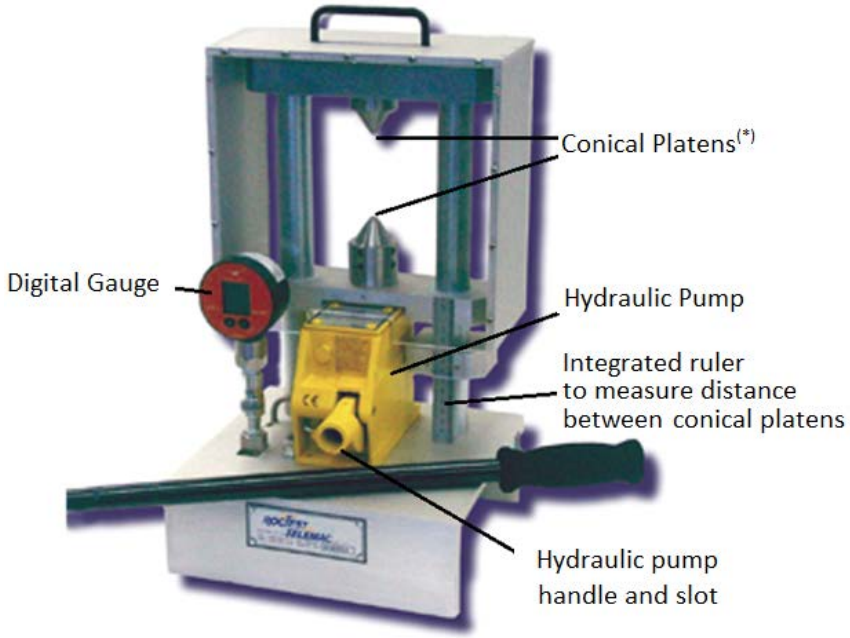

Figure 3-1 Typical PL Test Equipment

(*) Within the scope of this study, the test equipment with the conical platens shown in Figure 3-2 was used in PL tests. Also, the parameters shown in Figure 3-2 were used in PFC software, where 2 dimensional models of the PL tests were constructed.

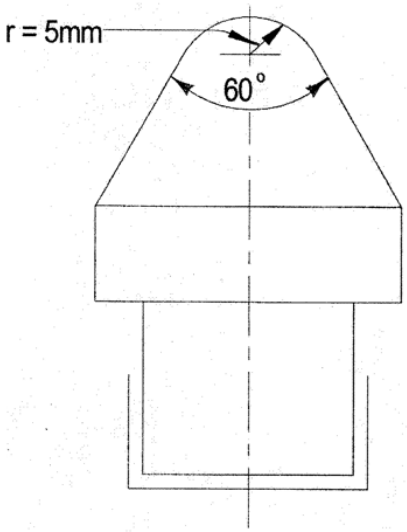

Figure 3-2 Conical platens

Rock specimens in the form of either core (the diametral and axial tests), cut blocks (the block test), or irregular lumps (the irregular lump test) are tested by application of concentrated load through a pair of truncated, conical platens. Little or no specimen preparation is required and can therefore be tested shortly after being obtained and any influence of moisture condition on the test data minimized.

Specimen to be tested is placed between the conical platens in perpendicular or parallel orientation depending on its shape. PL test can be performed in three different methods:

i. Diametral PL test
ii. Axial PL test
iii. PL test applied on blocks or irregular lumps

Examples of how specimens are placed during testing and the ratios between specimen dimensions are shown in Figure 3-3.

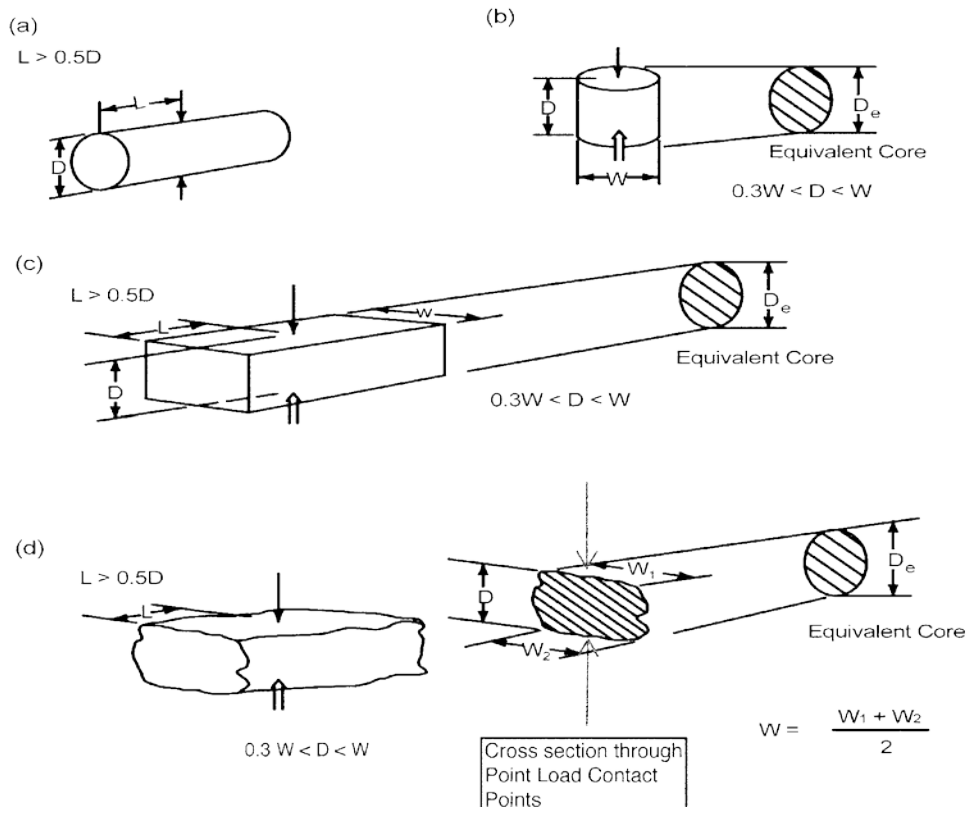

Legend:

L = distance between contact points and nearest free face

D_e = equivalent core diameter

Figure 3-3 Load Configurations and Specimen Shape Requirement for (a) the Diametral Test, (b) the Axial Test, (c) the Block Test and (d) the Irregular Lump Test

According to the test method, the specimen that is prepared to have the dimensions set forth in Figure 3-3 by measuring with a caliper is perpendicularly placed between conical platens for diametral testing and placed parallel for axial testing. Loading frame is raised with the help of the pump until the gap between conical platen and specimen is eliminated. Load is applied steadily in such a way that failure occurs within 10 to 60 seconds and failure load (P) shown on the gauge of test equipment is recorded. The test should be rejected if the fracture surface passes through only one loading point as shown in Figure 3-4(d)).

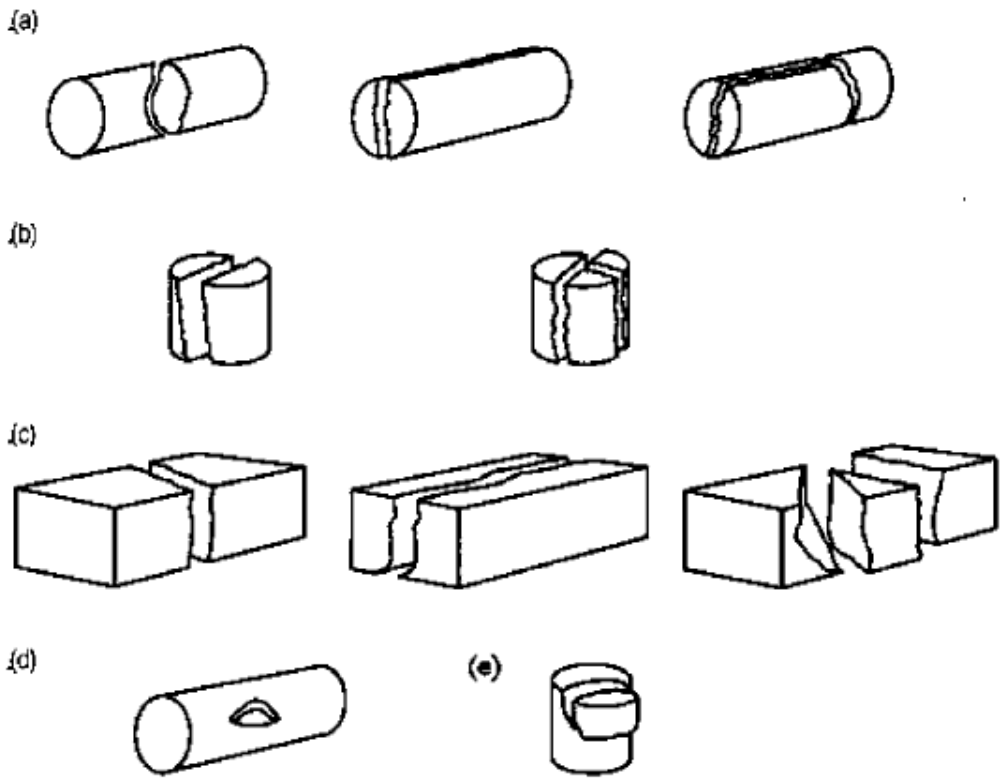

Figure 3-4 Typical Modes of Failure for Valid and Invalid PL Strength Index Tests – (a) Valid diametral tests; (b) valid axial tests; (c) valid block tests; (d) invalid core test; and (e) invalid axial test

Corrected value of PL strength index is calculated by using the following formula:

$$I_S = \frac{P}{D_e^2}\ (kPa) \qquad \text{Eq. 1}$$

In this equation P is the failure load (in terms of N) and D_e is the equivalent specimen diameter (in terms of mm).

i. For diametral PL test $D_e^2 = D^2$ and

ii. For axial, block or irregular lump PL tests $D_e^2 = 4A / \pi$ (where A = WD, minimum cross-sectional area of a plane through the platen contact points – See Figure 3-3).

I_S value is a function of D parameter for diametral PL tests and of De parameter for other types of PL tests. Accordingly, I_S value should be corrected as per the diameter of a standard specimen having a diameter of D = 50 mm. The index obtained as a result of correction is called I_{S50} and is calculated by using the following equation:

$$I_{S50} = FI_s \qquad \text{Eq. 2}$$

In this equation F is the size correction factor. Size correction factor (F) can be determined from the Equation 3 or from the graph given in Figure 3-5. The unit of De in Equation 3 is mm.

$$F = (D_e/50)^{0,45} \qquad \text{Eq. 3}$$

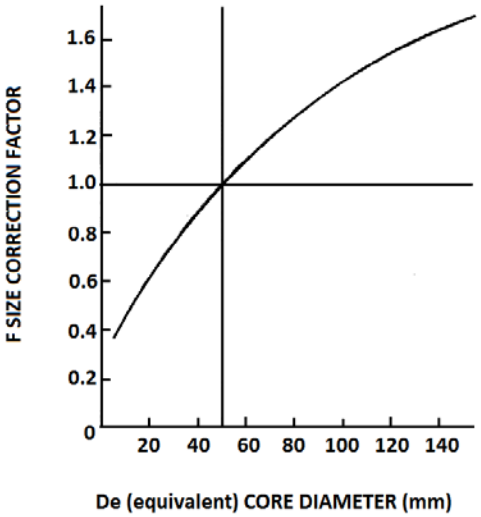

Figure 3-5 Graph for Size Correction Factor

- **Estimation of Uniaxial Compressive Strength**

The estimated UCS can be obtained for NX core by using Figure 3-6 or Equation 4.

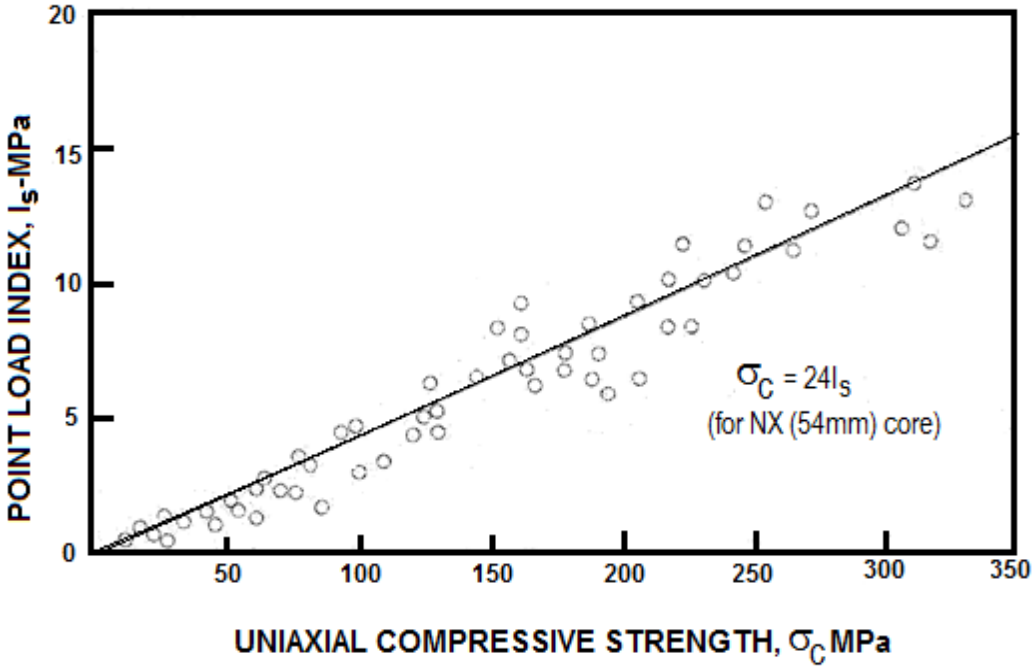

Figure 3-6 Correlation between PL Strength Index and UCS from 125 Tests On Sandstone, Quartzite, Marikana Norite, and Belfast Norite (ASTM D5731–08, 2008)

$$UCS = K * I_s \qquad \text{Eq. 4}$$

In this equation UCS is the uniaxial compressive strength (in terms of MPa), K is the index to strength conversion factor that depends on site-specific correlation between UCS and Is for a specific specimen with a test diameter (D) and I_S is the uncorrected PL strength index (in terms of MPa) from a specimen with a specific test diameter (D)

If site-specific correlation factor "K" is not available, the generalized values may be used in Table 3-1.

Table 3-1 Generalized Index to Strength Conversion Factor (K) (Bieniawski, 1975)

Core Size, mm	Value of "K" (Generalized)
21.5 (Ex Core)	18
30	19
42 (Bx Core)	21
50	23
54 (Nx Core)	24
60	24,5

PL tests analyzed in this study were carried out for axially loaded samples under field conditions and details for these tests are given for claystone in Table 3-2, for bituminous shale in Table 3-3 and for trona in Table 3-4, where the data of upper trona is between the rows 1 and 25 and the rest belongs to lower trona. A total of 16 rows were highlighted in gray in these three tables. These are the PL tests for which numerical models were constructed in PFC. Details of these modeling studies are given in Chapter 4.

Table 3-2 PL Tests – Claystone

No	**Specimen No**	**Drillhole Name**	**From (m)**	**To (m)**	**Interval (m)**	**Average Corrected PL Index I_{S50} (MPa)**	**Matching Code**
1	8	AGA-4	321.45	321.49	0.04	0.483	C-M1
2	40	AGA-4	400.20	400.25	0.05	0.426	C-M2
	42	AGA-4	400.30	400.34	0.04		
3	1	GT-1	410.55	410.61	0.06	0.637	C-M3
4	2	GT-1	411.40	411.44	0.04	1.024	C-M4
	3	GT-1	411.60	411.63	0.03		
	4	GT-1	411.65	411.69	0.04		

Table 3-2 PL Tests – Claystone (continued)

5	61	GT-1	455.96	455.99	0.03	0.218	C-M5
6	63	GT-1	456.05	456.10	0.05	0.325	C-M6
	64	GT-1	456.35	456.39	0.04		
7	58	GT-2	431.10	431.15	0.05	0.511	C-M7
	59	GT-2	431.15	431.20	0.05		
	60	GT-2	431.20	431.24	0.04		
8	79	GT-2	456.00	456.05	0.05	0.627	C-M8
	80	GT-2	456.05	456.09	0.04		
	81	GT-2	456.10	456.14	0.04		
9	87	GT-2	462.65	462.69	0.04	0.415	C-M9
	88	GT-2	462.70	462.74	0.04		
10	95	GT-2	466.40	466.44	0.04	0.344	C-M10
	96	GT-2	466.45	466.49	0.04		
11	102	GT-2	473.75	473.80	0.05	0.481	C-M11
	103	GT-2	473.80	473.85	0.05		
12	108	GT-2	482.05	482.11	0.06	0.927	C-M12
	109	GT-2	482.10	482.14	0.04		
	110	GT-2	482.15	482.21	0.06		
13	118	GT-2	492.55	492.59	0.04	1.400	C-M13
	119	GT-2	492.60	492.64	0.04		
14	120	GT-2	494.90	494.94	0.04	0.985	C-M14
15	121	GT-2	494.95	495.00	0.05	1.530	C-M15
16	122	GT-2	496.80	496.85	0.05	1.274	C-M16
	123	GT-2	496.85	496.89	0.04		

Table 3-3 PL Tests – Bituminous Shale

No	Specimen No	Drillhole Name	From (m)	To (m)	Interval (m)	Average Corrected PL Index I_{S50} (MPa)	Matching Code
1	8	GT-1	414.50	414.54	0.04	0.679	B-M1
	9	GT-1	414.55	414.59	0.04		
2	14	GT-1	419.00	419.04	0.04	1.008	B-M2
	15	GT-1	419.05	419.09	0.04		
	16	GT-1	419.10	419.15	0.05		
3	14	GT-2	383.50	383.55	0.05	0.918	B-M3
	15	GT-2	383.55	383.60	0.05		
4	16	GT-2	386.25	386.30	0.05	0.589	B-M4
5	18	GT-2	386.65	386.69	0.04	0.674	B-M5
6	19	GT-2	389.70	389.75	0.05	1.106	B-M6
	20	GT-2	389.75	389.80	0.05		
	21	GT-2	389.80	389.86	0.06		
7	52	GT-2	425.35	425.39	0.04	0.130	B-M7
	53	GT-2	425.40	425.44	0.04		
	54	GT-2	425.45	425.49	0.04		

Table 3-4 PL Tests – Trona (Upper and Lower)

No	Specimen No	Drillhole Name	From (m)	To (m)	Interval (m)	Average Corrected PL Index I_{S50} (MPa)	Matching Code
1	14	AGA-4	331.00	331.04	0.04	1.083	UT-M1
2	23	AGA-4	363.50	363.54	0.04	1.301	UT-M2
3	24	AGA-4	363.55	363.59	0.04	1.695	UT-M3
4	27	AGA-4	366.75	366.79	0.04	0.436	UT-M4
5	36	AGA-4	389.55	389.59	0.04	0.581	UT-M5
6	38	AGA-4	395.75	395.79	0.04	0.614	UT-M6
7	43	AGA-4	400.35	400.40	0.05	0.597	UT-M7

Table 3-4 PL Tests – Trona (Upper and Lower) (continued)

8	48	AGA-4	404.75	404.79	0.04	0.763	UT-M8
9	49	AGA-4	405.75	405.80	0.05	1.587	UT-M9
10	50	AGA-4	405.80	405.85	0.05	1.867	UT-M10
11	26	GT-1	433.70	433.74	0.04	1.969	UT-M11
12	27	GT-1	434.35	434.38	0.03	1.618	UT-M12
13	28	GT-1	434.40	434.43	0.03	1.846	UT-M13
14	31	GT-1	438.10	438.13	0.03	0.377	UT-M14
15	34	GT-1	439.15	439.18	0.03	0.684	UT-M15
16	50	GT-1	447.90	447.94	0.04	1.497	UT-M16
17	51	GT-1	450.20	450.23	0.03	2.545	UT-M17
	52	GT-1	450.25	450.28	0.03		
	53	GT-1	450.30	450.33	0.03		
18	24	GT-2	396.00	396.04	0.04	0.741	UT-M18
	26	GT-2	396.70	396.74	0.04		
	27	GT-2	396.75	396.79	0.04		
19	36	GT-2	407.95	407.99	0.04	1.788	UT-M19
20	37	GT-2	408.00	408.04	0.04	0.630	UT-M20
21	39	GT-2	412.85	412.89	0.04	1.221	UT-M21
22	40	GT-2	412.90	412.94	0.04	0.663	UT-M22
23	48	GT-2	421.15	421.19	0.04	1.827	UT-M23
24	55	GT-2	429.25	429.29	0.04	2.751	UT-M24
25	61	GT-2	432.20	432.24	0.04	1.078	UT-M25
	62	GT-2	432.25	432.30	0.05		
	63	GT-2	432.30	432.35	0.05		
26	84	GT-2	462.10	462.13	0.03	0.777	LT-M26
27	86	GT-2	462.20	462.23	0.03	0.607	LT-M27
28	92	GT-2	465.55	465.58	0.03	0.627	LT-M28
	93	GT-2	465.60	465.63	0.03		
	94	GT-2	465.65	465.69	0.04		
29	99	GT-2	471.30	471.33	0.03	0.739	LT-M29
	100	GT-2	471.35	471.38	0.03		
	101	GT-2	471.40	471.43	0.03		
30	104	GT-2	478.35	478.39	0.04	0.382	LT-M30
	105	GT-2	478.40	478.44	0.04		
31	114	GT-2	489.00	489.04	0.04	2.199	LT-M31

The coefficients of variations (CoV) were determined to evaluate the variability of the I_{S50} for each rock type. Table 3-5 presents the CoV values.

Table 3-5 I_{S50} and CoV Values of Different Units

Lithology	**Average I_{S50} (MPa)**	**Standard Deviation**	**CoV (%)**
CS	0.73	0.41	57
BS	0.73	0.33	45
UT	1.27	0.67	52
LT	0.89	0.66	74
T	1.2	0.67	56

As can be seen from Table 3-5, the I_{S50} CoV of the rock units changes between 45% and 74%. CoV calculations were carried out by including all the data. Although, ISRM (1985) suggests not including two highest and two lowest values, this was not applied here due to limited number data.

The histogram distribution of I_{S50} for each unit is shown in Figure 3-7.

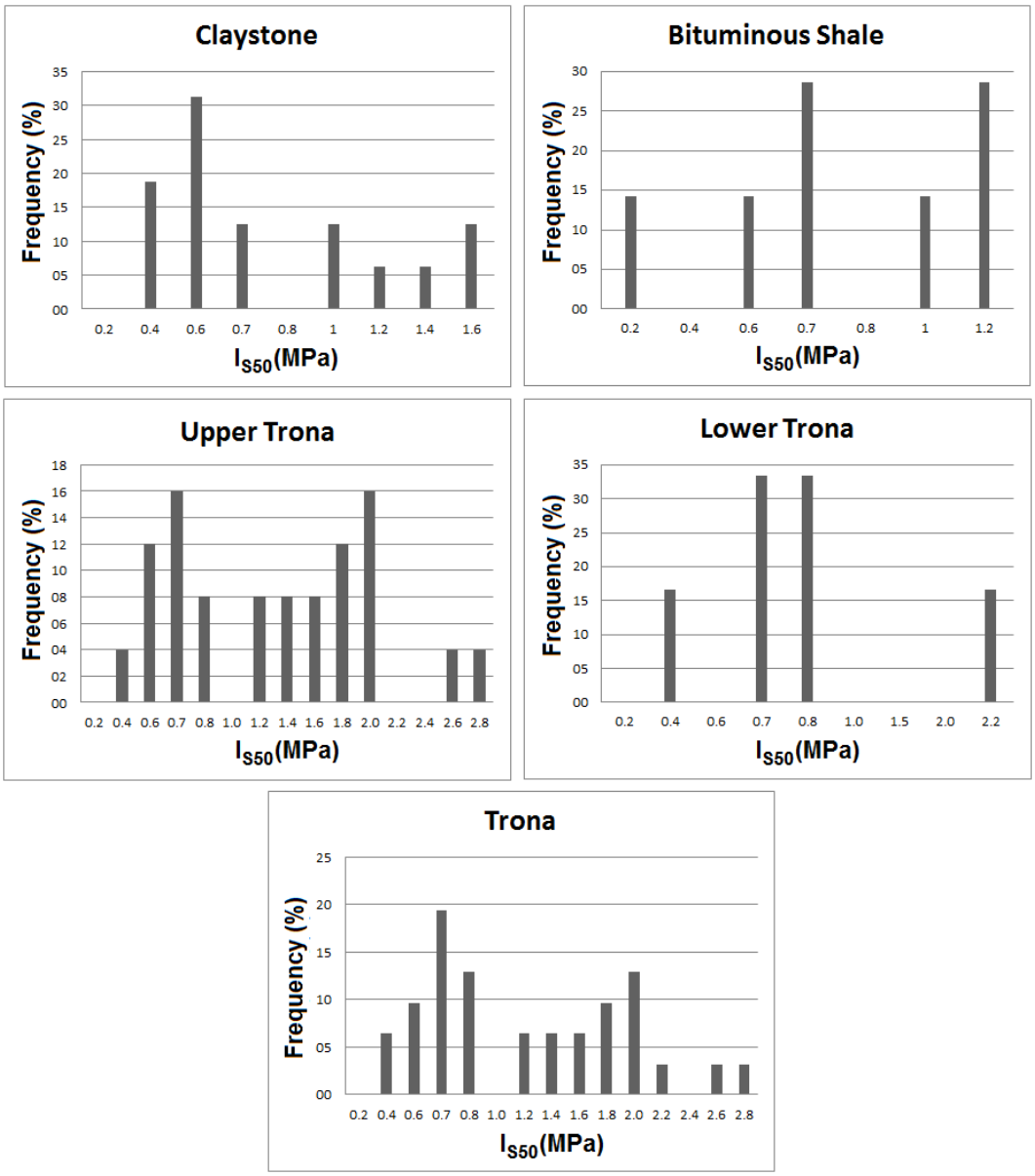

Figure 3-7 Histogram Showing Distribution of I_{S50} Values of Lithological Units

3.3 Uniaxial Compressive Strength (UCS) Tests

Compressive strength is one of the most commonly used and utilized rock mechanics engineering parameters. The maximum stress that a rock specimen can withstand under uniaxial loading conditions is called UCS and it is represented by σ_{ucs} or σ_c symbols.

USC test is used to determine compressive strengths of rock specimens. Test is generally applied on cubic or cylindrical core specimens. In general, cubic specimens are used for marble, concrete and coal tests and rock mechanics tests are applied on core specimens. As the length/diameter ratio of the specimen used in testing increases UCS value decreases. Specimens are prepared in such a way that they have a length (L) / diameter (D) ratio of 2.5 to 3.0. In rock mechanics laboratories NX cores having a diameter of 54.7mm are preferred. However, if it is not possible to take samples with appropriate lengths, this test can be applied on the cores with smaller diameters.

Since the objective of the test is to test the behavior of material under existing conditions, specimens should be conditioned in order to simulate their original environments. Dimensions of prepared specimens are recorded and specimens are placed between the hydraulic platens. In order to uniformly distribute the load on the specimen, steel spherical seats are placed on top the specimen. Figure 3-8 shows typical UCS test equipment.

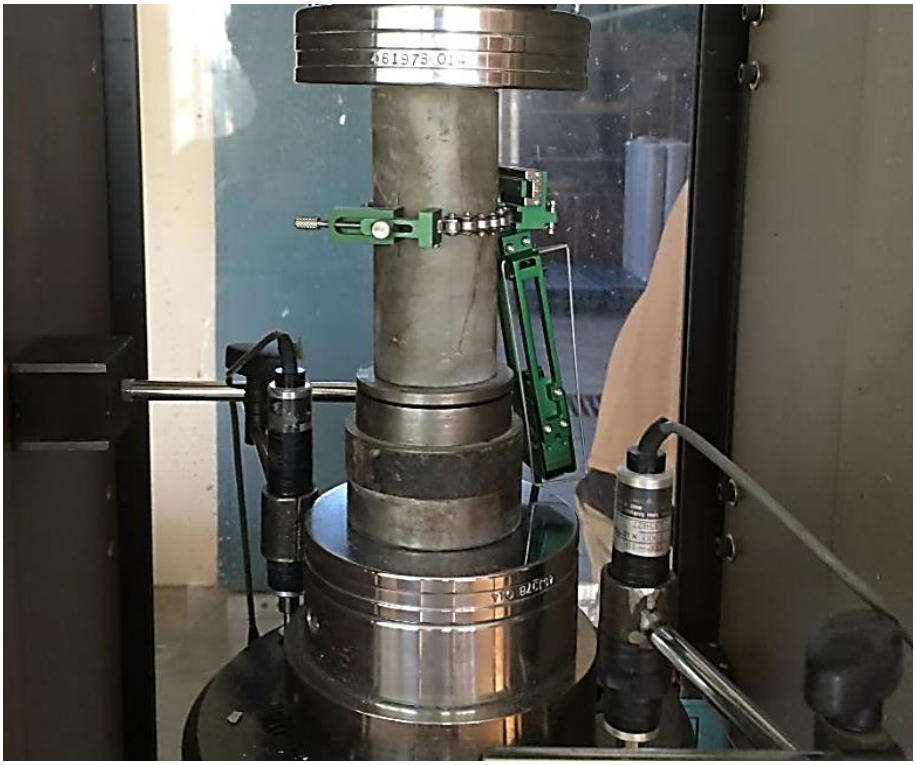

Figure 3-8 Typical UCS Test Equipment

After the discs are precisely aligned with the specimen, a small axial load of approximately 100 N is applied on the specimen to properly seat the platens. On hydraulic press equipment, the platen on which the specimen is placed moves upward. Rate (loading or displacement) can be manually or automatically controlled and loading condition can be monitored on dial indicator or digital gauge or on computer. Axial load is continuously applied until load stabilizes or decreases or reaches at a predetermined tension value. Load should be applied in such a way that a constant stress or tension rate is achieved as far as possible or that the specimen fails within 2 to 15 minutes. The maximum load value to which the specimen can withstand is recorded to be used for calculations. It should also be noted that deformability tests were carried out in order to generate stress-strain curves which were used during PFC modeling.

Compressive strength of the specimen is calculated by using the Equation 5 which incorporates the maximum applied compressive load and initially determined cross sectional area as parameters.

$$\sigma = \frac{P}{A} \qquad \text{Eq. 5}$$

In this equation σ is the compressive strength, P is the maximum load and A is the cross-sectional area.

UCS tests analyzed within the scope of this study were carried out in the laboratory environment. Intervals on which the tests are applied were determined and the cores taken from the corresponding intervals were prepared according to the standards before testing process. Details with regard to UCS tests were given for claystone in Table 3-6, for bituminous shale in Table 3-7 and for trona in Table 3-8, where the data of upper trona is between the rows 1 and 25 and the rest belongs to lower trona. A total of 16 rows were highlighted in gray in these three tables. These are the UCS tests for which numerical models were constructed in PFC. Details about these modeling studies are given in Chapter 4.

Table 3-6 UCS Tests – Claystone

No	Specimen No	Drillhole Name	From (m)	To (m)	Interval (m)	UCS (MPa)	Matching Code
1	364	AGA-4	324.35	324.58	0.23	12.00	C-M1
2	375	AGA-4	399.90	400.10	0.20	6.90	C-M2
3	851	GT-1	410.75	410.96	0.21	22.53	C-M3
4	854	GT-1	411.70	411.88	0.18	8.07	C-M4
5	904	GT-1	454.88	455.10	0.22	4.81	C-M5
6	908	GT-1	456.10	456.35	0.25	2.88	C-M6
7	698	GT-2	429.95	430.15	0.20	6.61	C-M7
8	712	GT-2	457.80	457.94	0.14	3.80	C-M8
9	717	GT-2	462.50	462.70	0.20	5.09	C-M9
10	721	GT-2	467.30	467.55	0.25	8.79	C-M10
11	725	GT-2	473.33	473.50	0.17	15.11	C-M11
12	728	GT-2	481.50	481.72	0.22	22.58	C-M12
13	738	GT-2	492.70	492.86	0.16	24.46	C-M13
14	739	GT-2	495.36	495.52	0.16	27.69	C-M14
15	741	GT-2	495.77	495.93	0.16	22.32	C-M15
16	742	GT-2	496.46	496.66	0.20	15.07	C-M16

Table 3-7 UCS Tests – Bituminous Shale

No	Specimen No	Drillhole Name	From (m)	To (m)	Interval (m)	UCS (MPa)	Matching Code
1	855	GT-1	414.58	414.75	0.17	20.18	B-M1
2	860	GT-1	418.80	419.00	0.20	28.44	B-M2
3	657	GT-2	384.00	384.22	0.22	28.14	B-M3
4	659	GT-2	385.11	385.26	0.15	21.56	B-M4
5	663	GT-2	388.32	388.49	0.17	11.73	B-M5
6	665	GT-2	390.13	390.31	0.18	24.61	B-M6
7	691	GT-2	425.70	425.96	0.26	9.37	B-M7

Table 3-8 UCS Tests – Trona (Upper and Lower)

No	Specimen No	Drillhole Name	From (m)	To (m)	Interval (m)	UCS (MPa)	Matching Code
1	365	AGA-4	327.70	327.98	0.28	22.60	UT-M1
2	368	AGA-4	363.70	363.98	0.28	25.30	UT-M2
3	369	AGA-4	364.65	364.90	0.25	30.70	UT-M3
4	370	AGA-4	365.95	366.26	0.31	3.30	UT-M4
5	372	AGA-4	391.85	392.10	0.25	1.80	UT-M5
6	374	AGA-4	396.50	396.70	0.20	19.50	UT-M6
7	376	AGA-4	402.67	402.90	0.23	6.40	UT-M7
8	378	AGA-4	406.10	406.27	0.17	19.50	UT-M8
9	379	AGA-4	406.80	406.98	0.18	18.00	UT-M9
10	380	AGA-4	406.98	407.18	0.20	32.00	UT-M10
11	871	GT-1	433.50	433.66	0.16	33.20	UT-M11
12	874	GT-1	435.02	435.20	0.18	11.17	UT-M12
13	875	GT-1	435.20	435.38	0.18	15.45	UT-M13
14	880	GT-1	438.32	438.50	0.18	3.89	UT-M14
15	883	GT-1	439.10	439.30	0.20	11.43	UT-M15
16	892	GT-1	448.40	448.62	0.22	28.19	UT-M16
17	899	GT-1	452.77	452.98	0.21	35.79	UT-M17
18	670	GT-2	396.16	396.35	0.19	14.35	UT-M18
19	674	GT-2	406.90	407.10	0.20	18.90	UT-M19
20	676	GT-2	408.88	409.08	0.20	18.61	UT-M20
21	679	GT-2	411.15	411.35	0.20	12.30	UT-M21
22	681	GT-2	413.08	413.27	0.19	3.09	UT-M22
23	686	GT-2	422.94	423.15	0.21	32.48	UT-M23
24	693	GT-2	427.62	427.82	0.20	29.95	UT-M24
25	700	GT-2	432.40	432.60	0.20	22.40	UT-M25
26	708	GT-2	456.88	457.02	0.14	7.33	LT-M26
27	714	GT-2	459.30	459.50	0.20	8.27	LT-M27
28	719	GT-2	465.05	465.30	0.25	6.90	LT-M28
29	723	GT-2	470.90	471.00	0.10	7.32	LT-M29
30	727	GT-2	478.11	478.31	0.20	7.20	LT-M30
31	733	GT-2	487.06	487.22	0.16	18.67	LT-M31

The coefficients of variations (CoV) were determined to evaluate the variability of the UCS for each rock type. Table 3-9 presents the CoV values.

Table 3-9 UCS and CoV Values of Different Units

Lithology	Average UCS (MPa)	Standard Deviation	CoV (%)
CS	13.04	8.42	65
BS	20.58	7.53	37
UT	18.81	10.45	56
LT	9.28	4.62	50
T	16.97	10.27	61

As can be seen from Table 3-9, the UCS CoV of the rock units changes between 37% and 65%. CoV calculations were carried out by including all the data. Although, ISRM (1985) suggests not including two highest and two lowest values, this was not applied here due to limited number data.

The histogram distribution of UCS for each unit is shown in Figure 3-9.

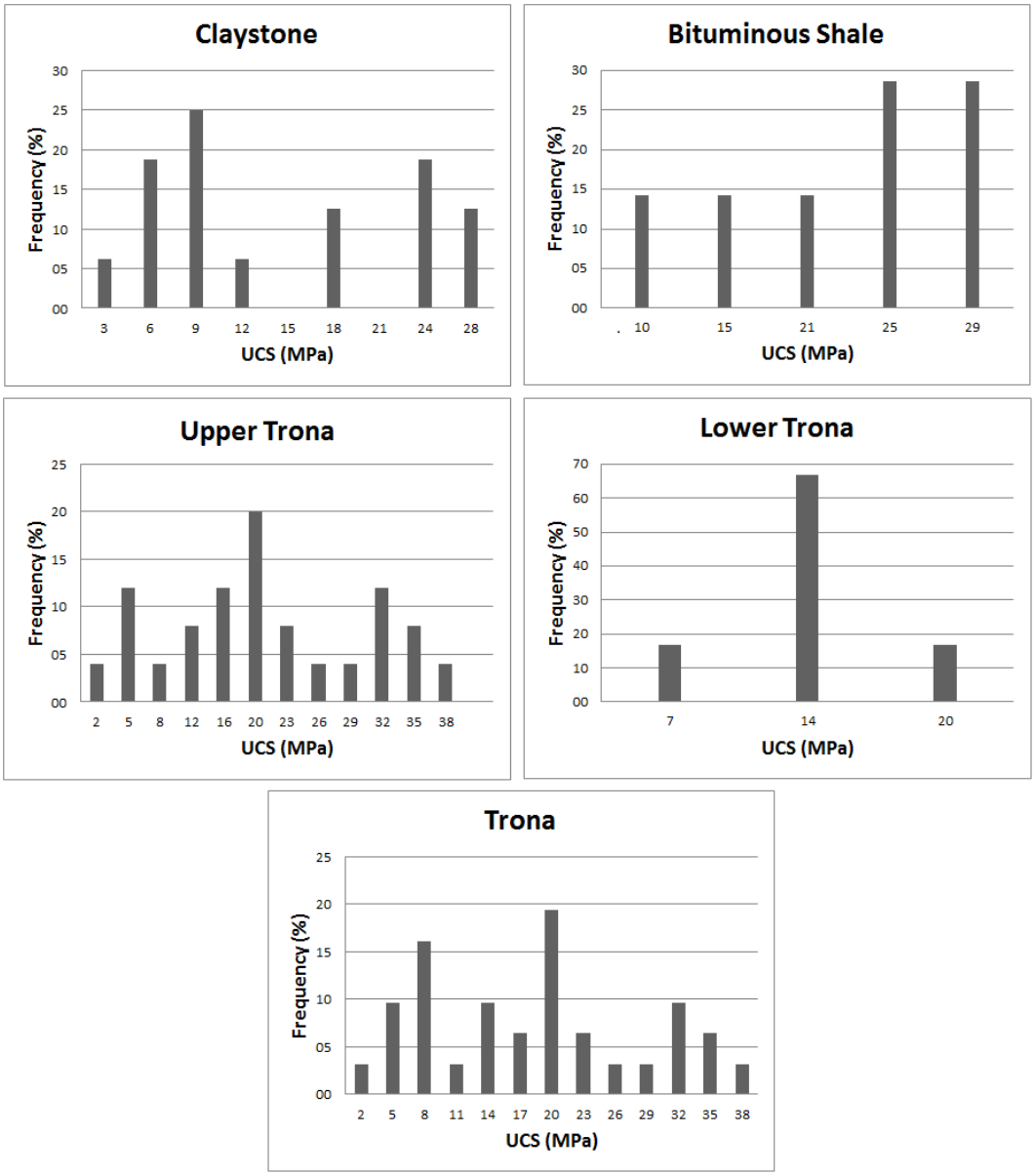

Figure 3-9 Histogram Showing Distribution of UCS Values of Lithological Units

3.4 Matching Drillhole Intervals Used in PL and UCS Tests

Some of the PL tests were combined for the purpose of matching PL and UCS tests. For example, the figures given in the second row of the Table 3-2 are the results of the PL tests applied on the samples 40 and 42 from AGA-4 drillhole. Since the From - To values of these tests and those of the UCS sample no 375, which is given in the second row of the Table 3-6, are close to each other, these tests are considered as a pair and

matched. Accordingly, in order to match 2 PL tests and 1 UCS test, results obtained from the PL tests applied on the specimens 40 and 42 were averaged and these 2 specimens were considered as 1 specimen. All PL and UCS tests that are close to each other as per their From - To values were matched and results from these tests were analyzed. For simplicity a "Matching Code", which can be seen in the last columns of Table 3-2, Table 3-3, Table 3-4, Table 3-6, Table 3-7 and Table 3-8, was assigned for each matching pair and the test pairs were created based on these codes. Data belonging to the test pairs that were matched based on the said matching codes are given in these tables.

3.5 Outlier Detection

Outliers are the extreme values which are not compatible with the other values in a data set. If there are too many outliers in a data set, this will cause the data set to deviate from normal distribution and statistical analyses to be negatively affected. For this reason outlier values should be detected and managed accordingly.

The "box plot" outlier detection method was used to determine whether there is an outlier within the results of the PL and UCS tests analyzed within the scope of this study or not. In this method, the first quartile (Q1) and the third quartile (Q3) of the data are calculated and the first quartile is subtracted from the third quartile in order to calculate the interquartile (IQR) value. IQR value is multiplied by 1.5, which is a constant found as a result of empirical studies. The value of 1.5*IQR is subtracted from Q1 to find the lower fence and added to the Q3 to find upper fence. Any data, which is below the lower fence and above the upper fence, is called as an outlier.

Lithological units for which the tests were carried out were considered as follows:

1. Claystone
2. Bituminous shale
3. Claystone + Bituminous shale
4. Upper trona

5. Lower trona
6. Upper + Lower trona

Median values as well as the first and the third quartiles were separately calculated for PL and UCS tests for each of the abovementioned lithological classifications and lower and upper fence limits were determined by using these parameters. Outlier detection parameters were summarized for PL tests in Table 3-10 and for UCS tests in Table 3-11.

Table 3-10 Outlier Detection for PL Tests

Parameter	**CS**	**BS**	**CS + BS**	**UT**	**LT**	**T (UT + LT)**
Q1	0.4177	0.5886	0.4258	0.6464	0.5510	0.6269
Q2, median	0.5693	0.6788	0.6372	1.2209	0.6828	1.0781
Q3	1.0147	1.0077	1.0077	1.8077	1.1328	1.7883
IQR	0.5970	0.4191	0.5819	1.1613	0.5818	1.1614
IQR * 1.5	0.8955	0.6286	0.8729	1.7419	0.8727	1.7420
Lower fence	-0.4777	-0.0400	-0.4471	-1.0954	-0.3218	-1.1151
Upper fence	1.9102	1.6363	1.8806	3.5496	2.0055	3.5303

Table 3-11 Outlier Detection for UCS Tests

Parameter	**CS**	**BS**	**CS + BS**	**UT**	**LT**	**T (UT + LT)**
Q1	5.4674	11.7350	6.9000	11.3018	7.1249	7.3153
Q2, median	10.3970	21.5600	15.0679	18.8981	7.3217	18.0000
Q3	22.4765	28.1400	22.5764	29.0667	10.8698	25.3000
IQR	17.0090	16.4050	15.6764	17.7649	3.7448	17.9847
IQR * 1.5	25.5136	24.6076	23.5146	26.6474	5.6173	26.9770
Lower fence	-20.0461	-12.8726	-16.6146	-15.3456	1.5077	-19.6617
Upper fence	47.9900	52.7476	46.0910	55.7141	16.4870	52.2770

According to the box plot method for outlier detection, values below lower limit and those above upper limit are deemed as outlier. Data given in Table 3-12 through Table 3-17 are the PL (I_{S50}) and UCS test results in terms of MPa and these data were compared with the lower and upper limits that were highlighted in gray in Table 3-10 and Table 3-11 above. Outlier statuses of the data are also stated in Table 3-12 through Table 3-17. In addition, these tables were also used for analyzing PL and UCS tests in Section 3.6.1 through 3.6.6.

Table 3-12 PL and UCS Test Results for Claystone

No	Hole ID	Average Corrected PL Index $I_{s(50)}$ (MPa)	Outlier?	UCS (MPa)	Outlier?	Matching Code
1	AGA-4	0.483	not	12.00	not	C-M1
2	AGA-4	0.426	not	6.90	not	C-M2
3	GT-1	0.637	not	22.53	not	C-M3
4	GT-1	1.024	not	8.07	not	C-M4
5	GT-1	0.218	not	4.81	not	C-M5
6	GT-1	0.325	not	2.88	not	C-M6
7	GT-2	0.511	not	6.61	not	C-M7
8	GT-2	0.627	not	3.80	not	C-M8
9	GT-2	0.415	not	5.09	not	C-M9
10	GT-2	0.344	not	8.79	not	C-M10
11	GT-2	0.481	not	15.11	not	C-M11
12	GT-2	0.927	not	22.58	not	C-M12
13	GT-2	1.400	not	24.46	not	C-M13
14	GT-2	0.985	not	27.69	not	C-M14
15	GT-2	1.530	not	22.32	not	C-M15
16	GT-2	1.274	not	15.07	not	C-M16

Table 3-13 PL and UCS Test Results for Bituminous Shale

No	Hole ID	Average Corrected PL Index $I_{s(50)}$ (MPa)	Outlier?	UCS (MPa)	Outlier?	Matching Code
1	GT-1	0.679	not	20.18	not	B-M1
2	GT-1	1.008	not	28.44	not	B-M2
3	GT-2	0.918	not	28.14	not	B-M3
4	GT-2	0.589	not	21.56	not	B-M4
5	GT-2	0.674	not	11.73	not	B-M5
6	GT-2	1.106	not	24.61	not	B-M6
7	GT-2	0.130	not	9.37	not	B-M7

Table 3-14 PL and UCS Test Results for Claystone and Bituminous Shale

No	Hole ID	Average Corrected PL Index $I_{s(50)}$ (MPa)	Outlier?	UCS (MPa)	Outlier?	Matching Code
1	AGA-4	0.483	not	12.00	not	C-M1
2	AGA-4	0.426	not	6.90	not	C-M2
3	GT-1	0.637	not	22.53	not	C-M3
4	GT-1	1.025	not	8.07	not	C-M4
5	GT-1	0.218	not	4.81	not	C-M5
6	GT-1	0.325	not	2.88	not	C-M6
7	GT-2	0.511	not	6.61	not	C-M7
8	GT-2	0.627	not	3.80	not	C-M8
9	GT-2	0.415	not	5.09	not	C-M9
10	GT-2	0.345	not	8.79	not	C-M10
11	GT-2	0.482	not	15.11	not	C-M11
12	GT-2	0.927	not	22.58	not	C-M12
13	GT-2	1.400	not	24.46	not	C-M13
14	GT-2	0.985	not	27.69	not	C-M14
15	GT-2	1.530	not	22.32	not	C-M15
16	GT-2	1.274	not	15.07	not	C-M16
17	GT-1	0.679	not	20.18	not	B-M1
18	GT-1	1.008	not	28.44	not	B-M2
19	GT-2	0.918	not	28.14	not	B-M3
20	GT-2	0.589	not	21.56	not	B-M4
21	GT-2	0.674	not	11.73	not	B-M5
22	GT-2	1.106	not	24.61	not	B-M6
23	GT-2	0.130	not	9.37	not	B-M7

Table 3-15 PL and UCS Test Results for Upper Trona

No	Hole ID	Average Corrected PL Index $I_{s(50)}$ (MPa)	Outlier?	UCS (MPa)	Outlier?	Matching Code
1	AGA-4	1.083	not	22.60	not	UT-M1
2	AGA-4	1.301	not	25.30	not	UT-M2
3	AGA-4	1.695	not	30.70	not	UT-M3
4	AGA-4	0.436	not	3.30	not	UT-M4
5	AGA-4	0.581	not	1.80	not	UT-M5
6	AGA-4	0.614	not	19.50	not	UT-M6
7	AGA-4	0.597	not	6.40	not	UT-M7
8	AGA-4	0.763	not	19.50	not	UT-M8
9	AGA-4	1.587	not	18.00	not	UT-M9
10	AGA-4	1.867	not	32.00	not	UT-M10
11	GT-1	1.969	not	33.20	not	UT-M11
12	GT-1	1.618	not	11.17	not	UT-M12
13	GT-1	1.846	not	15.45	not	UT-M13
14	GT-1	0.377	not	3.89	not	UT-M14
15	GT-1	0.684	not	11.43	not	UT-M15
16	GT-1	1.497	not	28.19	not	UT-M16
17	GT-1	2.545	not	35.79	not	UT-M17
18	GT-2	0.741	not	14.35	not	UT-M18
19	GT-2	1.788	not	18.90	not	UT-M19
20	GT-2	0.630	not	18.61	not	UT-M20
21	GT-2	1.221	not	12.30	not	UT-M21
22	GT-2	0.663	not	3.09	not	UT-M22
23	GT-2	1.827	not	32.48	not	UT-M23
24	GT-2	2.751	not	29.95	not	UT-M24
25	GT-2	1.078	not	22.40	not	UT-M25

Table 3-16 PL and UCS Test Results for Lower Trona

No	Hole ID	Average Corrected PL Index $I_{s(50)}$ (MPa)	Outlier?	UCS (MPa)	Outlier?	Matching Code
1	GT-2	0.777	not	7.33	not	LT-M26
2	GT-2	0.607	not	8.27	not	LT-M27
3	GT-2	0.627	not	6.90	not	LT-M28
4	GT-2	0.739	not	7.32	not	LT-M29
5	GT-2	0.382	not	7.20	not	LT-M30
6	GT-2	2.199	outlier	18.67	outlier	LT-M31

Table 3-17 PL and UCS Test Results for Trona (Upper and Lower)

No	Hole ID	Average Corrected PL Index $I_{s(50)}$ (MPa)	Outlier?	UCS (MPa)	Outlier?	Matching Code
1	AGA-4	1.083	not	22.60	not	UT-M1
2	AGA-4	1.301	not	25.30	not	UT-M2
3	AGA-4	1.695	not	30.70	not	UT-M3
4	AGA-4	0.436	not	3.30	not	UT-M4
5	AGA-4	0.581	not	1.80	not	UT-M5
6	AGA-4	0.614	not	19.50	not	UT-M6
7	AGA-4	0.597	not	6.40	not	UT-M7
8	AGA-4	0.763	not	19.50	not	UT-M8
9	AGA-4	1.587	not	18.00	not	UT-M9
10	AGA-4	1.867	not	32.00	not	UT-M10
11	GT-1	1.969	not	33.20	not	UT-M11
12	GT-1	1.618	not	11.17	not	UT-M12
13	GT-1	1.846	not	15.45	not	UT-M13
14	GT-1	0.377	not	3.89	not	UT-M14
15	GT-1	0.684	not	11.43	not	UT-M15
16	GT-1	1.497	not	28.19	not	UT-M16
17	GT-1	2.545	not	35.79	not	UT-M17
18	GT-2	0.741	not	14.35	not	UT-M18
19	GT-2	1.788	not	18.90	not	UT-M19
20	GT-2	0.630	not	18.61	not	UT-M20
21	GT-2	1.221	not	12.30	not	UT-M21
22	GT-2	0.663	not	3.09	not	UT-M22
23	GT-2	1.827	not	32.48	not	UT-M23
24	GT-2	2.751	not	29.95	not	UT-M24
25	GT-2	1.078	not	22.40	not	UT-M25
26	GT-2	0.777	not	7.33	not	LT-M26
27	GT-2	0.607	not	8.27	not	LT-M27
28	GT-2	0.627	not	6.90	not	LT-M28
29	GT-2	0.739	not	7.32	not	LT-M29
30	GT-2	0.382	not	7.20	not	LT-M30
31	GT-2	2.199	not	18.67	not	LT-M31

When the results for PL and UCS tests, which are given in Table 3-12 through Table 3-17, are compared to the lower and upper limits, which are highlighted in gray in Table 3-10 and Table 3-11 above, I_{S50} and UCS values of the 6th test given in Table 3-16 for lower trona are deemed as outlier. These rows are also highlighted in gray in the said table.

It is not a good approach to exclude an outlier from the data set only by considering it from a mathematical and/or statistical point of view. First of all, the factors that make a value be an outlier should be investigated. The first thing to do is to investigate whether a mistake was made during data entry stage or not. When this was investigated, it was understood that these data are not wrong. Secondly, the tests (observations) generating these values should be investigated and also it should be ensured that the procedures of the tests are followed. It was determined that the tests stated were duly performed. In the third place it should be investigated that how close the outliers are to lower and upper limit values. I_{S50} = 2.199 and UCS = 18.67 values, which are the results of the 6th test pair given in the table for lower trona, were around the corresponding lithology's upper fence limits, which are 2.055 and 16.487, respectively. Since these results, which are deemed as outlier according to the box plot method, are slightly above the corresponding upper limits, they were not excluded from the data set in order not to cause a data loss.

Consequently, due to the reasons set forth above, no data were excluded from the data set as a result of outlier detection study and statistical analyses were conducted by assuming all of the tests were valid.

3.6 Analyzing PL and UCS Tests

This section presents graphs for the test results, which were obtained from PL and UCS tests applied on the lithological units of claystone, bituminous shale and trona and which were matched in a manner described in Section 3.4. Data were analyzed based on lithological unit classification stated in Table 3-18 and graphs were generated as per the corresponding classifications.

Table 3-18 Lithological Unit Classifications

Lith. Unit No	Lithological Unit	# of Test Pairs Analyzed	Total # of PL Tests	Total # of UCS Tests
1	Claystone	16	151	32
2	Bituminous Shale	7	39	12
3	Claystone + Bituminous Shale	23	190	44
4	Upper Trona	25	55	38
5	Lower Trona	6	32	9
6	Trona	31	87	47
7	All	54	277	91

3.6.1 Analysis of Claystone

The results obtained from the tests, which were applied on the lithological unit of claystone and which were statistically analyzed by being matched with each other, are given in Table 3-12 and the graph is shown in Figure 3-10.

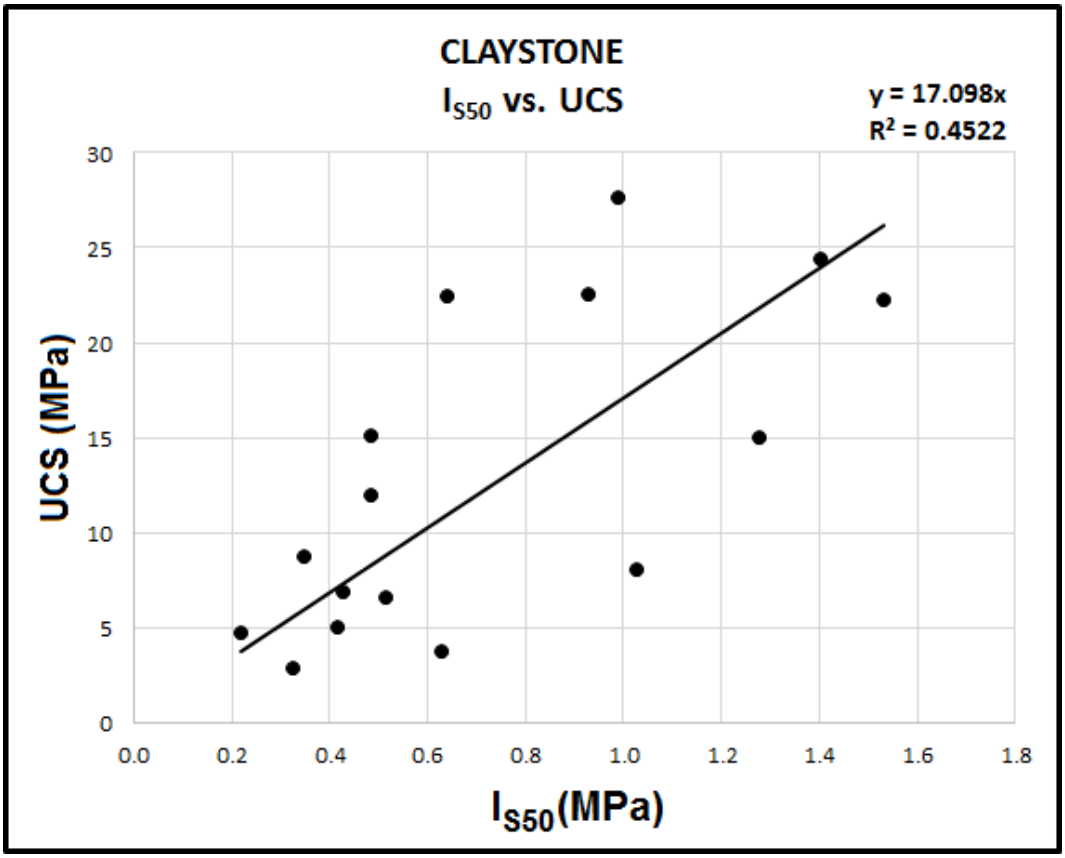

Figure 3-10 PL vs. UCS Graph for Claystone

3.6.2 Analysis of Bituminous Shale

The results obtained from the tests, which were applied on the lithological unit of bituminous shale and which were statistically analyzed by being matched with each other, are given in Table 3-13 and the graph is shown in Figure 3-11.

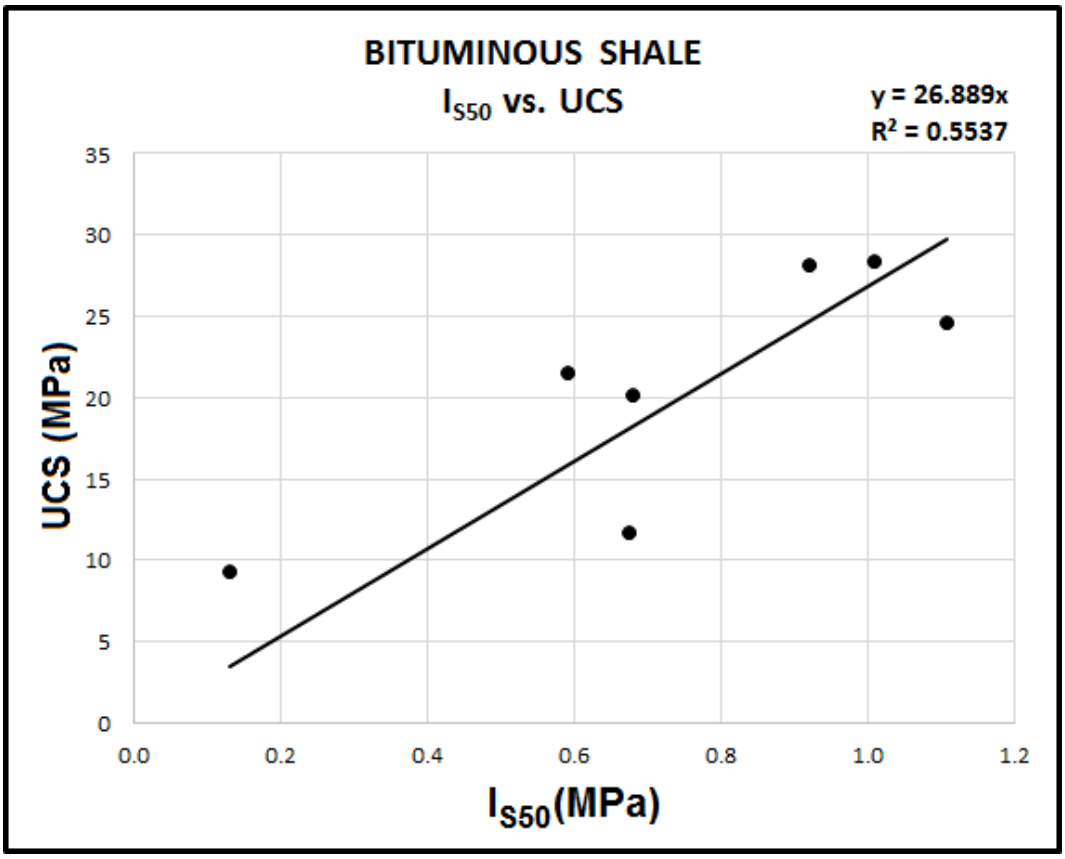

Figure 3-11 PL vs. UCS Graph for Bituminous Shale

3.6.3 Common Analysis of Claystone and Bituminous Shale

The results obtained from the tests, which were applied on the lithological units of claystone and bituminous shale and which were statistically analyzed by being matched with each other, are given in Table 3-14 and the graph is shown in Figure 3-12.

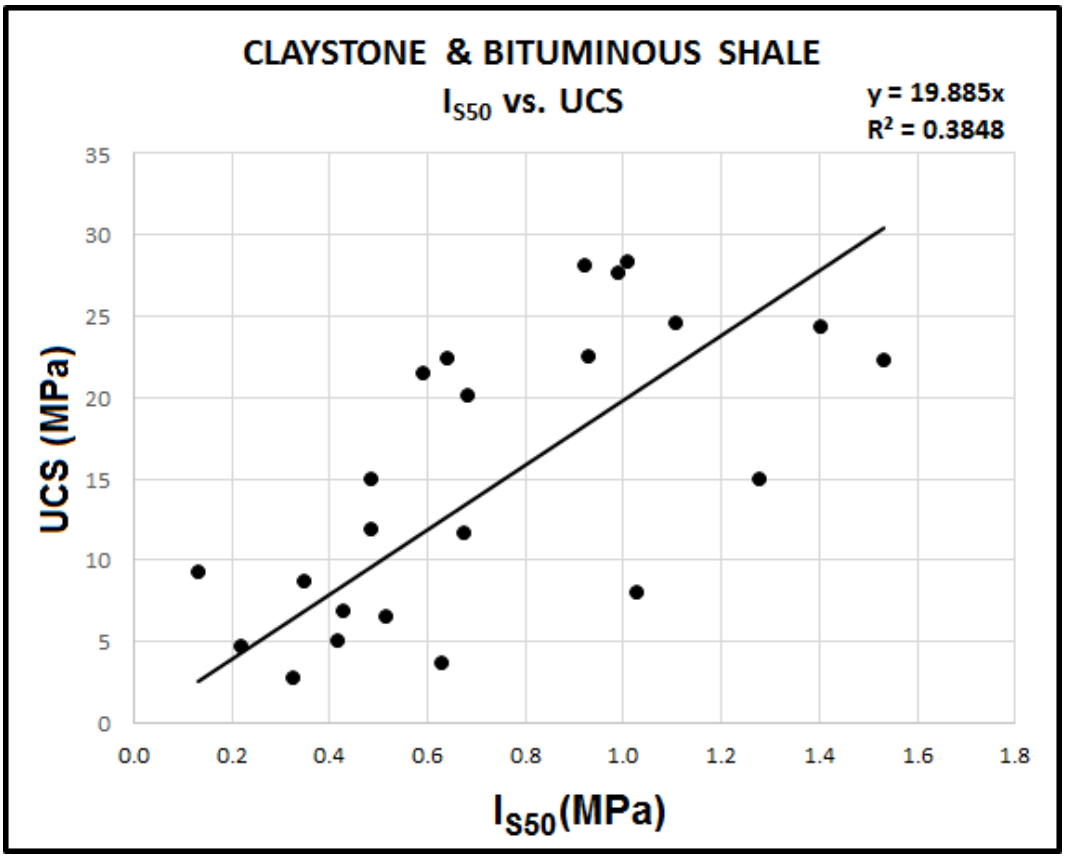

Figure 3-12 PL vs. UCS Graph for Claystone and Bituminous Shale

3.6.4 Analysis of Upper Trona

The results obtained from the tests, which were applied on the lithological unit of upper trona and which were statistically analyzed by being matched with each other, are given in Table 3-15 and the graph is shown in Figure 3-13.

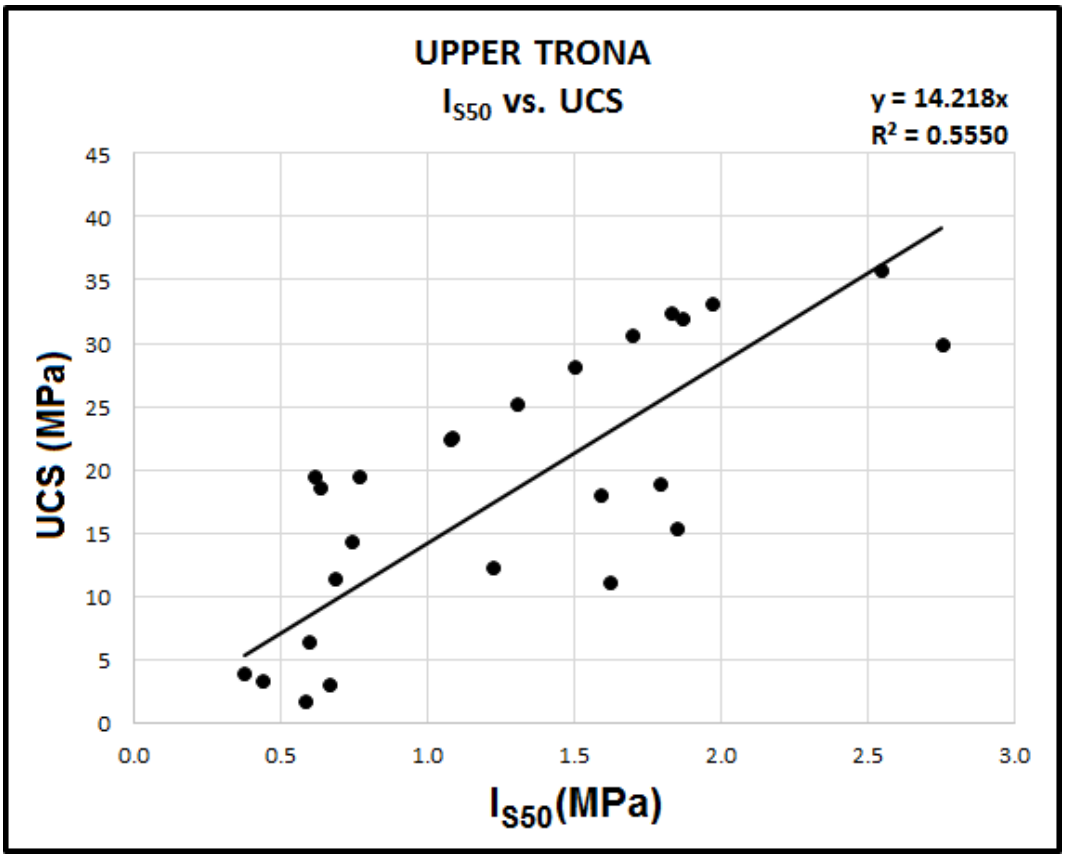

Figure 3-13 PL vs. UCS Graph for Upper Trona

3.6.5 Analysis of Lower Trona

The results obtained from the tests, which were applied on the lithological unit of lower trona and which were statistically analyzed by being matched with each other, are given in Table 3-16 and the graph is shown in Figure 3-14.

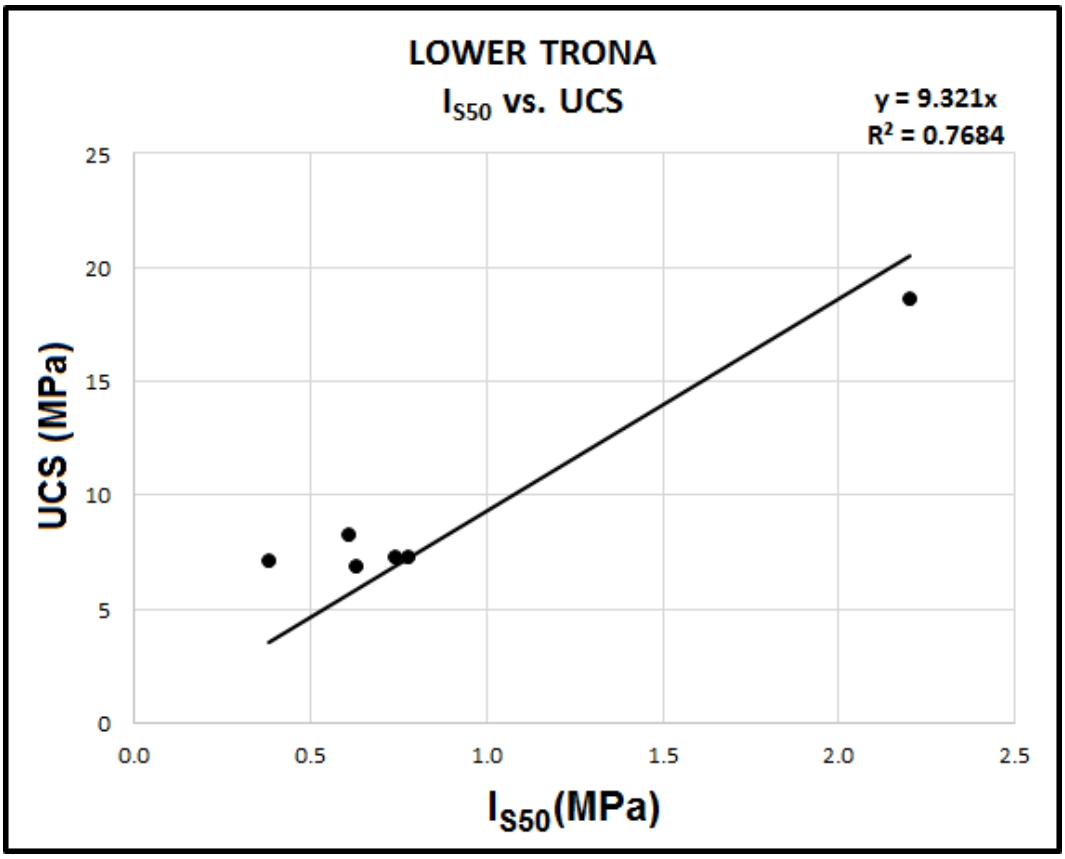

Figure 3-14 PL vs. UCS Graph for Lower Trona

3.6.6 Common Analysis of Upper and Lower Trona

The results obtained from the tests, which were applied on the lithological units of upper and lower trona and which were statistically analyzed by being matched with each other, are given in Table 3-17 and the graph is shown in Figure 3-15.

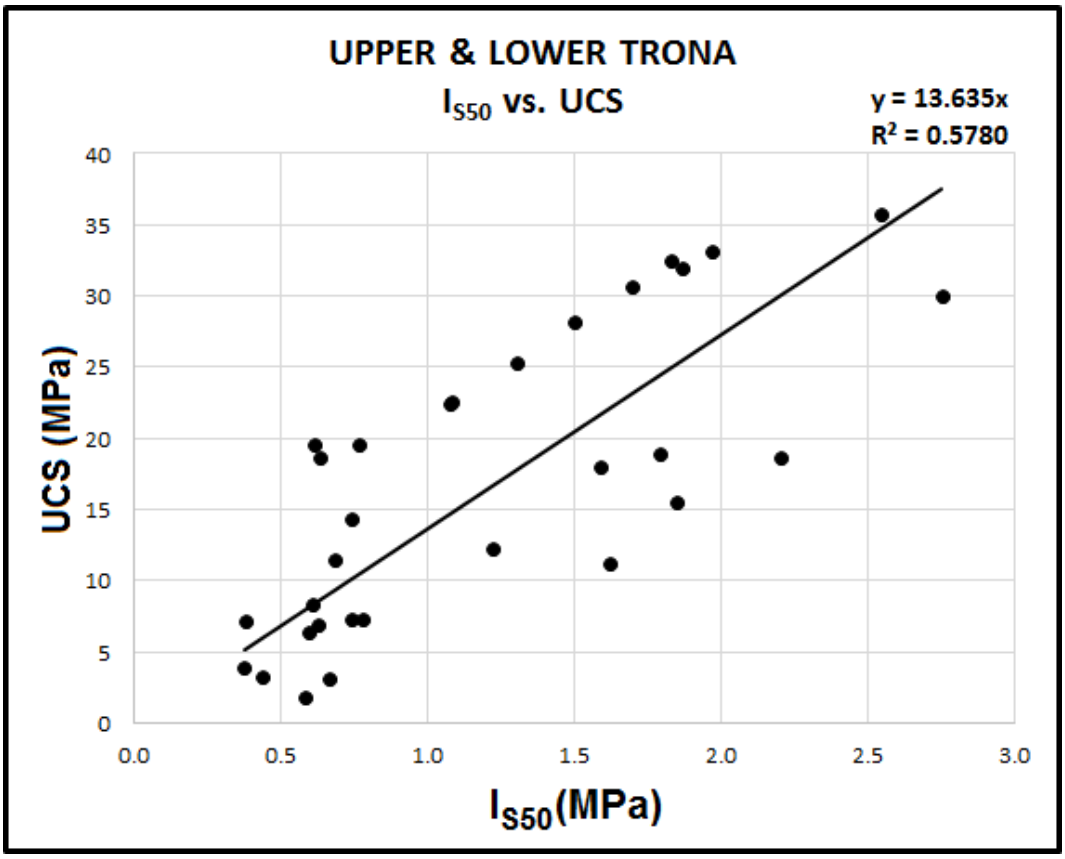

Figure 3-15 PL vs. UCS Graph for Upper and Lower Trona

3.7 Material Properties Obtained by Analyzing the PL and UCS Tests

This section presents a table, which includes the data with respect to the conversion factors and correlation coefficient (R^2) values that were calculated from the graphs given in Sections 3.6.1 through 3.6.6, as well as a comparison of these data to those included in the studies of the other researchers.

Table 3-19 Conversion Factors and Correlation Coefficients

Lithological Unit No	Lithological Unit	# of Test Pairs Analyzed	Correlation Coefficient (R^2)(*)	Conversion Factor(*)
1	CS	16	0.45	17.1
2	BS	7	0.55	26.9
3	CS + BS	23	0.39	19.9
4	UT	25	0.56	14.2
5	LT	6	0.77	9.3
6	T (UT + LT)	31	0.58	13.6

(*) Graphs shown in Figure 3-10 to Figure 3-15 are generated by using "Set Intercept" feature of MS Excel. Since UCS of a specimen is "0.00" when PL is "0.00", Set Intercept value was entered as "0.00". Hence, rather than using the phrase “correlation between PL and UCS”, the phrase “conversion factor” from PL to UCS, which is also a correlation, was used.

The figures under the column “Correlation Coefficient (R^2)” in Table 3-19 are said to be within the range of the figures given in Table 2-1. Correlation coefficients found in the studies of Kahraman (2001) and Mishra and Basu (2013) are relatively high (range from 0.72 to 0.88). This may be explained by considering that these equations are the original equations, which were not forced to pass through the origin. Correlation coefficients given in the study of Vallejo et al. (1989), however, are relatively low (between 0.38 and 0.62) as the data is scattered, and this situation is explained by the small number of tests.

Since the data in this study are also scattered, correlation coefficients are relatively low for sedimentary rocks (between 0.39 and 0.55). Scattered data is caused by specimens’ heterogeneous natures which create anisotropy. Although the lithological units are the same, specimens are not identical and thus they produced different results at the end of the tests.

Conversion factor of 17.1 given in Table 3-19 for claystone, which is a clastic sedimentary rock, is close to those given in the literature for sedimentary rocks (Read et al., 1980). Conversion factor of 26.9 found for bituminous shale is about twice the conversion factors existing in the literature for shale, for example, suggested by Vallejo et al. (1989) as 12.5. This is caused by the relatively soft nature of bituminous shale as compared to shale. Conversion factors of 14.2, 9.3 and 13.6 were calculated for upper trona, lower trona and trona units, respectively, for which there has been no study so far. These conversion factors are the subject matter of this study.

CHAPTER 4

NUMERICAL MODELING

This chapter includes the details of the numerical models constructed for the PL and UCS tests that were highlighted in gray in Table 3-2, Table 3-3, Table 3-4, Table 3-6, Table 3-7 and Table 3-8. A total of 16 PL and 16 UCS tests were numerically modeled within the scope of this study by using 2-dimensional Particle Flow Code (PFC2D, ItascaTM, 2008) software, which is based on Discrete Element Method (DEM). The theory of DEM is discussed in the following section.

4.1 Discrete Element Method (DEM)

DEM was first proposed by Cundall and Strack (1979) and it can be described as a type of modeling, which is used to solve rock and soil mechanics problems by analyzing the motions of and the interaction between circular particles that come together. In addition to existing circular particles, constraining conditions can be constructed by defining walls in DEM. Uniaxial and multi-axial compressing and tensioning simulations can be achieved by defining constant or variable velocity conditions for walls. Balls and the defined walls are in interaction with each other through the forces assigned on interaction points.

This method is generally used for the materials with granular structure. Constructed representative model is comprised of hundreds to thousands small circular particles.

Rock behaves like a cemented granular material of complex-shaped grains in which both the grains and the cement are deformable and may break, and that such a

conceptual model can, in principle, explain all aspects of the mechanical behavior. The bonded-particle model (BPM) for rock directly mimics this system and thus exhibits a rich set of emergent behaviors that correspond very well with those of real rock. The mechanical behavior of rock is governed by the formation, growth and eventual interaction of microcracks (Potyondy & Cundall, 2004).

According to the literature, numerical simulations are generally based on rock mass, which is heterogeneous in nature due to random micro discontinuities like fractures or voids between the grains. Particle Flow Code (PFC) can overcome this problem. PFC is based on DEM proposed by Cundall and Strack (1979). Two elements called walls and particles are required only to generate a model in PFC. The contact model, the contact bond model and the parallel bond model are the common contact models that are available in PFC and the parallel bond model was used in this study. A contact model can be explained as a pair of elastic springs with constant normal and shear stiffness acting at a point. Therefore, it cannot resist a moment. The parallel bond model assumes an elastic interaction between particles that act in parallel with the slip or contact bond models. For the parallel bond, bonding is activated over a finite area, thus it can resist a moment (Figure 4-1).

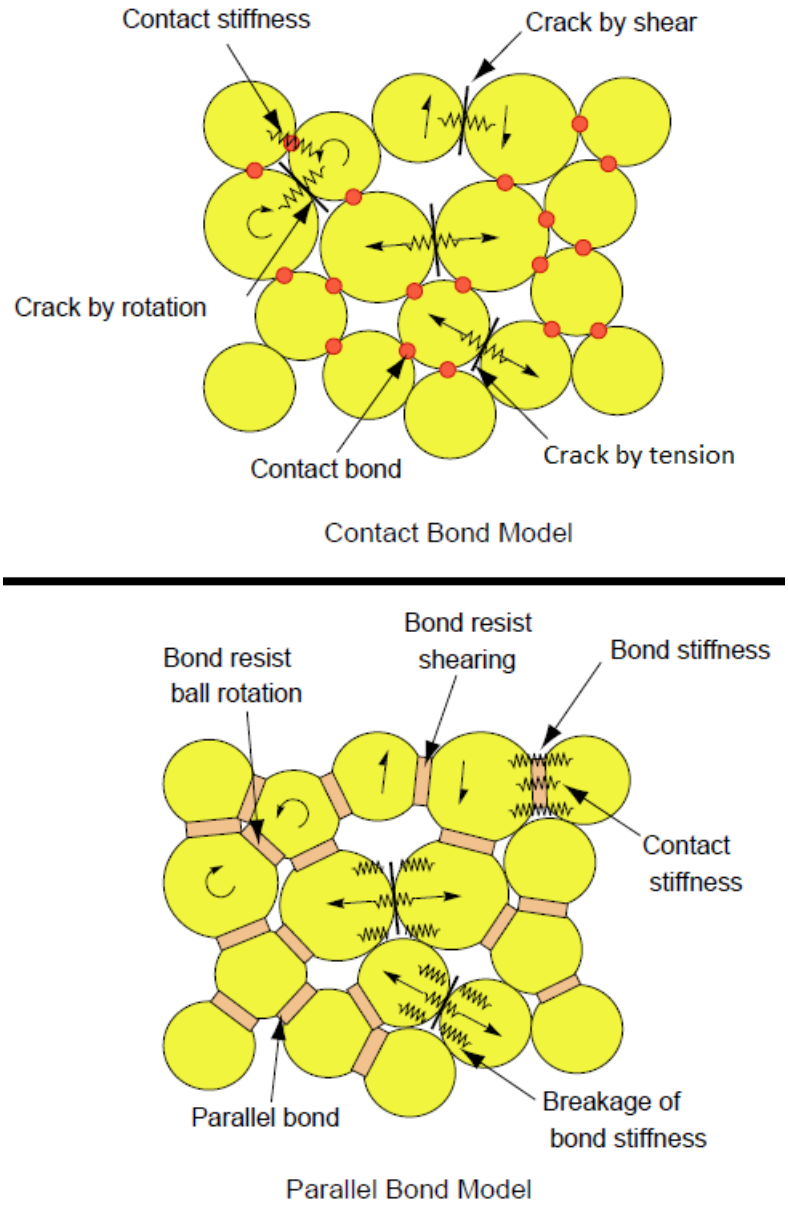

Figure 4-1 Illustration of Bond Models Provided in PFC (Cho et al., 2007)

Selection of micro properties is the most important step in modeling with PFC. The phenomena observed in laboratory are simulated by calibrating the micro-mechanical properties of the models by using UCS tests as well as direct tension tests. In PFC, the BPM with parallel bonds are treated as a set of elastic springs with limited shear and tensile strengths as well as rotation constraints. Two particles are well connected and locked with low interlocking force.

PFC software basically constructs model for finite displacements and rotation of discrete objects in a manner to include total separation. Newton's Second Law of Motion and the procedure of explicit finite element differential are used in each time interval. Equation of motion is automatically arranged for local conditions and it is solved for each step and time interval. In PFC, only two forces and a momentum component exist.

In DEM software, calculations are performed through transitions between Newton's Second Law of Motion and the law of load-displacement. While Newton's Second Law of Motion defines motion of each particle by using contact forces and body forces between particles, load-displacement law is used to update relative motion of each contact point. For the walls defined in the software, only the law of load-displacement is used to identify the contact between ball and wall.

In DEM software, interaction between particles is a dynamic process until internal forces reach equilibrium. Contact forces and displacements observed in the particles under loading are determined by monitoring each particle's motion. As disturbance within the particle system spreads, particles start to move. Factors affecting this spread are defined walls, motions of particles and/or body forces.

As stated in the user's guide of PFC (Itasca, 2008), dynamic behavior is numerically represented by assuming that velocity and acceleration values are constant in each time step. In the beginning of time interval, contact sets are renewed according to locations of walls and known particles. Contact forces, which are based on relative velocities of particles, are updated by immediately applying the law of force-displacement on each contact. Afterwards, the moment value, which is arising out of particle's velocity, resultant force based on particle's location and contact and body forces acting on particle, is updated by applying law of motion on each particle. Additionally, wall locations are updated according to the wall velocities (Figure 4-2).

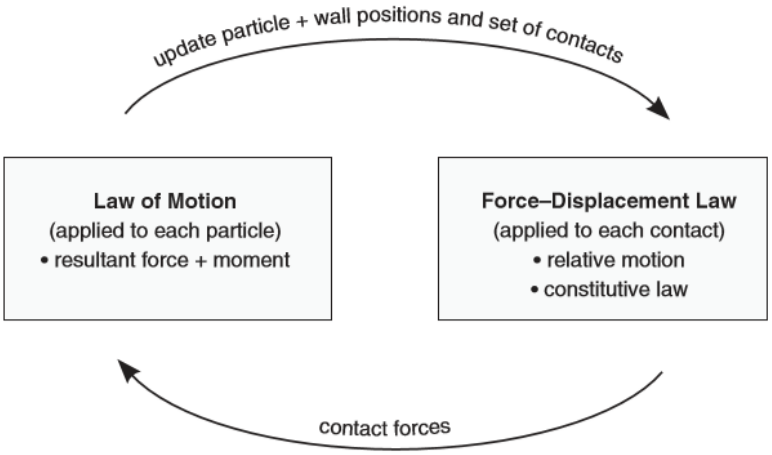

Figure 4-2 Calculation Cycle in PFC (Itasca, 2008)

It was propounded in the study carried out by Potyondy and Cundall (2004) that it is possible to model mechanical behavior of rocks by assuming that rocks are formed by particles and bonding material (deformable, breakable). Since the BPM enables this conceptual model, it can be used to simulate mechanical behaviors of rocks.

BPM enables user to generate models for model contacts and bonds at the micro feature level by taking Newton's Second Law of Motion into consideration. By this method, micro features can be determined by using bond failures, shear movements and contact properties.

In this field a lot of different test modeling studies were carried out by using bonded particle model method. Rock, soil and asphalt specimens were modeled in these studies in order to obtain DEM input parameters. In addition to these studies, some researchers performed underground space modeling studies by PFC or coupled with FLAC (Potyondy, 2015) under large-strain mode (since particle positions are updated) by using the corresponding input parameters that they obtained.

PFC software incorporates a coding language called FISH. This code enables user defined functions and features to be added. For example, graphs can be generated for defined variables, special particles can be produced, servo-control feature can be added to test simulations and particle size distributions can be specified in different ways. Moreover, coding software belonging to the study of Potyondy and Cundall is also

included in the FISH library. This function can be used to determine micro and macro parameters that were written on BPM. 5 different laboratory test simulations are present in the existing function (indirect tensile, direct tensile, UCS, TCS and fracture toughness tests can be modeled for simple and complex particle configurations). Within the scope of this study the existing code was used to create UCS specimens and to model UCS tests, but a new routine was developed to create PL specimens and to model PL tests.

4.2 Determining Model Input Parameters

In this section, the details of determining the parameters to be used as input for modeling studies are discussed. Parameters used in modeling studies are the same for UCS and PL tests and they are given below.

4.2.1 Particle Radius

These are the radii of particles, which are assumed to exist in the test specimen and on which the model is based. Microscopic analyses for the lithological units of claystone, bituminous shale and upper trona are present in the detailed geotechnical report prepared by Dokuz Eylül University (DEU, 2001). Hence, detailed particle size determination studies were able to be carried out by using the said microscopic analyses for these lithological units. The same study was carried out for all of the lithological units and the one performed for claystone specimen GT2-698 was described in detailed below, as an example.

Microscopic view given in Figure 4-3 was used for claystone. The length and the width and then the area of the claystone crystal (tct) were determined with the help of the scale in Figure 4-3 and the radius of the equivalent circular particle was calculated. The minimum particle radius for claystone is found as $R_{min} = 2.5x10^{-3}m$.

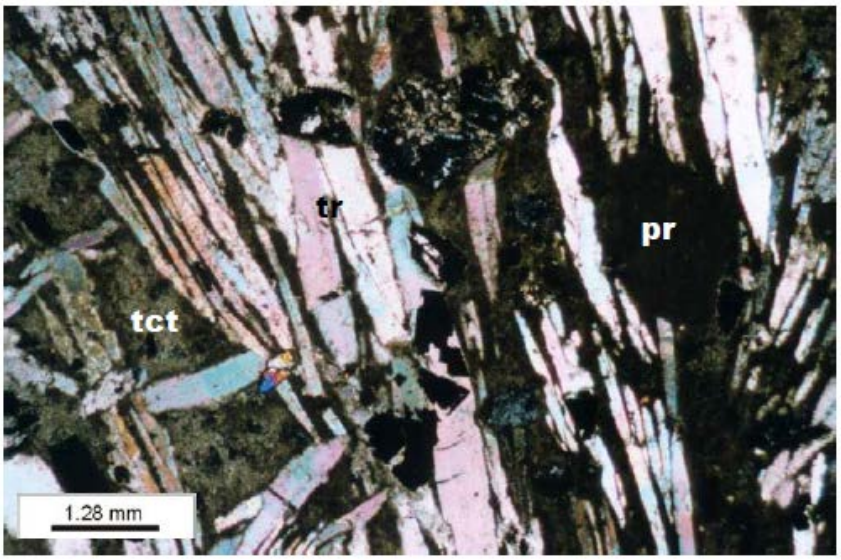

Figure 4-3 Microscopic View for Claystone (tct – tuffitic claystone)

In PFC, ratio of the maximum particle radius to the minimum particle radius is entered and the software normally distributes particle sizes by using this ratio. This ratio was taken as 1.66. In other words, while the minimum particle radius is R_{min} = 2.5x10^{-3}m, the maximum particle radius is calculated as R_{max} = 4.15x10^{-3}m as the ratio is 1.66 and the average particle radius for claystone is R_{ave} = 3.3x10^{-3}m. Claystone specimen GT2-698 has a length of 126.18x10^{-3}m and a width of 61.88x10^{-3}m. 225 particles with the radius of 3.3x10^{-3}m can fit into a specimen having these dimensions. However, Cai (2013) suggested in his modeling study for granular asphalt that the optimum particle size should be around 6,000. In order to carry out a more realistic modeling study, the minimum particle radius was selected as R_{min} = 0.42x10^{-3}m and the ratio of the maximum to minimum radius was taken as 1.66 and the resultant number of particles in the specimen was found as 7327.

This method and also the microscopic views in the geotechnical report of DEU (2001), which were used to determine the particle size of claystone specimen GT2-698, were also used and similar calculations were carried out to determine the particle sizes of bituminous shale (Figure 4-4) and upper trona (Figure 4-5). For UCS tests, calculations and assumptions to determine particle sizes of lithological units are summarized in Table 4-1(a) through (d).

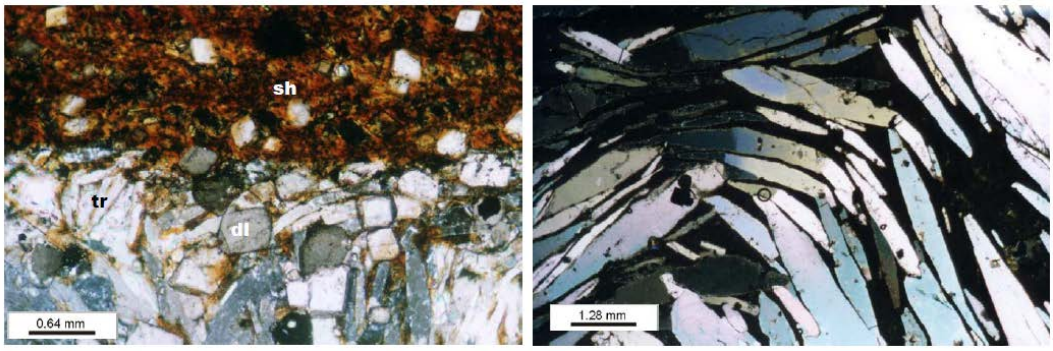

Figure 4-4 Microscopic View for Bituminous Shale (on the left: sh = bituminous shale, on the right: black sections = bituminous shale)

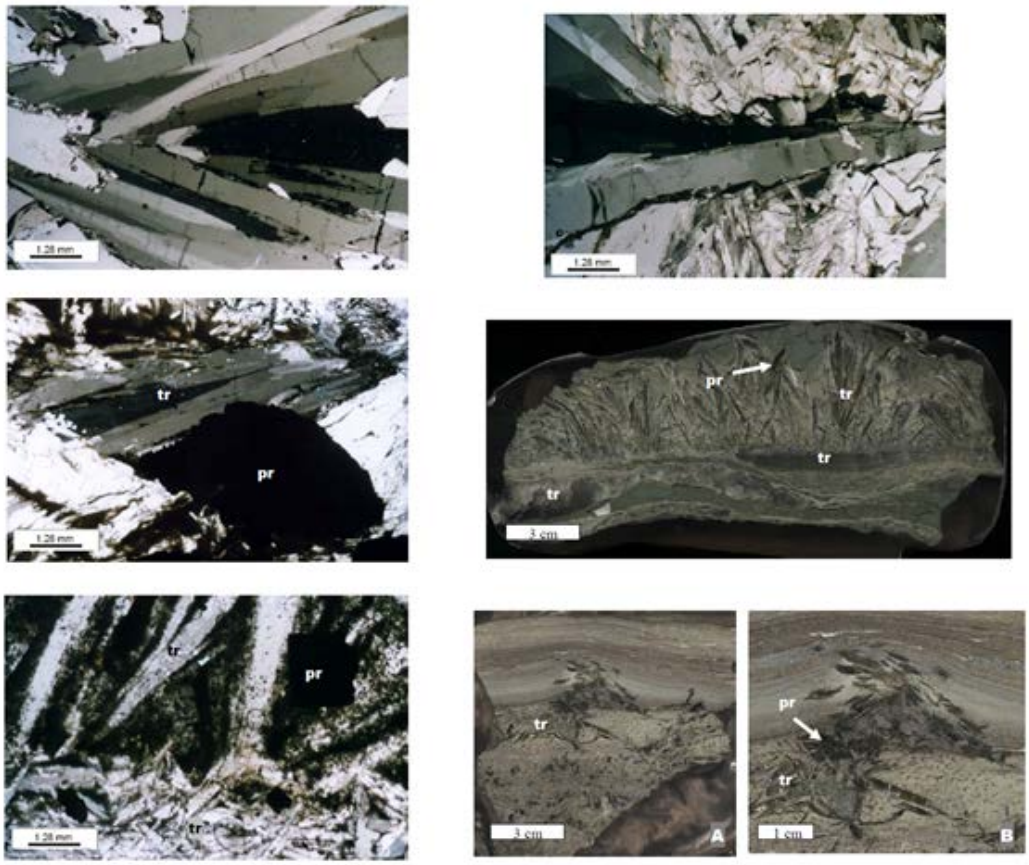

Figure 4-5 Microscopic View for Upper Trona (tr = upper trona)

Since there is no microscopic analysis for lower trona in the geotechnical report, assumptions made for the other three lithological units were also used for lower trona.

Table 4-1 Particle Radius Determination of UCS Tests for (a) Claystone, (b) Bituminous Shale, (c) Upper Trona and (d) Lower Trona Specimens

(a)

No	METU Test Sample No	Calc. R_{min} (mm)	Max / Min Ratio	Calc. R_{max} (mm)	Calc. R_{ave} (mm)	Length of Specimen (mm)	Width of Specimen (mm)	# of Particles	Assumed R_{min} (mm)	# of Particles Based on Assumed R_{min}
1	GT1-904	2.50	1.66	4.15	3.33	131.15	61.80	233	0.42	7080
2	GT1-908	2.50	1.66	4.15	3.33	134.31	62.51	241	0.42	7879
3	GT2-698	2.50	1.66	4.15	3.33	126.18	61.88	225	0.42	7327
4	GT2-712	2.50	1.66	4.15	3.33	107.21	61.92	191	0.42	6230

(b)

No	METU Test Sample No	Calc. R_{min} (mm)	Max / Min Ratio	Calc. R_{max} (mm)	Calc. R_{ave} (mm)	Length of Specimen (mm)	Width of Specimen (mm)	# of Particles	Assumed R_{min} (mm)	# of Particles Based on Assumed R_{min}
5	GT1-855	1.07	1.66	1.78	1.42	130.22	61.78	1269	0.42	7550
6	GT1-860	1.07	1.66	1.78	1.42	128.94	58.77	1196	0.42	7111
7	GT2-657	1.07	1.66	1.78	1.42	131.59	59.59	1237	0.42	7359
8	GT2-659	1.07	1.66	1.78	1.42	106.13	59.37	994	0.42	5913

(c)

No	METU Test Sample No	Calc. R_{min} (mm)	Max / Min Ratio	Calc. R_{max} (mm)	Calc. R_{ave} (mm)	Length of Specimen (mm)	Width of Specimen (mm)	# of Particles	Assumed R_{min} (mm)	# of Particles Based on Assumed R_{min}
9	GT1-874	3.74	1.66	6.21	4.97	129.97	57.70	96	0.42	7038
10	GT1-875	3.74	1.66	6.21	4.97	130.59	59.98	101	0.42	7351
11	GT2-674	3.74	1.66	6.21	4.97	130.43	59.71	100	0.42	7309
12	GT2-679	3.74	1.66	6.21	4.97	131.70	59.74	101	0.42	7383

Table 4-2 Particle Radius Determination of UCS Tests for (a) Claystone, (b) Bituminous Shale, (c) Upper Trona and (d) Lower Trona Specimens (continued)

(d)

No	METU Test Sample No	Calc. R_{min} (mm)	Max / Min Ratio	Calc. R_{max} (mm)	Calc. R_{ave} (mm)	Length of Specimen (mm)	Width of Specimen (mm)	# of Particles	Assumed R_{min} (mm)	# of Particles Based on Assumed R_{min}
13	GT2-708	-	-	-	-	124.97	60.37	-	0.42	7080
14	GT2-719	-	-	-	-	131.57	60.80	-	0.42	7507
15	GT2-723	-	-	-	-	132.21	58.82	-	0.42	7298
16	GT2-733	-	-	-	-	130.50	61.69	-	0.42	7555

The same particle size values were also used for PL modeling studies.

4.2.2 The Rest of the Input Parameters for PFC

The rest of the input parameters for PFC modeling studies are discussed in this section.

- **Platen Positioning Stress**

It is the stress applied before the test in order to fix the test specimen between the platens. 0.1MPa for UCS tests and 100Pa for PL tests were used.

- **Particle Density**

Test specimen's density in terms of kg/m^3 was used.

- **Loading Rate**

Loading rate is a parameter which is determined both for field PL tests and laboratory UCS tests. The study carried out by Kias (2013) on the effect of loading rate on a Bonded Particle Model (BPM) for which UCS tests were performed by using different

loading rates sets forth that loading rate does not have a significant effect on the elastic region of the stress strain curve.

For numerical models constructed in PFC, the parameter of loading rate is set by specifying a value for platen strain rate (PSR) parameter. Güner (2014) performed a study to verify that the loading rate does not have a significant influence on failure load and he constructed 6 different models with PSR values of 0.05, 0.01, 0.50, 1.00, 2.00 and 5.00. It is concluded in the said study that high loading rate (PSR ≥ 5.00) causes higher tensile strength and tensile modulus and that the optimum value for PSR is 1.00 (64E-3m/s)

In the light of these studies and by considering the processing time of the computer, PSR was selected as 1 in this study.

- **Particle Elasticity Modulus**

Test specimen's elasticity modulus in terms of Pa was used. Elasticity modulus is the slope of stress strain curve within the elastic deformation range, which is typically the linear region of the curve. This value is obtained from the stress strain curves plotted as a result of the UCS tests that were carried out in the laboratory.

- **Particle Friction Coefficient**

This coefficient was calculated by taking the tangent of friction angle that was obtained as a result of the triaxial compressive strength test applied on the specimen.

- **Iteration Input Parameters**

All the parameters described above were used as known inputs for each model constructed for lithological units. In addition to these parameters, elasticity modulus and mean normal strength for parallel bonds were used as variable input parameters and

iteration studies were performed by changing these two parameters. Outputs, which are uniaxial compressive strength and elasticity modulus for UCS models and failure load for PL models, were recorded and iterations were continued until the same results of the laboratory UCS (stress-strain curve) and field PL (failure load) tests were obtained.

4.3 Modeling UCS Tests

4 specimens from each lithological unit i.e. in total 16 UCS specimens were modeled within the scope of this study. Modeled tests are highlighted in gray in Table 3-6 for claystone, in Table 3-7 for bituminous shale and in Table 3-8 for trona.

During the modeling process, model input parameters used in iterations were changed in order to obtain the same stress-strain behavior for the specimen as the laboratory test does. Details of model geometry are shown in Figure 4-6. Parameters given in Table 4-2 were used for numerical modeling studies of UCS tests. Iterations were performed by using the PFC's existing code for UCS testing.

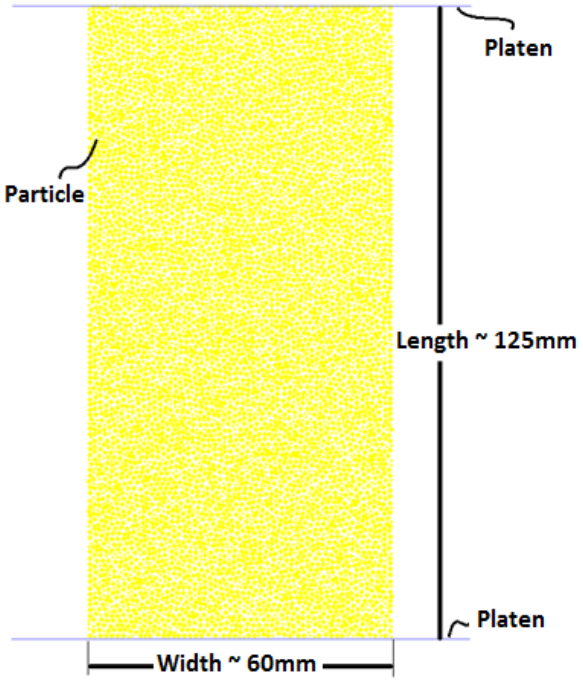

Figure 4-6 Typical Model Geometry in PFC for UCS Test

Table 4-3 Parameters Used For Numerical Modeling Studies of UCS Tests

No	Parameter	Description
1	Particle density (kg/m^3)	Density of specimen in kilograms per cubic meter
2	Particle elasticity modulus (Pa)	Elasticity modulus of specimen in Pascal
3	Particle friction coefficient	Friction coefficient
4	Parallel bond elasticity modulus (Pa)	Parallel bond elasticity modulus in Pascal (iteration input)
5	Parallel bond normal strength (Pa)	Mean normal strength between parallel bonds in Pascal (iteration input)
6	Width of the specimen (m)	Width of specimen in meter
7	Length of the specimen (m)	Length of specimen in meter
8	R_{min} (m) (*)	The minimum particle radius in meter
9	Ratio (*)	Ratio of the maximum particle size to the minimum
10	Initial loading (Pa) (*)	Platen positioning stress in Pascal

(*) Since these values are repeated for each iteration process, they were not given in the individual tables of the numerically modeled specimens. They were given under the corresponding headings in Section 4.2.

As the models are two dimensional (2D), shear strength values used in the parameter input file of PFC software for all of the materials are taken as the same as normal strength values.

4.3.1 Numerical Modeling of UCS Tests for Claystone Specimens

Among the UCS tests performed in the laboratory environment for claystone, the specimens with the number of:

- GT1-904
- GT1-908
- GT2-698 and
- GT2-712

were numerically modeled. Modeling studies for these specimens are discussed in detail in the following sections.

4.3.1.1 Numerical Modeling of UCS Test for CS GT1-904

The parameters given in Table 4-3 were used in this modeling study.

Table 4-4 Parameters of CS GT1-904

No	Parameter	Value
1	Particle density (kg/m^3)	2100
2	Particle elasticity modulus (Pa)	0.85E+09
3	Particle friction coefficient	0.90
4	Parallel bond elasticity modulus (Pa)	Iteration input
5	Parallel bond normal strength (Pa)	Iteration input
6	Width of the specimen (m)	61.80E-03
7	Length of the specimen (m)	131.15E-03

Figure 4-7 shows the status of the specimen GT1-904 before and after the laboratory test.

Figure 4-7 Numerically Modeled CS GT1-904

Figure 4-8 shows the fracture model (red: tension, blue: shear) developed during modeling of claystone specimen GT1-904.

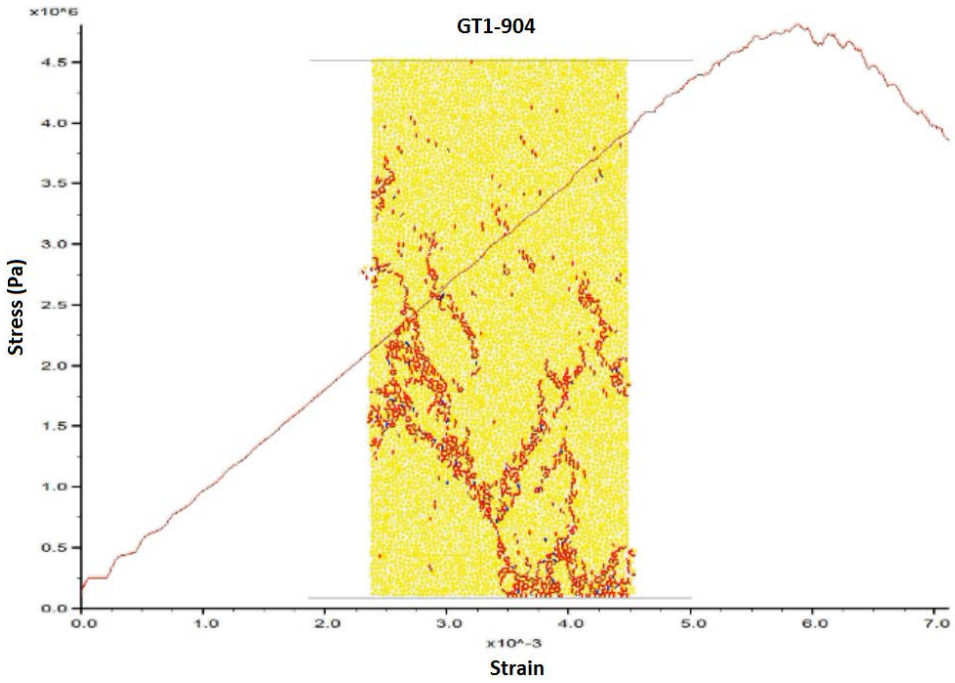

Figure 4-8 PFC Model of CS GT1-904 and Fractures Developed

Stress-strain relationships were obtained both from laboratory tests and numerically modeled tests and the graph given in Figure 4-9 shows these relationships. According to the figure, slope of the curve (Young's Modulus) and the maximum strength (compressive strength) value of the laboratory test and those of the numerically modeled test are the same. Multiple trial and error iterations were completed until reproducing the laboratory stress-strain curve in PFC model. The non-linear portion of the laboratory stress-strain curve is because of closing pre-existing cracks. The same behavior was observed by Yoon (2007). This phenomenon is also observed for the rest of the UCS models.

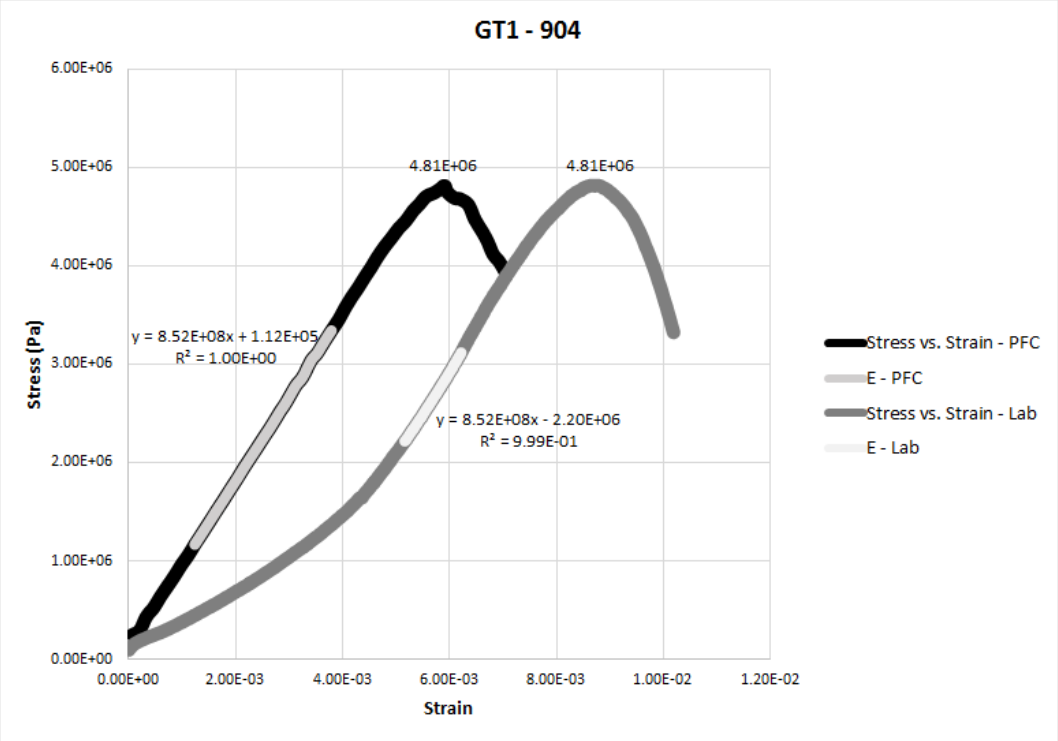

Figure 4-9 Stress-Strain Curves of Lab. Test vs. Modeled Test for CS GT1-904

4.3.1.2 Numerical Modeling of UCS Test for CS GT1-908

The parameters given in Table 4-4 were used in this modeling study.

Table 4-5 Parameters of CS GT1-908

No	Parameter	Value
1	Particle density (kg/m^3)	2050
2	Particle elasticity modulus (Pa)	0.16E+09
3	Particle friction coefficient	0.90
4	Parallel bond elasticity modulus (Pa)	Iteration input
5	Parallel bond normal strength (Pa)	Iteration input
6	Width of the specimen (m)	62.51E-03
7	Length of the specimen (m)	134.31E-03

Figure 4-10 shows the status of the specimen GT1-908 before and after the laboratory test.

Figure 4-10 Numerically Modeled CS GT1-908

Figure 4-11 shows the fracture model (red: tension, blue: shear) developed during modeling of claystone specimen GT1-908.

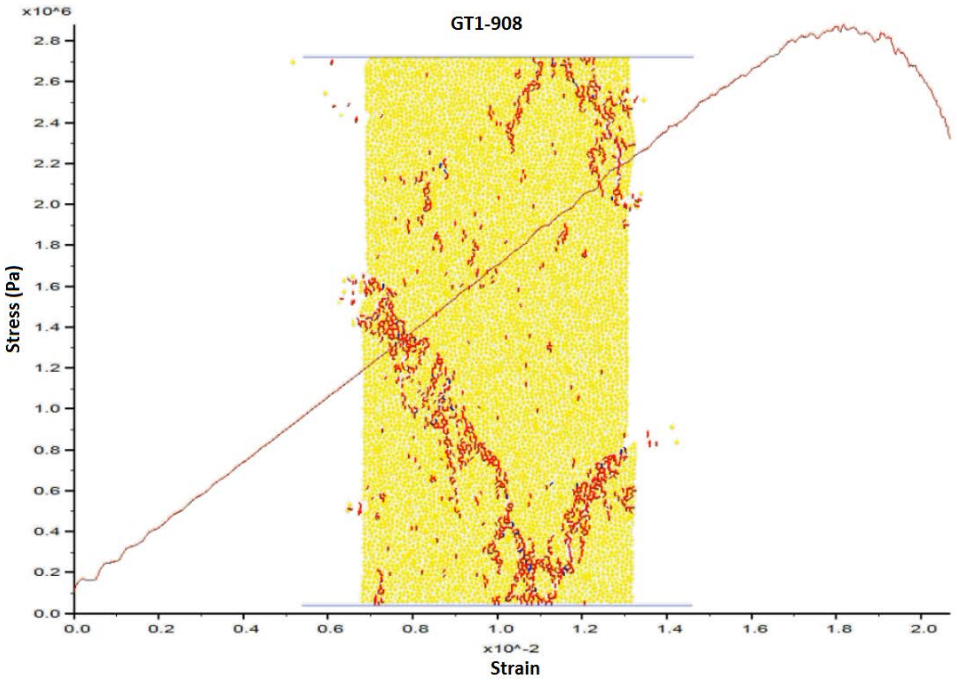

Figure 4-11 PFC Model of CS GT1-908 and Fractures Developed

Stress-strain relationships were obtained both from laboratory tests and numerically modeled tests and the graph given in Figure 4-12 shows these relationships. According to the figure, slope of the curve (Young's Modulus) and the maximum strength (compressive strength) value of the laboratory test and those of the numerically modeled test are the same.

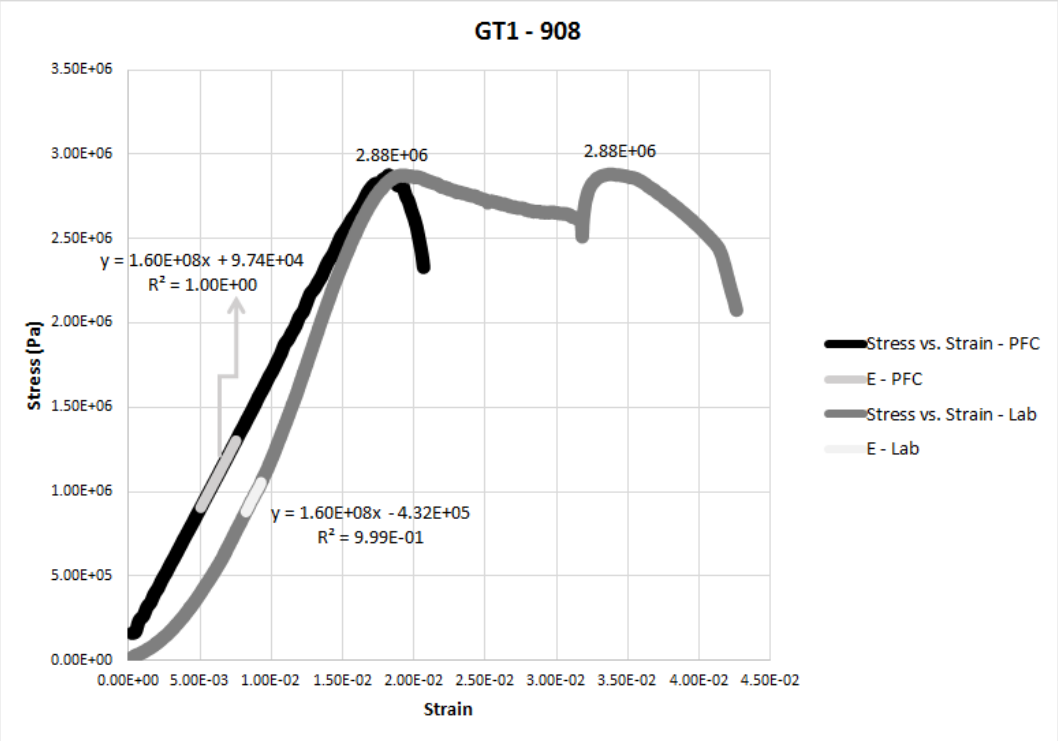

Figure 4-12 Stress-Strain Curves of Lab. Test vs. Modeled Test for CS GT1-908

4.3.1.3 Numerical Modeling of UCS Test for CS GT2-698

The parameters given in Table 4-5 were used in this modeling study.

Table 4-6 Parameters of CS GT2-698

No	Parameter	Value
1	Particle density (kg/m^3)	2130
2	Particle elasticity modulus (Pa)	1.77E+09
3	Particle friction coefficient	0.90
4	Parallel bond elasticity modulus (Pa)	Iteration input
5	Parallel bond normal strength (Pa)	Iteration input
6	Width of the specimen (m)	61.88E-03
7	Length of the specimen (m)	126.18E-03

Figure 4-13 shows the status of the specimen GT2-698 before and after the laboratory test.

Figure 4-13 Numerically Modeled CS GT2-698

Figure 4-14 shows the fracture model (red: tension, blue: shear) developed during modeling of claystone specimen GT2-698.

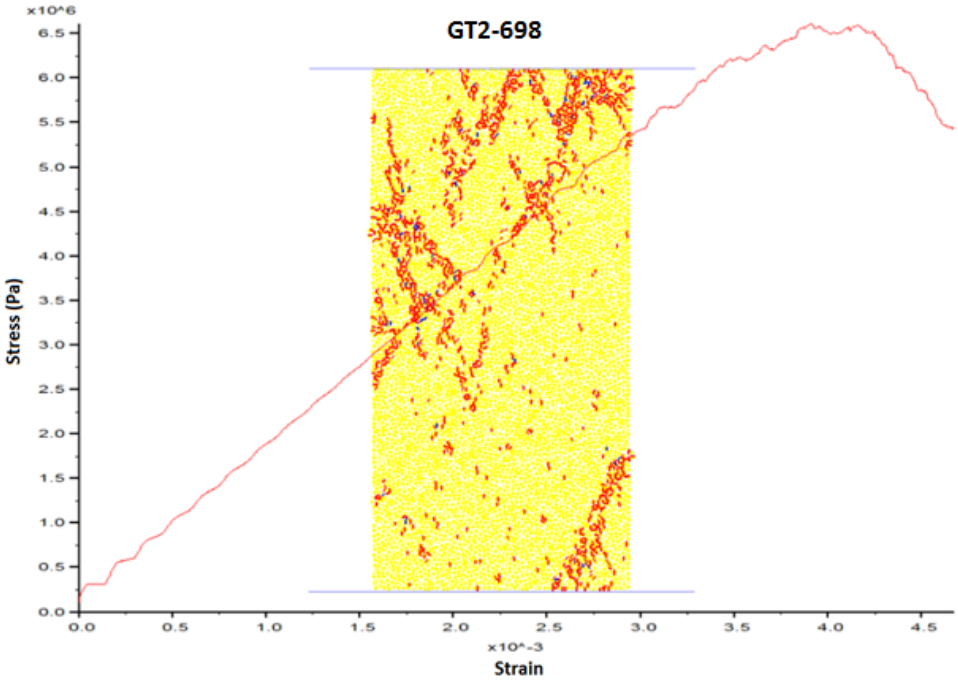

Figure 4-14 PFC Model of CS GT2-698 and Fractures Developed

Stress-strain relationships were obtained both from laboratory tests and numerically modeled tests and the graph given in Figure 4-15 shows these relationships. According to the figure, slope of the curve (Young's Modulus) and the maximum strength (compressive strength) value of the laboratory test and those of the numerically modeled test are the same.

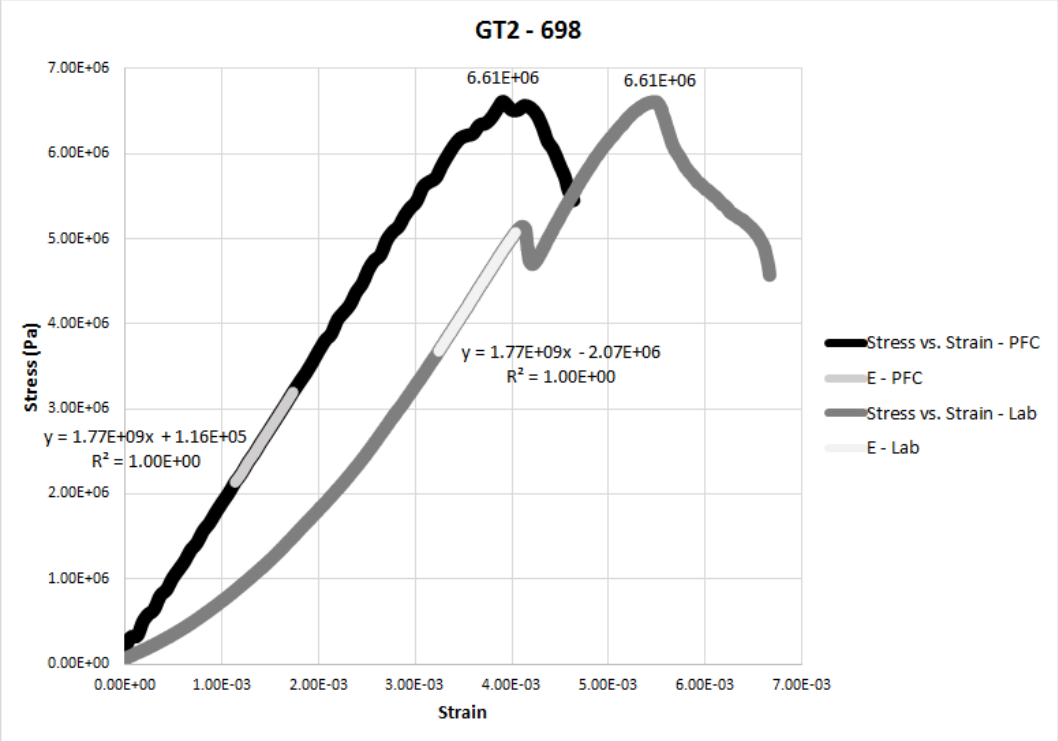

Figure 4-15 Stress-Strain Curves of Lab. Test vs. Modeled Test for CS GT2-698

4.3.1.4 Numerical Modeling of UCS Test for CS GT2-712

The parameters given in Table 4-6 were used in this modeling study.

Table 4-7 Parameters of CS GT2-712

No	Parameter	Value
1	Particle density (kg/m^3)	2030
2	Particle elasticity modulus (Pa)	0.64E+09
3	Particle friction coefficient	1.46
4	Parallel bond elasticity modulus (Pa)	Iteration input
5	Parallel bond normal strength (Pa)	Iteration input
6	Width of the specimen (m)	61.92E-03
7	Length of the specimen (m)	107.21E-03

Figure 4-16 shows the status of the specimen GT2-712 before and after the laboratory test.

Figure 4-16 Numerically Modeled CS GT2-712

Figure 4-17 shows the fracture model (red: tension, blue: shear) developed during modeling of claystone specimen GT2-712.

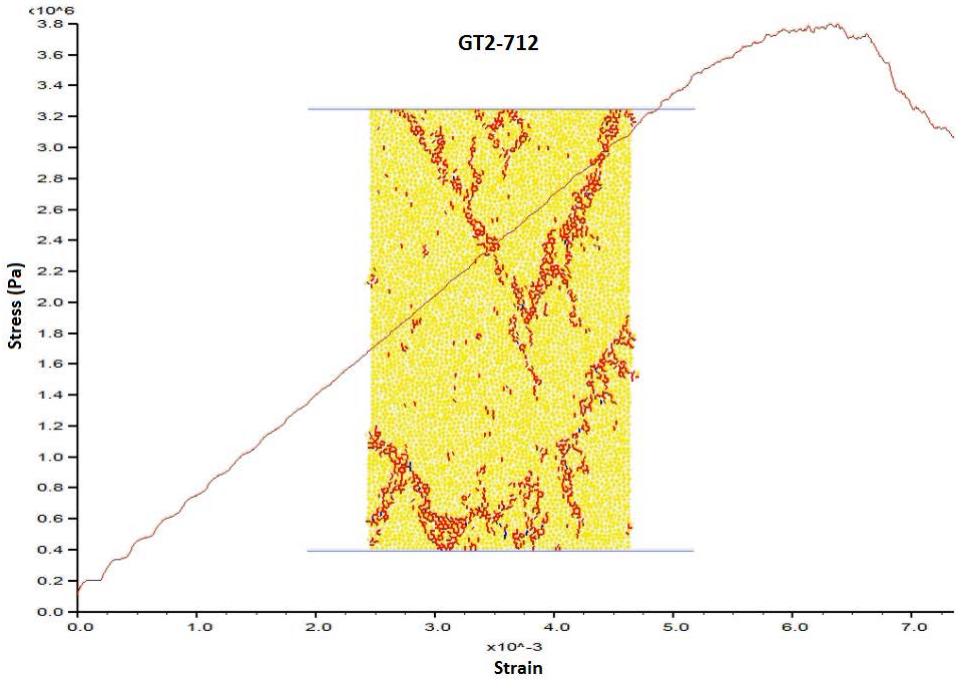

Figure 4-17 PFC Model of CS GT2-712 and Fractures Developed

Stress-strain relationships were obtained both from laboratory tests and numerically modeled tests and the graph given in Figure 4-18 shows these relationships. According

to the figure, slope of the curve (Young's Modulus) and the maximum strength (compressive strength) value of the laboratory test and those of the numerically modeled test are the same.

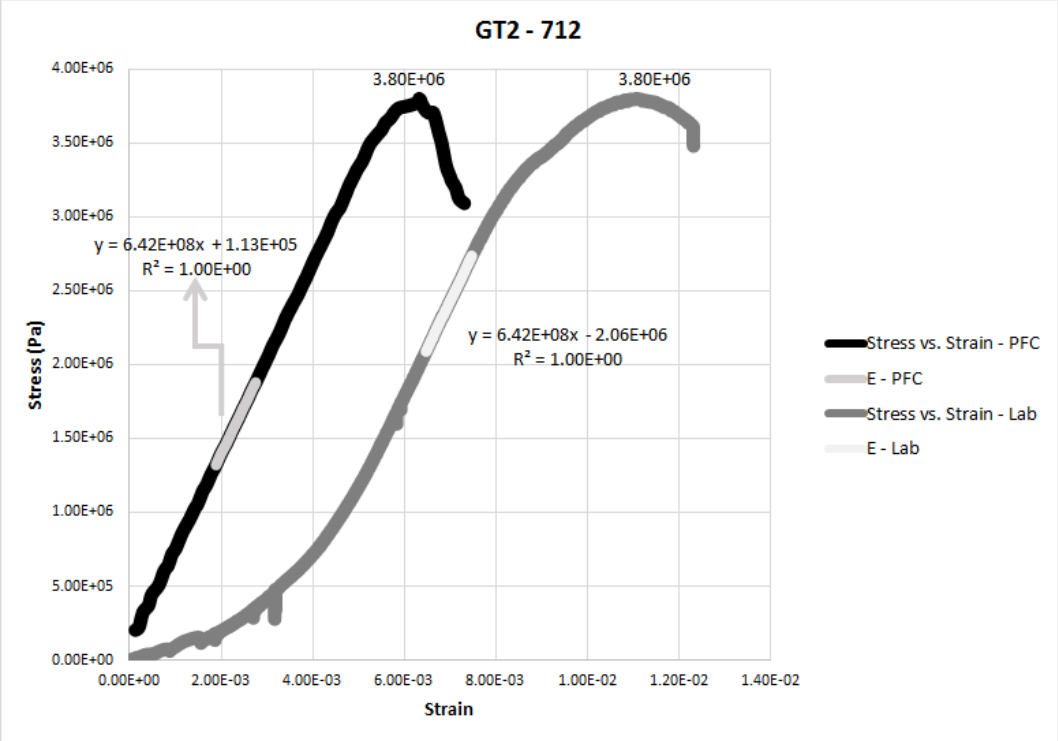

Figure 4-18 Stress-Strain Curves of Lab. Test vs. Modeled Test for CS GT2-712

4.3.2 Numerical Modeling of UCS Tests for Bituminous Shale Specimens

Among the UCS tests performed in the laboratory environment for bituminous shale, the specimens with the number of:

- GT1-855
- GT1-860
- GT2-657 and
- GT2-659

were numerically modeled. Modeling studies for these specimens are discussed in detail in the following sections.

4.3.2.1 Numerical Modeling of UCS Test for BS GT1-855

The parameters given in Table 4-7 were used in this modeling study.

Table 4-8 Parameters of BS GT1-855

No	Parameter	Value
1	Particle density (kg/m^3)	2260
2	Particle elasticity modulus (Pa)	1.77E+09
3	Particle friction coefficient	0.98
4	Parallel bond elasticity modulus (Pa)	Iteration input
5	Parallel bond normal strength (Pa)	Iteration input
6	Width of the specimen (m)	61.78E-03
7	Length of the specimen (m)	130.22E-03

Figure 4-19 shows the status of the specimen GT1-855 before and after the laboratory test.

Figure 4-19 Numerically Modeled BS GT1-855

Figure 4-20 shows the fracture model (red: tension, blue: shear) developed during modeling of bituminous shale specimen GT1-855.

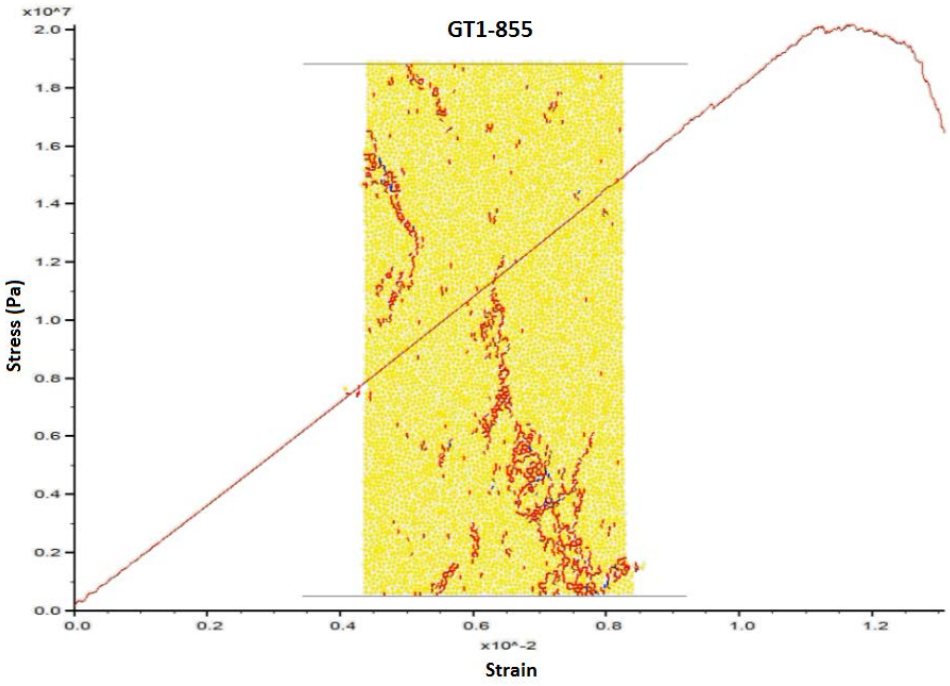

Figure 4-20 PFC Model of BS GT1-855 and Fractures Developed

Stress-strain relationships were obtained both from laboratory tests and numerically modeled tests and the graph given in Figure 4-21 shows these relationships. According to the figure, slope of the curve (Young's Modulus) and the maximum strength (compressive strength) value of laboratory test and those of numerically modeled test are the same.

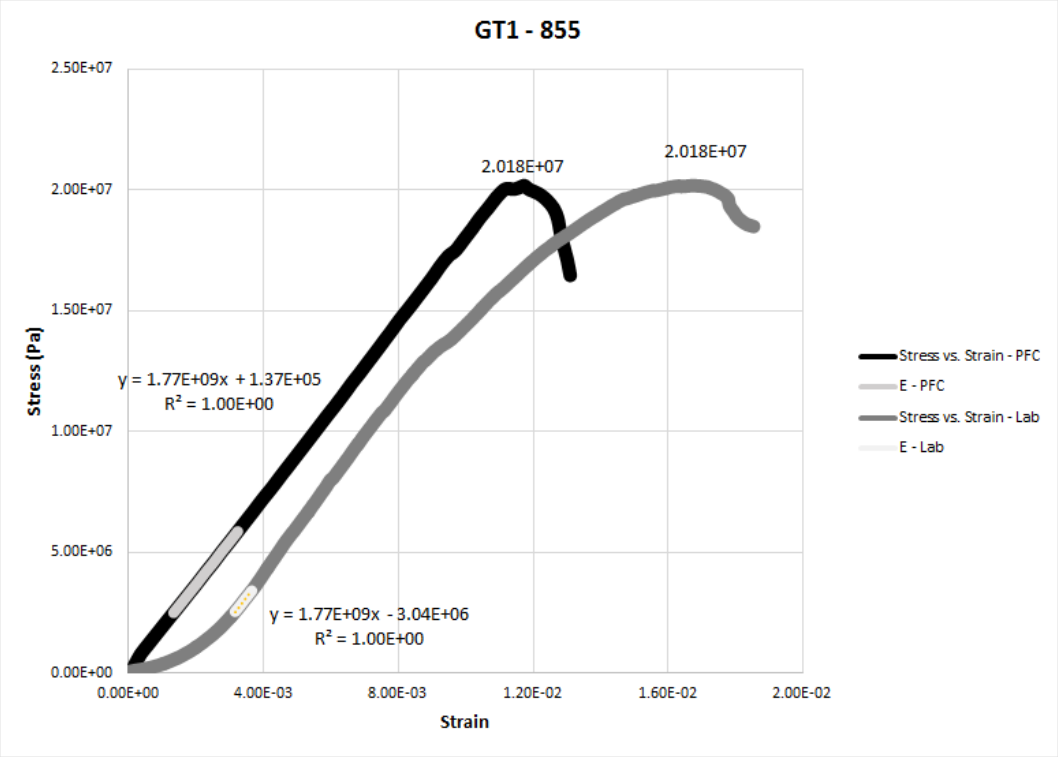

Figure 4-21 Stress-Strain Curves of Lab. Test vs. Modeled Test for BS GT1-855

4.3.2.2 Numerical Modeling of UCS Test for BS GT1-860

The parameters given in Table 4-8 were used in this modeling study.

Table 4-9 Parameters of BS GT1-860

No	Parameter	Value
1	Particle density (kg/m^3)	2310
2	Particle elasticity modulus (Pa)	5.44E+09
3	Particle friction coefficient	0.98
4	Parallel bond elasticity modulus (Pa)	Iteration input
5	Parallel bond normal strength (Pa)	Iteration input
6	Width of the specimen (m)	58.77E-03
7	Length of the specimen (m)	128.94E-03

Figure 4-22 shows the status of the specimen GT1-860 before and after the laboratory test.

Figure 4-22 Numerically Modeled BS GT1-860

Figure 4-23 shows the fracture model (red: tension, blue: shear) developed during modeling of bituminous shale specimen GT1-860.

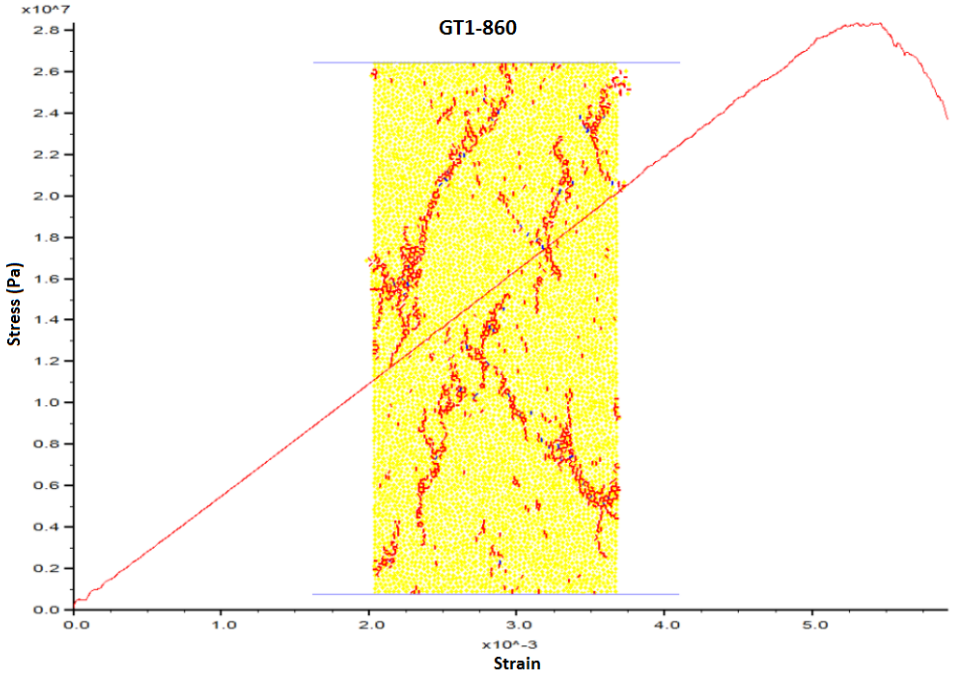

Figure 4-23 PFC Model of BS GT1-860 and Fractures Developed

Stress-strain relationships were obtained both from laboratory tests and numerically modeled tests and the graph given in Figure 4-24 shows these relationships. According

to the figure, slope of the curve (Young's Modulus) and the maximum strength (compressive strength) value of laboratory test and those of numerically modeled test are the same.

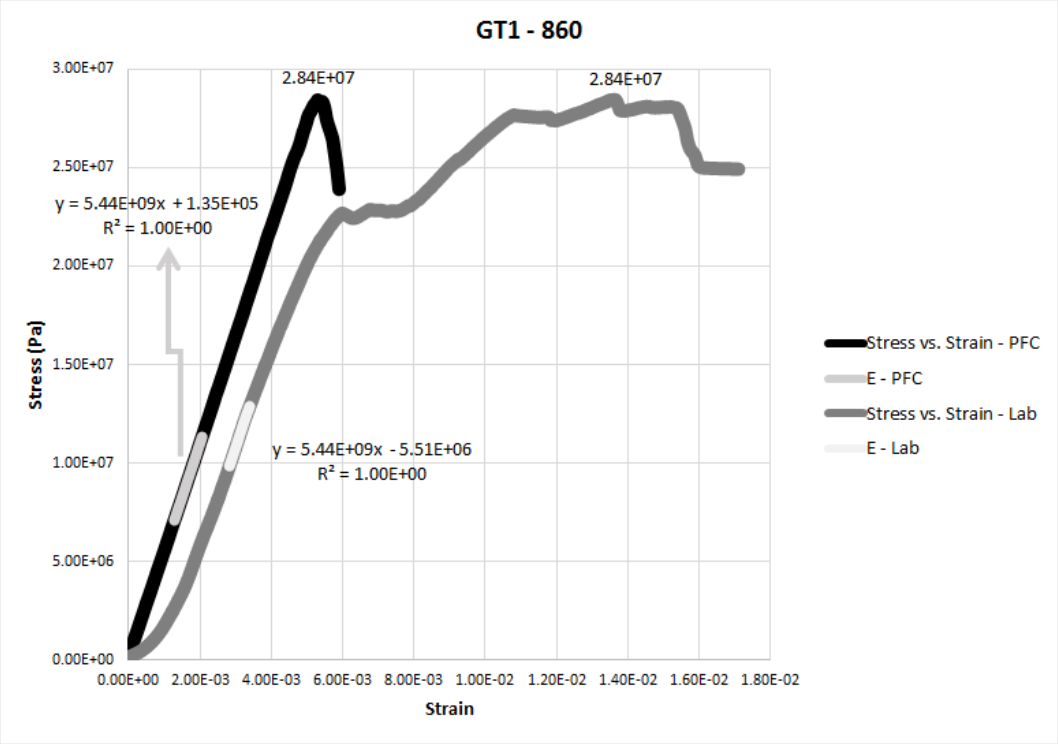

Figure 4-24 Stress-Strain Curves of Lab. Test vs. Modeled Test for BS GT1-860

4.3.2.3 Numerical Modeling of UCS Test for BS GT2-657

The parameters given in Table 4-9 were used in this modeling study.

Table 4-10 Parameters of BS GT2-657

No	Parameter	Value
1	Particle density (kg/m^3)	2160
2	Particle elasticity modulus (Pa)	2.87E+09
3	Particle friction coefficient	0.47
4	Parallel bond elasticity modulus (Pa)	Iteration input
5	Parallel bond normal strength (Pa)	Iteration input
6	Width of the specimen (m)	59.59E-03
7	Length of the specimen (m)	131.59E-03

No core photo is available for the bituminous shale specimen no GT2-657.

Figure 4-25 shows the fracture model (red: tension, blue: shear) developed during modeling of bituminous shale specimen GT2-657.

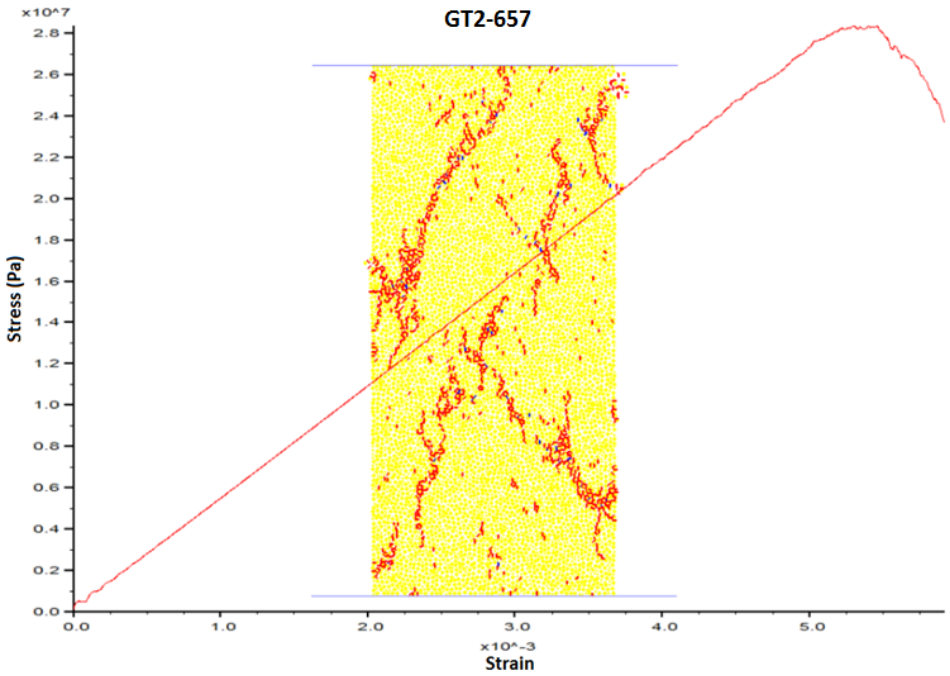

Figure 4-25 PFC Model of BS GT2-657 and Fractures Developed

Stress-strain relationships were obtained both from laboratory tests and numerically modeled tests and the graph given in Figure 4-26 shows these relationships. According to the figure, slope of the curve (Young's Modulus) and the maximum strength (compressive strength) value of laboratory test and those of numerically modeled test are the same.

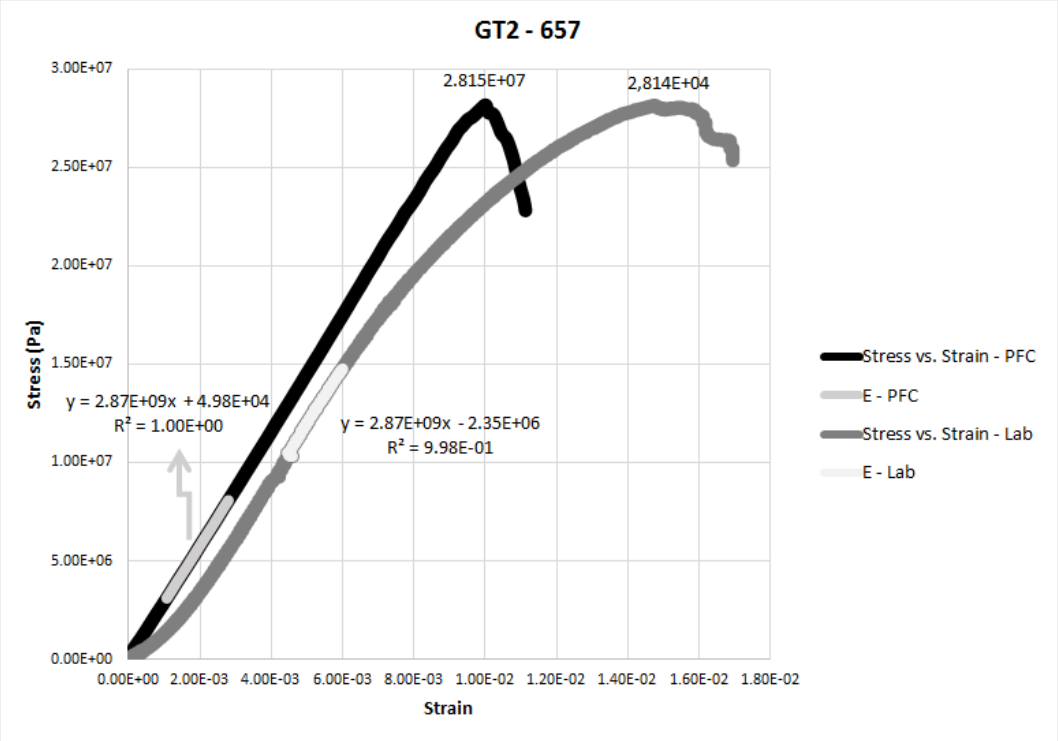

Figure 4-26 Stress-Strain Curves of Lab. Test vs. Modeled Test for BS GT2-657

4.3.2.4 Numerical Modeling of UCS Test for BS GT2-659

The parameters given in Table 4-10 were used in this modeling study.

Table 4-11 Parameters of BS GT2-659

No	Parameter	Value
1	Particle density (kg/m^3)	2180
2	Particle elasticity modulus (Pa)	2.84E+09
3	Particle friction coefficient	0.47
4	Parallel bond elasticity modulus (Pa)	Iteration input
5	Parallel bond normal strength (Pa)	Iteration input
6	Width of the specimen (m)	59.37E-03
7	Length of the specimen (m)	106.13E-03

No core photo is available for the bituminous shale specimen no GT2-659.

Figure 4-27 shows the fracture model (red: tension, blue: shear) developed during modeling of bituminous shale specimen GT2-659.

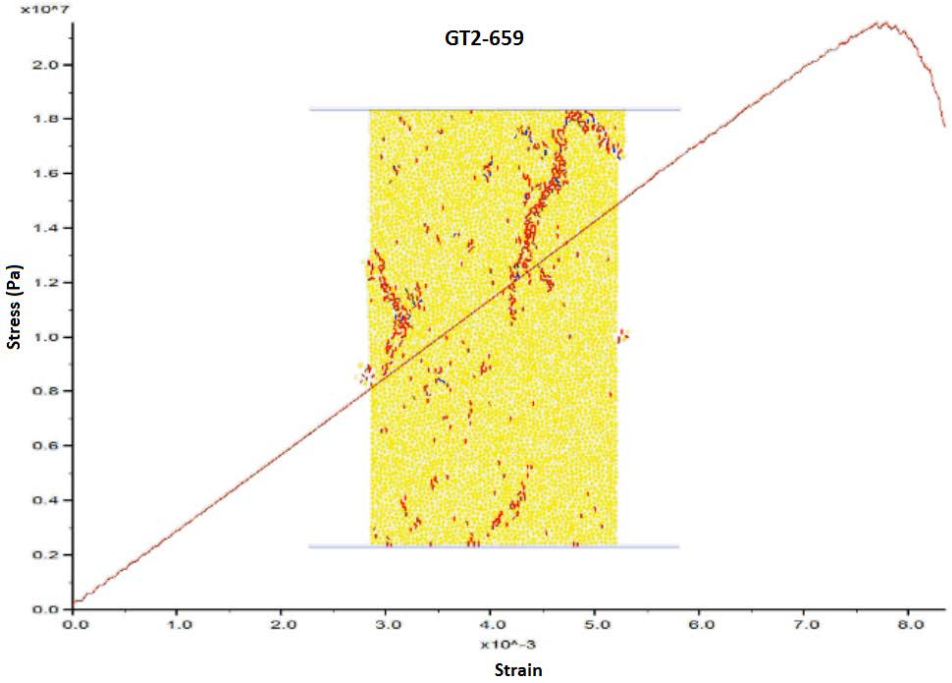

Figure 4-27 PFC Model of BS GT2-659 and Fractures Developed

Stress-strain relationships were obtained both from laboratory tests and numerically modeled tests and the graph given in Figure 4-28 shows these relationships. According to the figure, slope of the curve (Young's Modulus) and the maximum strength (compressive strength) value of laboratory test and those of numerically modeled test are the same.

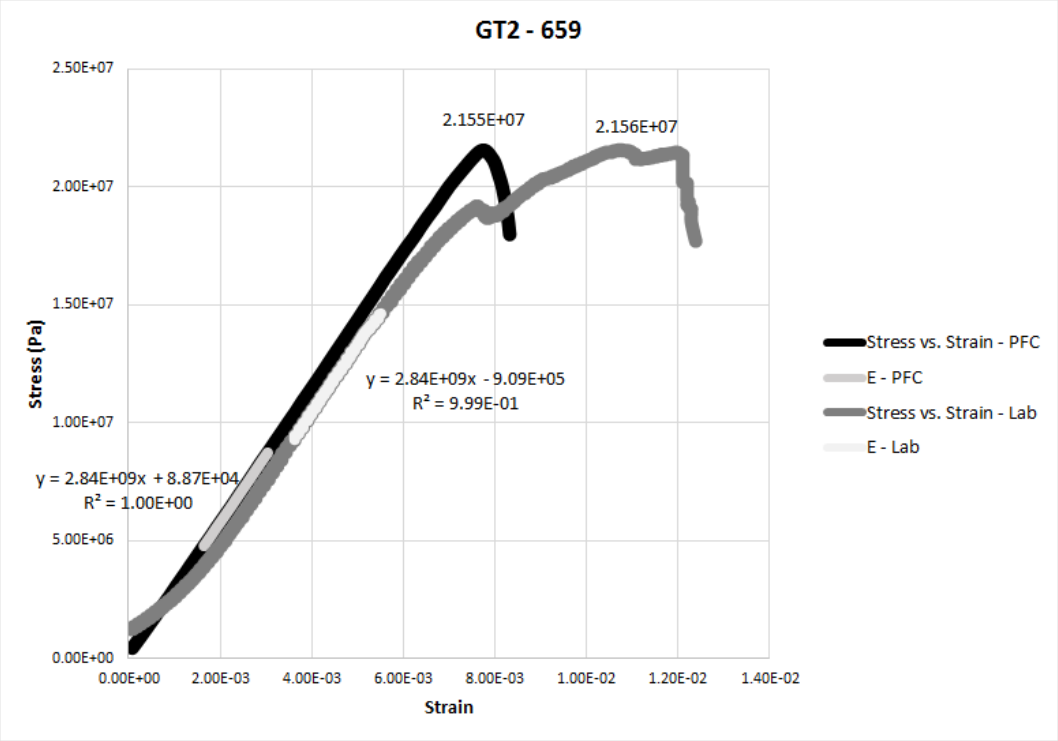

Figure 4-28 Stress-Strain Curves of Lab. Test vs. Modeled Test for BS GT2-659

4.3.3 Numerical Modeling of UCS Tests for Upper Trona Specimens

Among the UCS tests performed in the laboratory environment for upper trona, the specimens with the number of:

- GT1-874
- GT1-875
- GT2-674 and
- GT2-679

were numerically modeled. Modeling studies for these specimens are discussed in detail in the following sections.

4.3.3.1 Numerical Modeling of UCS Test for UT GT1-874

The parameters given in Table 4-11 were used in this modeling study.

Table 4-12 Parameters of UT GT1-874

No	Parameter	Value
1	Particle density (kg/m^3)	2040
2	Particle elasticity modulus (Pa)	4.82E+09
3	Particle friction coefficient	0.91
4	Parallel bond elasticity modulus (Pa)	Iteration input
5	Parallel bond normal strength (Pa)	Iteration input
6	Width of the specimen (m)	57.70E-03
7	Length of the specimen (m)	129.97E-03

Figure 4-29 shows the status of the specimen GT1-874 before and after the laboratory test.

Figure 4-29 Numerically Modeled UT GT1-874

Figure 4-30 shows the fracture model (red: tension, blue: shear) developed during modeling of upper trona specimen GT1-874.

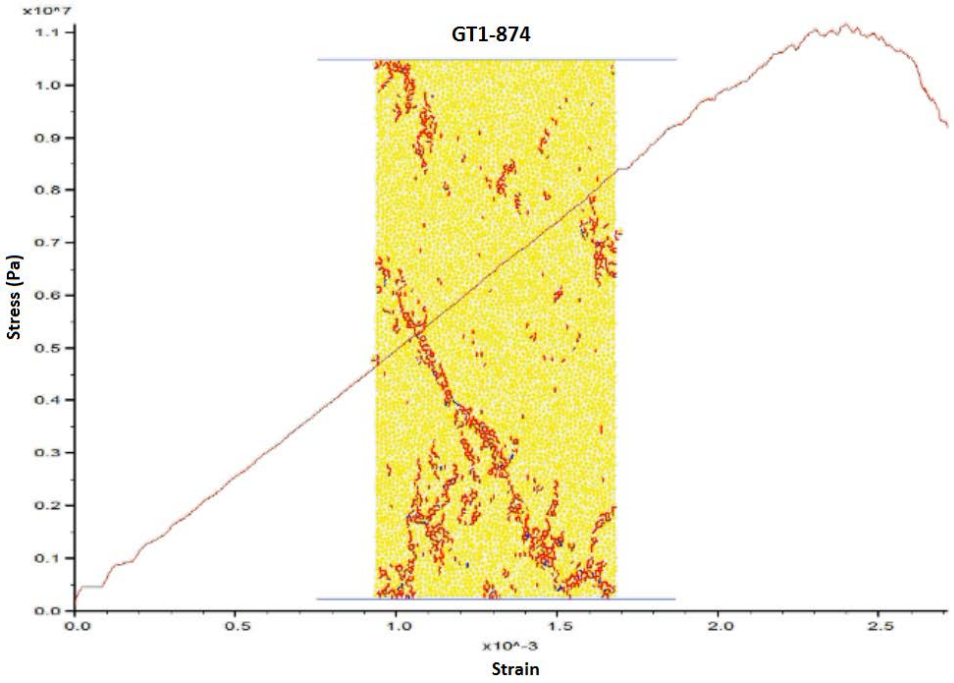

Figure 4-30 PFC Model of UT GT1-874 and Fractures Developed

Stress-strain relationships were obtained both from laboratory tests and numerically modeled tests and the graph given in Figure 4-31 shows these relationships. According to the figure, slope of the curve (Young's Modulus) and the maximum strength (compressive strength) value of laboratory test and those of numerically modeled test are the same.

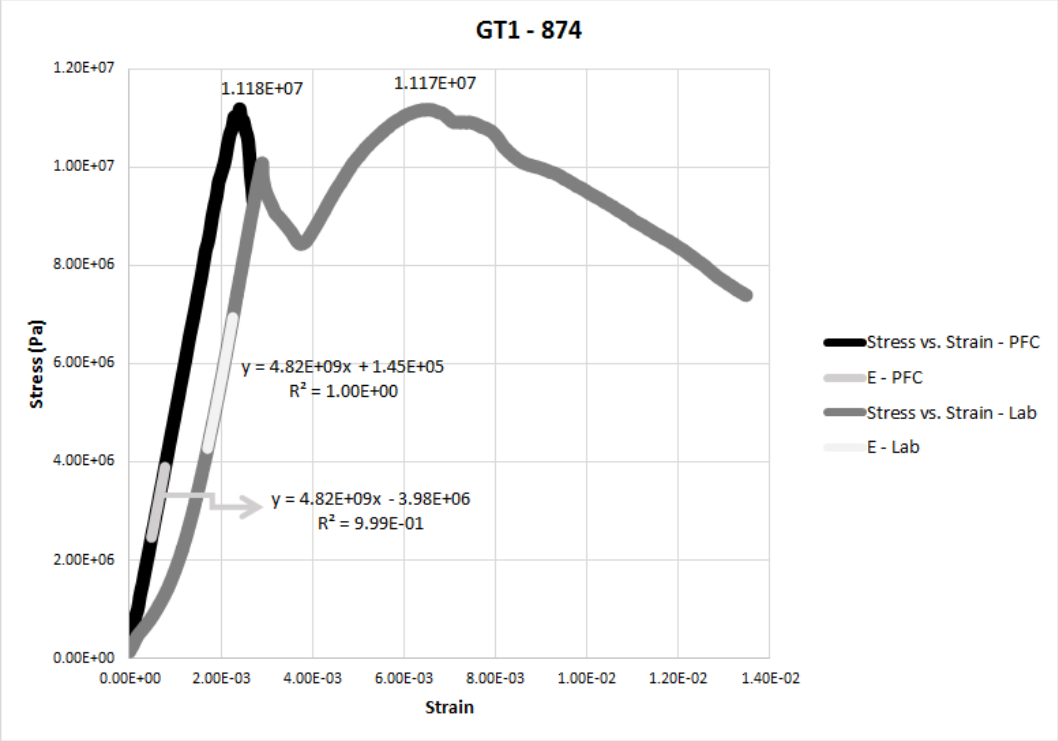

Figure 4-31 Stress-Strain Curves of Lab. Test vs. Modeled Test for UT GT1-874

4.3.3.2 Numerical Modeling of UCS Test for UT GT1-875

The parameters given in Table 4-12 were used in this modeling study.

Table 4-13 Parameters of UT GT1-875

No	Parameter	Value
1	Particle density (kg/m^3)	1980
2	Particle elasticity modulus (Pa)	4.64E+09
3	Particle friction coefficient	0.91
4	Parallel bond elasticity modulus (Pa)	Iteration input
5	Parallel bond normal strength (Pa)	Iteration input
6	Width of the specimen (m)	59.98E-03
7	Length of the specimen (m)	130.50E-03

Figure 4-32 shows the status of the specimen GT1-875 before and after the laboratory test.

Figure 4-32 Numerically Modeled UT GT1-875

Figure 4-33 shows the fracture model (red: tension, blue: shear) developed during modeling of upper trona specimen GT1-875.

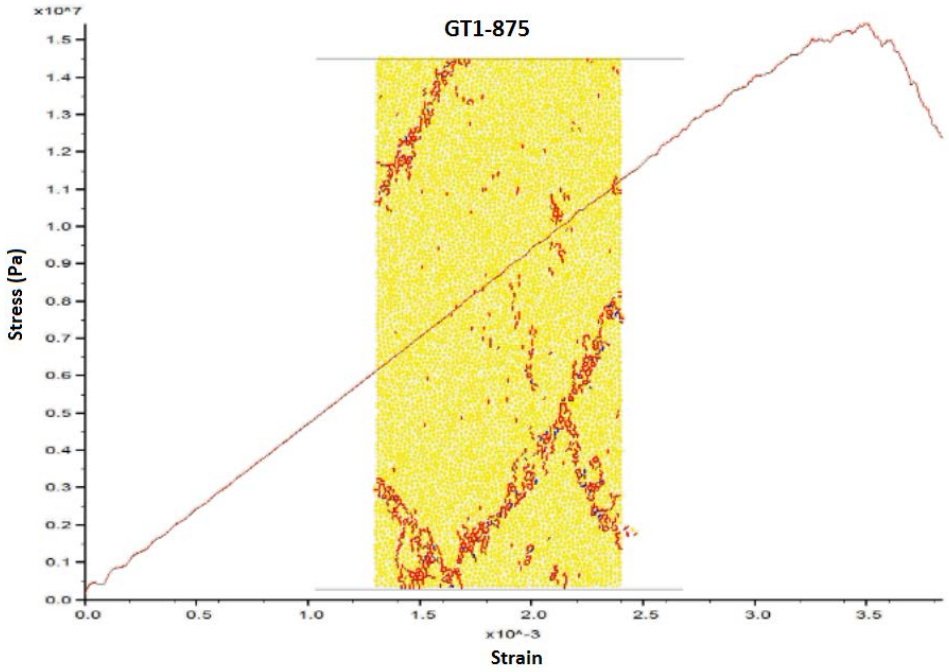

Figure 4-33 PFC Model of UT GT1-875 and Fractures Developed

Stress-strain relationships were obtained both from laboratory tests and numerically modeled tests and the graph given in Figure 4-34 shows these relationships. According

to the figure, slope of the curve (Young's Modulus) and the maximum strength (compressive strength) value of laboratory test and those of numerically modeled test are the same.

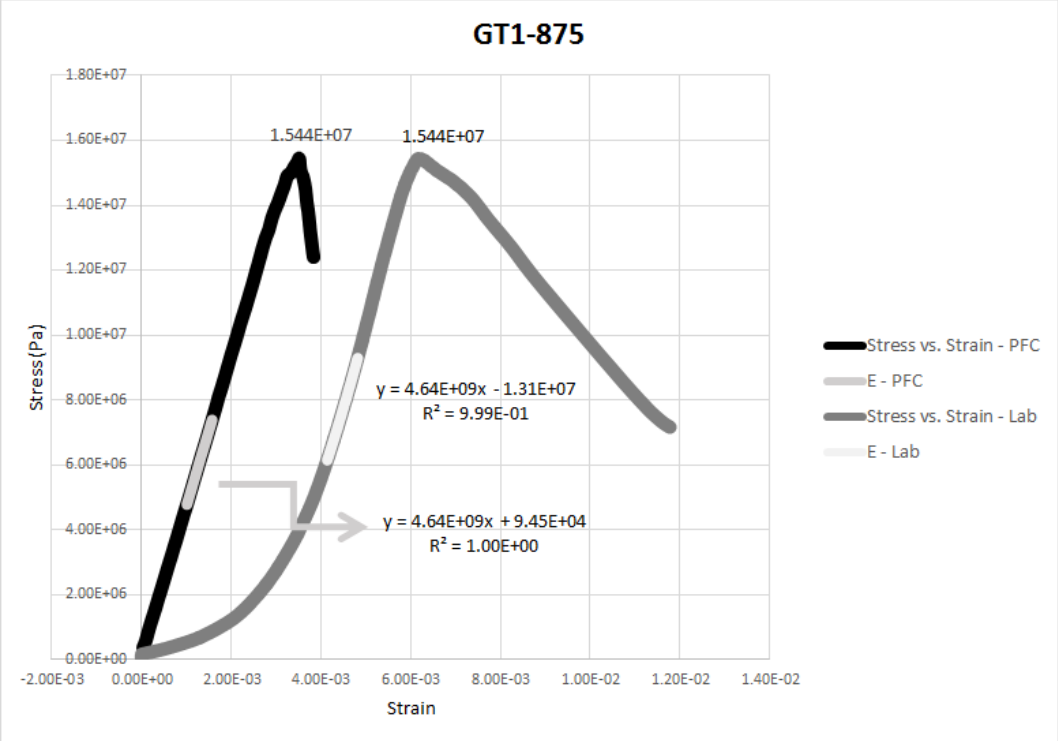

Figure 4-34 Stress-Strain Curves of Lab. Test vs. Modeled Test for UT GT1-875

4.3.3.3 Numerical Modeling of UCS Test for UT GT2-674

The parameters given in Table 4-13 were used in this modeling study.

Table 4-14 Parameters of UT GT2-674

No	Parameter	Value
1	Particle density (kg/m^3)	2070
2	Particle elasticity modulus (Pa)	7.50E+09
3	Particle friction coefficient	0.68
4	Parallel bond elasticity modulus (Pa)	Iteration input
5	Parallel bond normal strength (Pa)	Iteration input
6	Width of the specimen (m)	59.71E-03
7	Length of the specimen (m)	130.43E-03

Figure 4-35 shows the status of the specimen GT2-674 before and after the laboratory test.

Figure 4-35 Numerically Modeled UT GT2-674

Figure 4-36 shows the fracture model (red: tension, blue: shear) developed during modeling of upper trona specimen GT2-674.

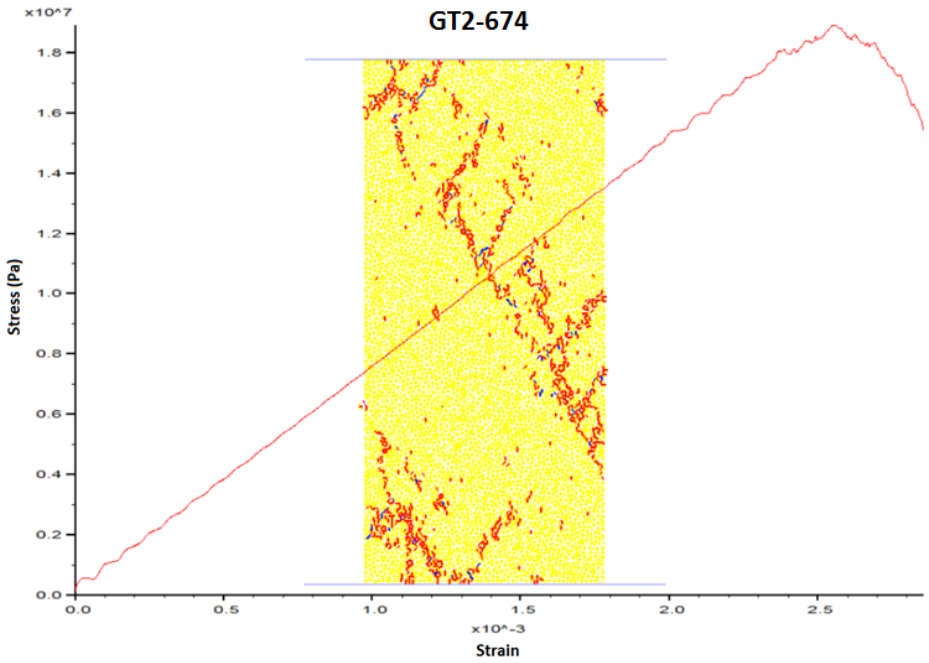

Figure 4-36 PFC Model of UT GT2-674 and Fractures Developed

Stress-strain relationships were obtained both from laboratory tests and numerically modeled tests and the graph given in Figure 4-37 shows these relationships. According to the figure, slope of the curve (Young's Modulus) and the maximum strength (compressive strength) value of laboratory test and those of numerically modeled test are the same.

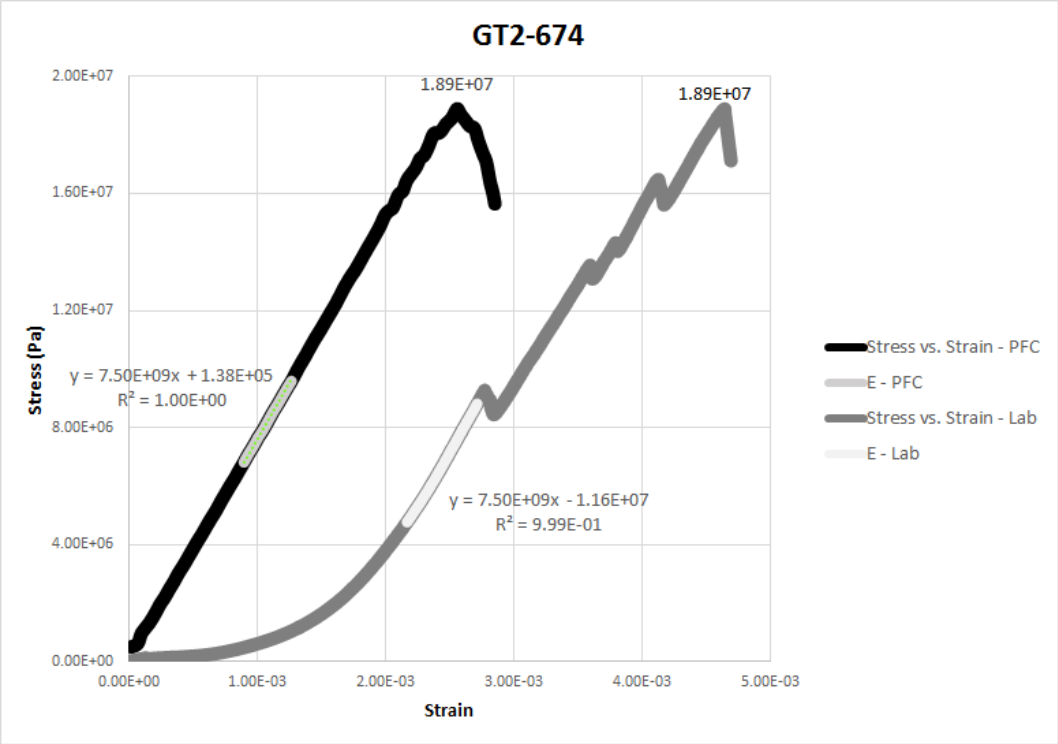

Figure 4-37 Stress-Strain Curves of Lab. Test vs. Modeled Test for UT GT2-674

4.3.3.4 Numerical Modeling of UCS Test for UT GT2-679

The parameters given in Table 4-14 were used in this modeling study.

Table 4-15 Parameters of UT GT2-679

No	Parameter	Value
1	Particle density (kg/m^3)	2020
2	Particle elasticity modulus (Pa)	1.294E+10
3	Particle friction coefficient	0.49
4	Parallel bond elasticity modulus (Pa)	Iteration input
5	Parallel bond normal strength (Pa)	Iteration input
6	Width of the specimen (m)	59.74E-03
7	Length of the specimen (m)	131.70E-03

Figure 4-38 shows the status of the specimen GT2-679 before and after the laboratory test.

Figure 4-38 Numerically Modeled UT GT2-679

Figure 4-39 shows the fracture model (red: tension, blue: shear) developed during modeling of upper trona specimen GT2-679.

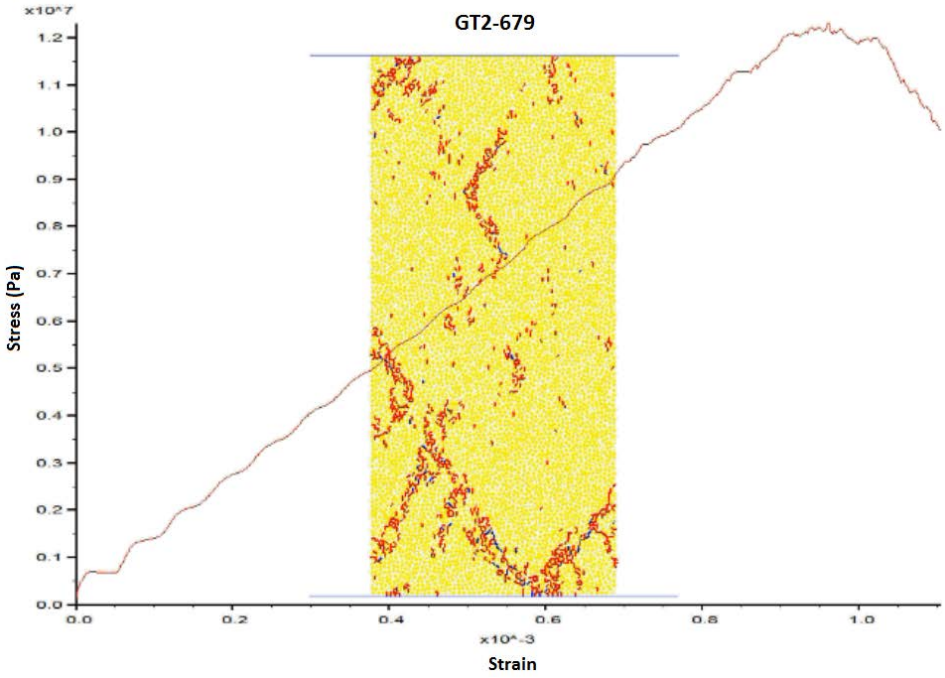

Figure 4-39 PFC Model of UT GT2-679 and Fractures Developed

Stress-strain relationships were obtained both from laboratory tests and numerically modeled tests and the graph given in Figure 4-40 shows these relationships. According to the figure, slope of the curve (Young's Modulus) and the maximum strength (compressive strength) value of laboratory test and those of numerically modeled test are the same.

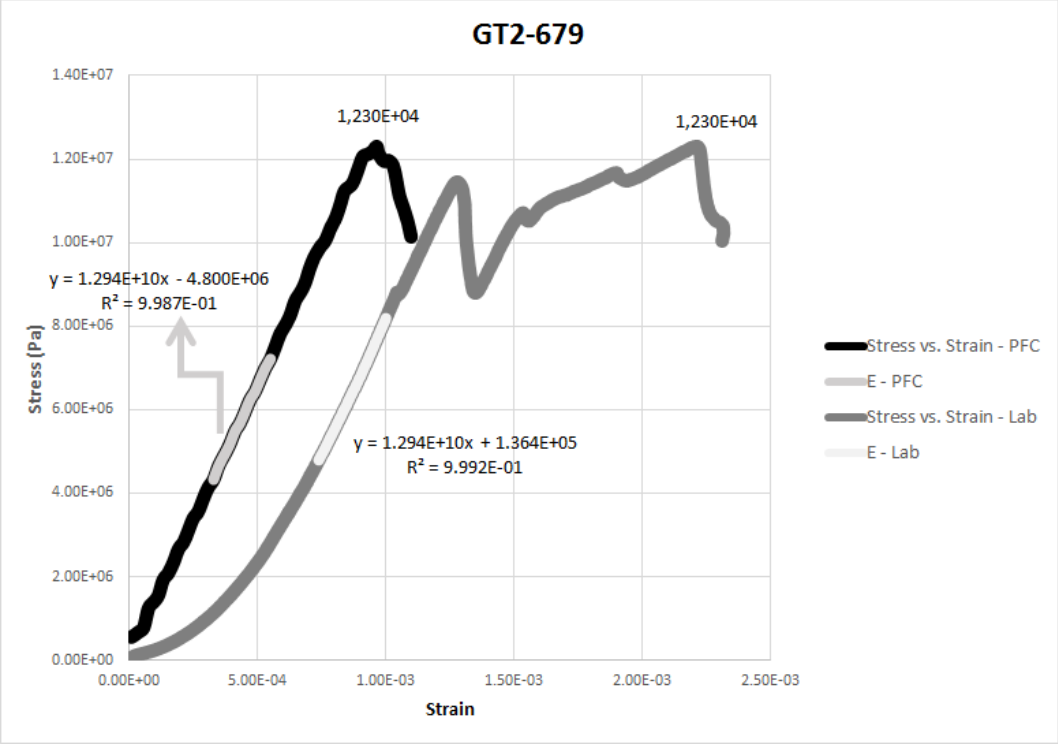

Figure 4-40 Stress-Strain Curves of Lab. Test vs. Modeled Test for UT GT2-679

4.3.4 Numerical Modeling of UCS Tests for Lower Trona Specimens

Among the UCS tests performed in the laboratory environment for lower trona, the specimens with the number of:

- GT2-708
- GT2-719
- GT2-723 and
- GT2-733

were numerically modeled. Modeling studies for these specimens are discussed in detail in the following sections.

4.3.4.1 Numerical Modeling of UCS Test for LT GT2-708

The parameters given in Table 4-15 were used in this modeling study.

Table 4-16 Parameters of LT GT2-708

No	Parameter	Value
1	Particle density (kg/m^3)	2020
2	Particle elasticity modulus (Pa)	1.01E+09
3	Particle friction coefficient	1.23
4	Parallel bond elasticity modulus (Pa)	Iteration input
5	Parallel bond normal strength (Pa)	Iteration input
6	Width of the specimen (m)	60.37E-03
7	Length of the specimen (m)	124.97E-03

Figure 4-41 shows the status of the specimen GT2-708 before and after the laboratory test.

Figure 4-41 Numerically Modeled LT GT2-708

Figure 4-42 shows the fracture model (red: tension, blue: shear) developed during modeling of lower trona specimen GT2-708.

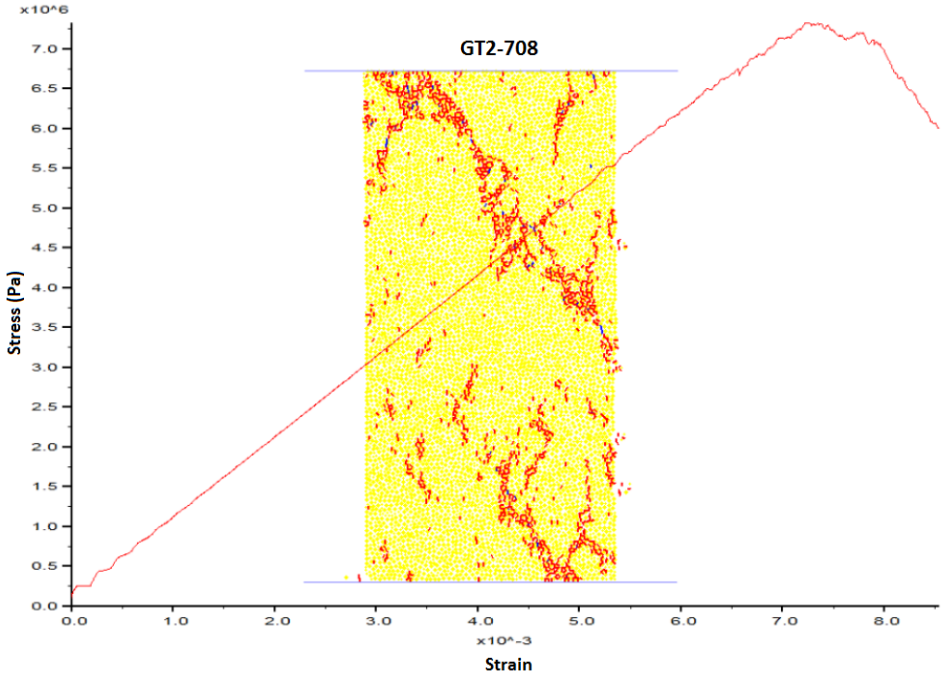

Figure 4-42 PFC Model of LT GT2-708 and Fractures Developed

Stress-strain relationships were obtained both from laboratory tests and numerically modeled tests and the graph given in Figure 4-43 shows these relationships. According to the figure, slope of the curve (Young's Modulus) and the maximum strength (compressive strength) value of laboratory test and those of numerically modeled test are the same.

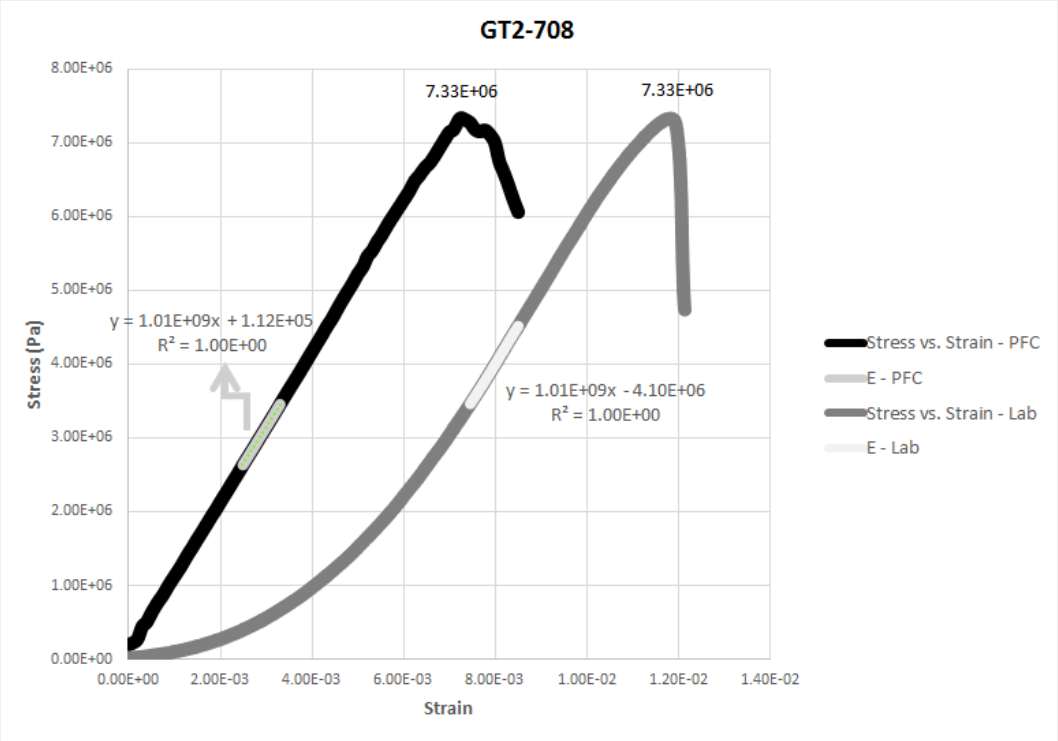

Figure 4-43 Stress-Strain Curves of Lab. Test vs. Modeled Test for LT GT2-708

4.3.4.2 Numerical Modeling of UCS Test for LT GT2-719

The parameters given in Table 4-16 were used in this modeling study.

Table 4-17 Parameters of LT GT2-719

No	Parameter	Value
1	Particle density (kg/m^3)	2070
2	Particle elasticity modulus (Pa)	1.86E+09
3	Particle friction coefficient	0.71
4	Parallel bond elasticity modulus (Pa)	Iteration input
5	Parallel bond normal strength (Pa)	Iteration input
6	Width of the specimen (m)	60.80E-03
7	Length of the specimen (m)	131.57E-03

Figure 4-44 shows the status of the specimen GT2-719 before and after the laboratory test.

Figure 4-44 Numerically Modeled LT GT2-719

Figure 4-45 shows the fracture model (red: tension, blue: shear) developed during modeling of lower trona specimen GT2-719.

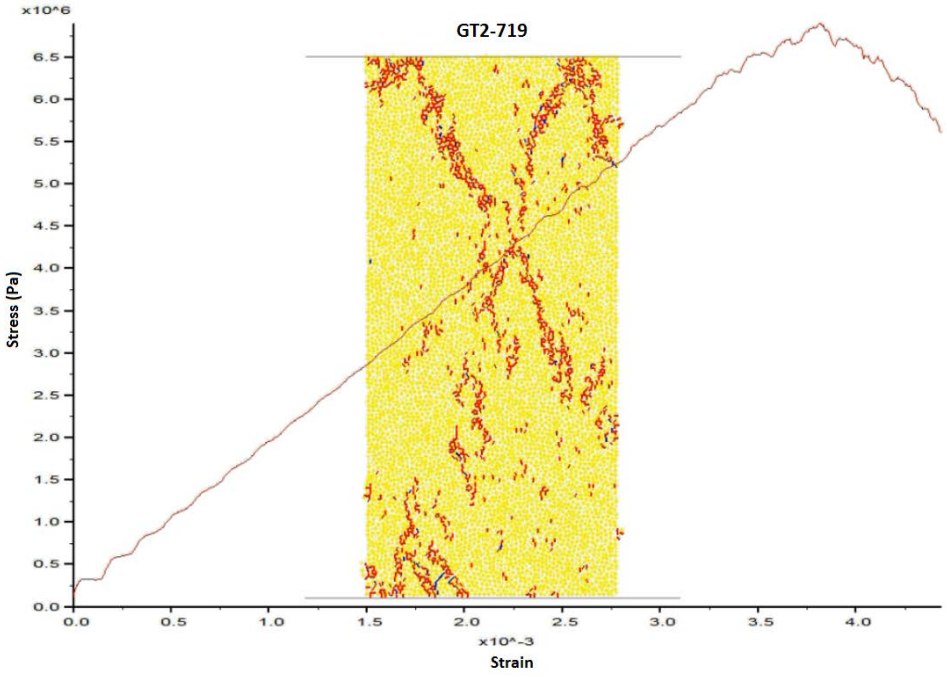

Figure 4-45 PFC Model of LT GT2-719 and Fractures Developed

Stress-strain relationships were obtained both from laboratory tests and numerically modeled tests and the graph given in Figure 4-46 shows these relationships. According to the figure, slope of the curve (Young's Modulus) and the maximum strength (compressive strength) value of laboratory test and those of numerically modeled test are the same.

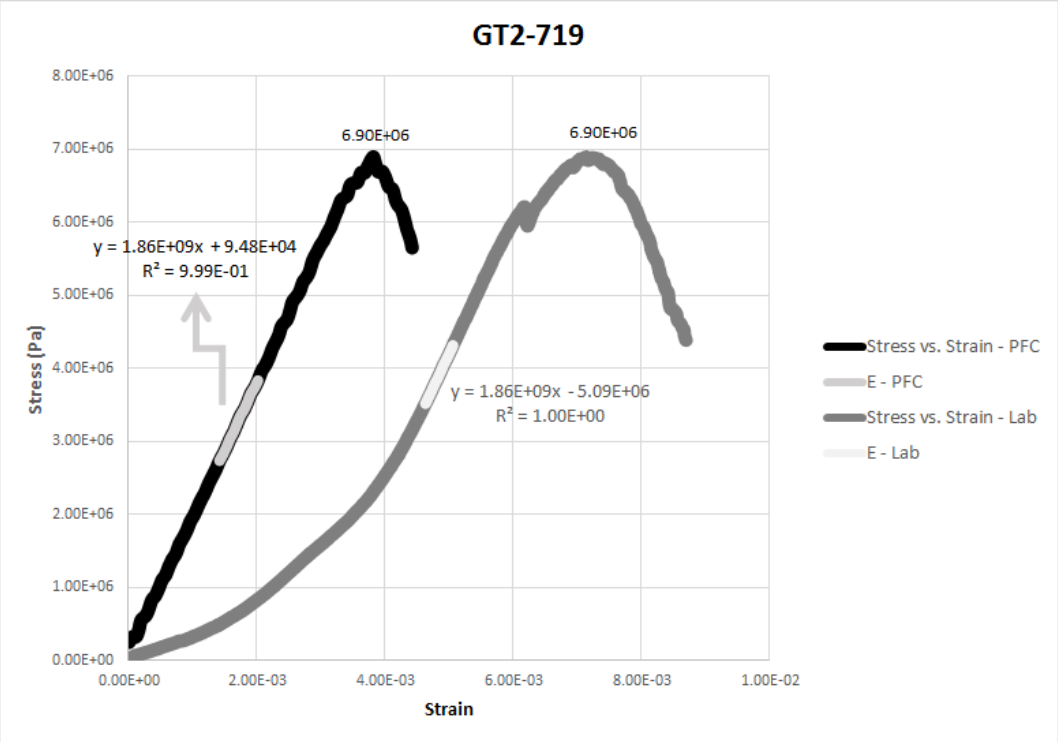

Figure 4-46 Stress-Strain Curves of Lab. Test vs. Modeled Test for LT GT2-719

4.3.4.3 Numerical Modeling of UCS Test for LT GT2-723

The parameters given in Table 4-17 were used in this modeling study.

Table 4-18 Parameters of LT GT2-723

No	Parameter	Value
1	Particle density (kg/m^3)	2080
2	Particle elasticity modulus (Pa)	2.74E+09
3	Particle friction coefficient	0.71
4	Parallel bond elasticity modulus (Pa)	Iteration input
5	Parallel bond normal strength (Pa)	Iteration input
6	Width of the specimen (m)	58.82E-03
7	Length of the specimen (m)	132.21E-03

Figure 4-47 shows the status of the specimen GT2-723 before and after the laboratory test.

Figure 4-47 Numerically Modeled LT GT2-723

Figure 4-48 shows the fracture model (red: tension, blue: shear) developed during modeling of lower trona specimen GT2-723.

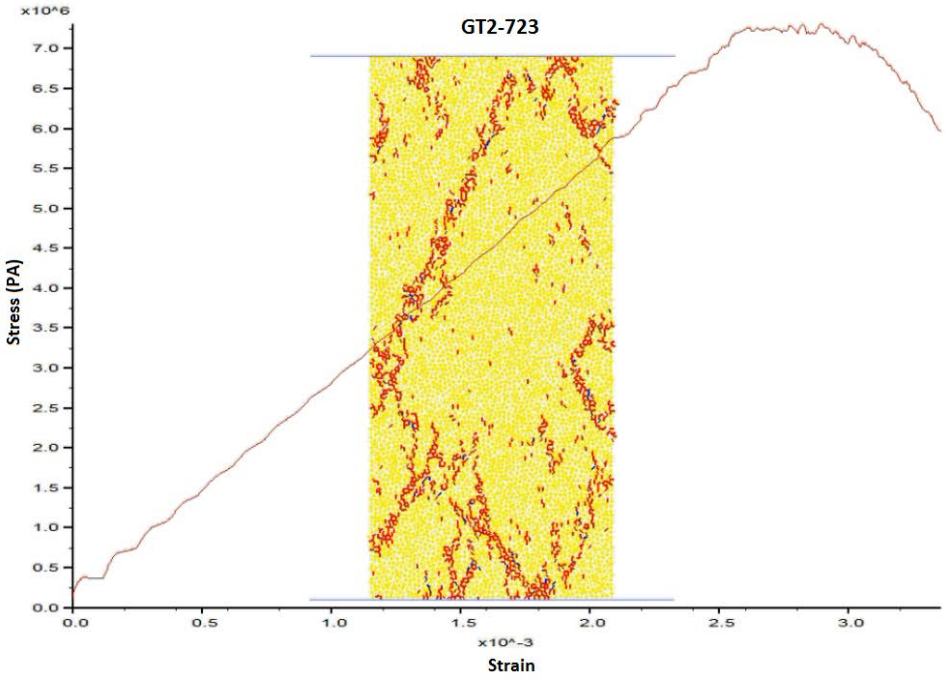

Figure 4-48 PFC Model of LT GT2-723 and Fractures Developed

Stress-strain relationships were obtained both from laboratory tests and numerically modeled tests and the graph given in Figure 4-49 shows these relationships. According to the figure, slope of the curve (Young's Modulus) and the maximum strength (compressive strength) value of laboratory test and those of numerically modeled test are the same.

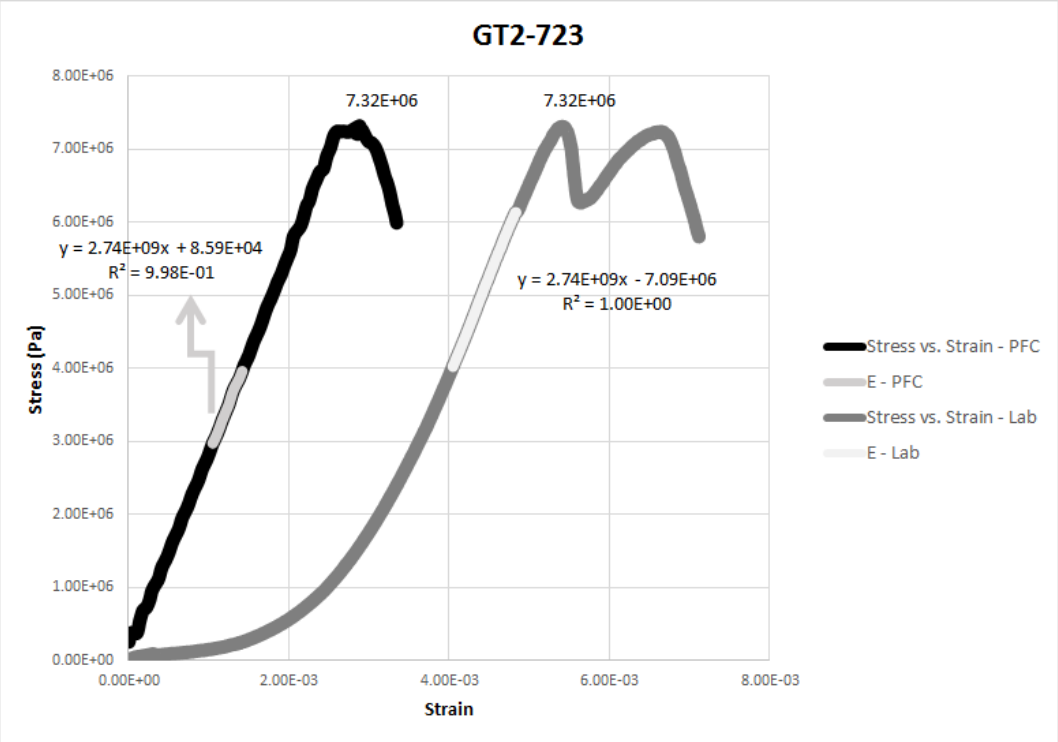

Figure 4-49 Stress-Strain Curves of Lab. Test vs. Modeled Test for LT GT2-723

4.3.4.4 Numerical Modeling of UCS Test for LT GT2-733

The parameters given in Table 4-18 were used in this modeling study.

Table 4-19 Parameters of LT GT2-733

No	Parameter	Value
1	Particle density (kg/m^3)	2090
2	Particle elasticity modulus (Pa)	8.80E+09
3	Particle friction coefficient	1.25
4	Parallel bond elasticity modulus (Pa)	Iteration input
5	Parallel bond normal strength (Pa)	Iteration input
6	Width of the specimen (m)	61.69E-03
7	Length of the specimen (m)	130.50E-03

Figure 4-50 shows the status of the specimen GT2-733 before and after the laboratory test.

Figure 4-50 Numerically Modeled LT GT2-733

Figure 4-51 shows the fracture model (red: tension, blue: shear) developed during modeling of lower trona specimen GT2-733.

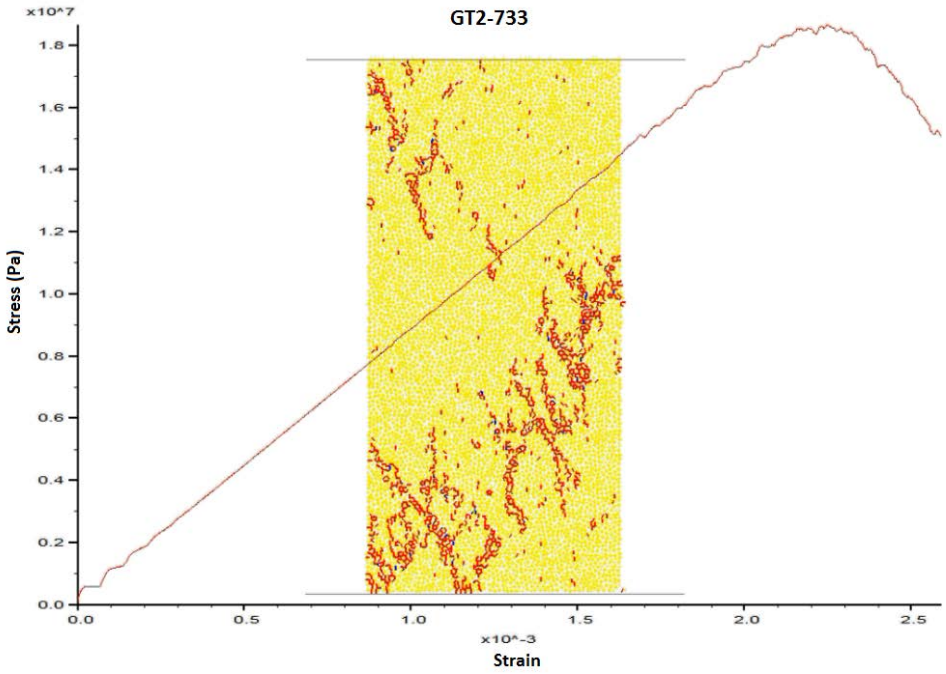

Figure 4-51 PFC Model of LT GT2-733 and Fractures Developed

Stress-strain relationships were obtained both from laboratory tests and numerically modeled tests and the graph given in Figure 4-52 shows these relationships. According to the figure, slope of the curve (Young's Modulus) and the maximum strength (compressive strength) value of laboratory test and those of numerically modeled test are the same.

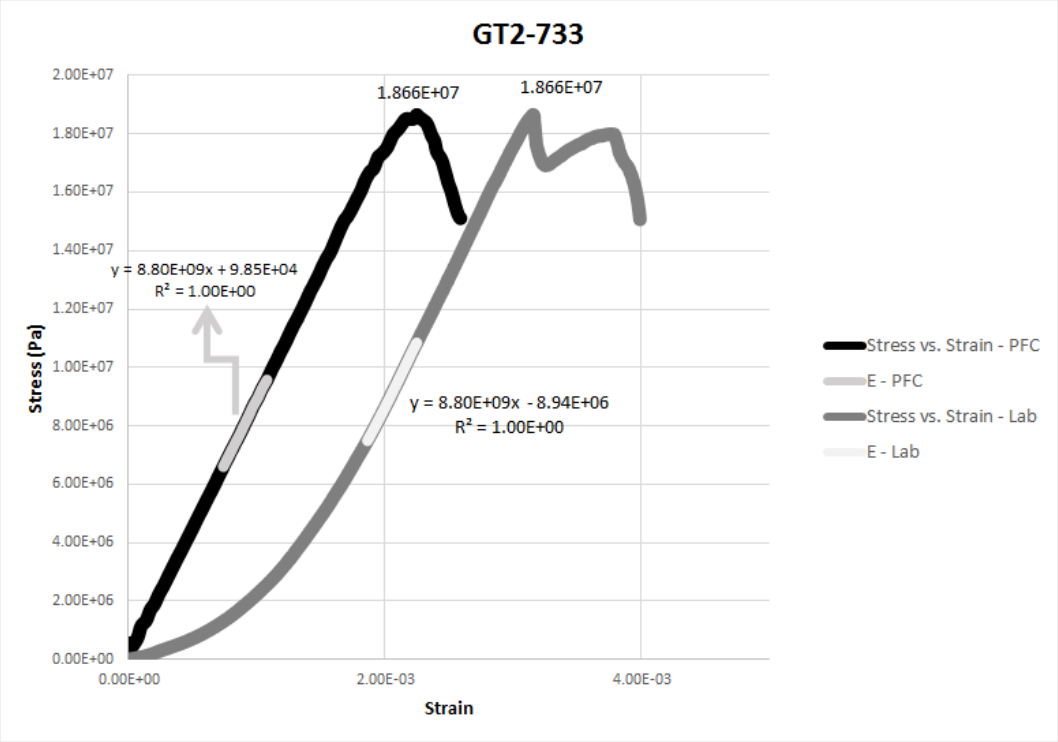

Figure 4-52 Stress-Strain Curves of Lab. Test vs. Modeled Test for LT GT2-733

4.3.5 Material Properties Obtained from Iterations for UCS Tests

Values obtained as a result of aforementioned iterations are given in Table 4-19. In Table 4-19 the values under the columns of "Parallel Bond Normal Strength (MPa) (input)" and "Parallel Bond EM (GPa) (input)" are the input parameters for iteration processes. These parameters were changed for each iteration process in PFC and the values given under the corresponding columns are the final input values by which the correct output values for UCS and elasticity modulus were obtained. These input parameters were also used as direct inputs for subsequent PL test modeling studies, whose details are given in Section 4.4, by assuming that the PL tests were calibrated with UCS tests. Therefore, these input parameters are called as UCS calibrated input parameters.

Table 4-20 Material Properties Obtained from Iterations for UCS Tests

No	Lith.	Hole ID	Spec. No.	Parallel Bond Normal Strength (MPa) (input)	Parallel Bond EM (GPa) (input)	# of Iterations	# of Particles	UCS (test result) (MPa)	UCS (iterated) (MPa) (output)	Precision (%)	EM (test result) (GPa)	EM (iterated) (GPa) (output)	Precision (%)
1	CS	GT1	904	29.645	0.4652	14	7080	4.81	4.81	99.94	0.8500	0.8502	99.97
2	CS	GT1	908	1.65905	0.0775	14	7879	2.88	2.88	99.97	0.1600	0.1601	99.92
3	CS	GT2	698	3.910	1.0043545	15	7327	6.61	6.61	99.94	1.7700	1.7738	99.79
4	CS	GT2	712	2.20002	0.324	14	6230	3.80	3.80	99.94	0.6400	0.6442	99.35
5	BS	GT1	855	12.635392	0.977	40	7550	20.18	20.19	99.97	1.7700	1.7722	99.88
6	BS	GT1	860	17.470	3.105	9	7111	28.44	28.41	100.12	5.4400	5.4418	99.97
7	BS	GT2	657	18.999	1.809	35	7359	28.14	28.17	99.91	2.8700	2.8728	99.90
8	BS	GT2	659	13.810	1.795	6	5913	21.56	21.56	99.98	2.8400	2.8436	99.87
9	UT	GT1	874	68.467	2.871	17	7038	11.17	11.17	99.99	4.8200	4.8232	99.93
10	UT	GT1	875	9.898	2.7443	9	7351	15.45	15.44	100.05	4.6400	4.6359	100.09
11	UT	GT2	674	11.698	4.58	7	7309	18.90	18.93	99.84	7.5000	7.5037	99.95
12	UT	GT2	679	7.7109	8.71524	43	7383	12.30	12.30	99.97	12.9400	12.9260	100.11
13	LT	GT2	708	4.085	0.521	11	7080	7.33	7.33	99.98	1.0100	1.0109	99.91
14	LT	GT2	719	4.065	1.060	8	7507	6.90	6.90	99.96	1.8600	1.8624	99.87
15	LT	GT2	723	4.3568	1.5886	22	7298	7.32	7.32	100.04	2.7400	2.7428	99.90
16	LT	GT2	733	11.3455	4.8271	19	7555	18.67	18.67	100.01	8.8000	8.7994	100.01
					TOTAL	283							

When the UCS and elasticity modulus values obtained from numerical models were compared with the ones obtained from laboratory tests, it is concluded that iterations were successfully completed for all of the lithological units. The average deviation for UCS estimations is 0.0524% and the one for EM estimations is 0.1246%. However, as can be seen in Figure 4-9, Figure 4-12, Figure 4-15, Figure 4-18, Figure 4-21, Figure 4-24, Figure 4-26, Figure 4-28, Figure 4-31, Figure 4-34, Figure 4-37, Figure 4-40, Figure 4-43, Figure 4-46, Figure 4-49 and Figure 4-52, stress-strain curves of the test specimens are not linear for all lithological units and also strain values are different from the real tests. This can be explained by the micro cracks within the real specimens. Similar behaviors were also observed in the literature (Yoon et al., 2012).

4.4 Modeling PL Index Tests

This section provides the details of the numerical modeling studies carried out for the PL tests that were matched with UCS specimens, whose numerical modeling details are given in Section 4.3. Modeled tests are highlighted in gray in Table 3-2 for claystone, in Table 3-3 for bituminous shale and in Table 3-4 for trona.

Geometric shapes of the specimens and the conical platens were taken into consideration during PFC modeling. Details of model geometry are shown in Figure 4-53. Radii of lower and upper conical platens are 5mm and angles of them are 60^{o}.

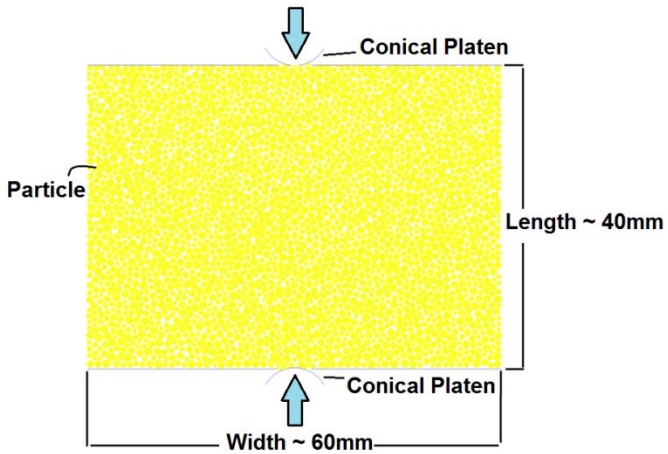

Figure 4-53 Typical Model Geometry in PFC for PL Test

The conical platen indentation is taken as a plane problem without considering the tangential rolling. Appropriateness of 2-D equivalent model has been verified by many researchers (Innaurato et al., 2007 and Gong et al., 2005). Therefore, PFC was used in this study for numerical modeling.

In order to generate numerical models for PL tests, a new routine was developed by revising the existing code in PFC.

Specifying the constraining conditions for PL test models is a crucial part of developing the said routine. These constraining conditions are the walls that confine the particles within test specimen. The code in the file named "et2.fis", which is one of the original files of the software, was revised by adding a new code.

Parameters given in Table 4-20 were used for numerical modeling studies of PL tests. These parameters are the same as the ones used for numerical modeling studies of UCS tests. These parameters were also discussed in detail in Section 4.2.

Table 4-21 Parameters Used For Numerical Modeling Studies of PL Tests

No	Parameter	Description
1	Particle density (kg/m^3)	Density of specimen in kilograms per cubic meter
2	Particle elasticity modulus (Pa)	Elasticity modulus of specimen in Pascal
3	Particle friction coefficient	Friction coefficient
4	Parallel bond elasticity modulus (Pa)	Parallel bond elasticity modulus in Pascal (iteration input)
5	Parallel bond normal strength (Pa)	Mean normal strength between parallel bonds in Pascal (iteration input)
6	Length of the specimen (m)	Length of specimen in meter
7	Width of the specimen m)	Width of specimen in meter
8	R_{min} (m) (*)	The minimum particle radius in meter
9	Ratio (*)	Ratio of the maximum particle size to the minimum
10	Initial loading (Pa) (*)	Platen positioning stress in Pascal

(*) Since these values are repeated for each iteration process, they were not given in the individual tables of the numerically modeled specimens. They were given under the corresponding headings in Section 4.2.

Note: For simplicity the following phrases were used in the following sections.

1- PL Model Representing Field PL Test: Field PL Model
2- PL Model Constructed By Using UCS Input Parameters: UCS Calibrated PL Model

4.4.1 Numerical Modeling of PL Tests for Claystone Specimens

Among the PL tests performed under the field conditions for claystone, the specimens with the number of:

- GT1-61
- GT1-63
- GT2-58 and
- GT2-79

were numerically modeled. Modeling studies for these specimens are discussed in detail in the following sections.

4.4.1.1 Numerical Modeling of PL Test for CS GT1-61

PL test applied on the specimen GT1-61 under field conditions was matched with the laboratory UCS test specimen GT1-904 and it was numerically modeled in PFC and the results were compared to each other. Parameters given in Table 4-21 were used for numerical modeling.

Table 4-22 Parameters of CS GT1-61

No	Parameter	Value (input parameters of the last UCS iteration)	Value (estimated input values)
1	Particle density (kg/m^3)	2100	2100
2	Particle elasticity modulus (Pa)	0.85E+9	0.85E+9
3	Particle friction coefficient	0.90	0.90
4	Parallel bond elasticity modulus (Pa)	4.6520E+08	Iteration input
5	Parallel bond normal strength (Pa)	2.9645E+07	Iteration input
6	Length (m)	34.00E-03	34.00E-03
7	Width (m)	61.00E-03	61.00E-03

The first numerical model was constructed by using the parameters that were used as the inputs for the last iteration of the UCS test with which this PL test is matched and to which a relationship is to be established. These parameters are given in the 4th and 5th rows of the "Value (input parameters of the last UCS iteration)" column of Table 4-21. Micro cracks and the time dependent variations in the load, which is exerted on the specimen through the conical platens in the PFC model, are given in Figure 4-54.

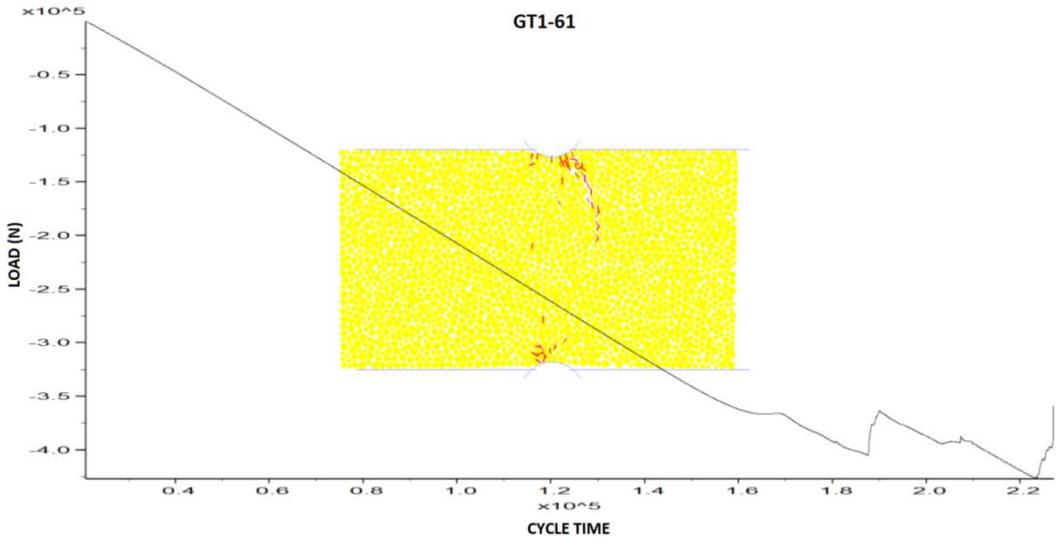

Figure 4-54 UCS Calibrated PL Model of CS GT1-61

At the end of PL test, only failure load is obtained. Failure load found as a result of the field PL test is 568N. However, this load was read as 426,000N from the graph

shown in Figure 4-54 given for the numerical modeling study, which was carried out by using the input parameters of the last iteration for the matched UCS test. The ratio between the two failure loads is 750. Consequently, it can be said that the PL test model that was calibrated by using UCS parameters cannot yield the correct PL failure load value. Therefore, in order to find the actual model parameters and represent the PL test applied under field conditions, PL numerical modeling study was performed by changing iteration input parameters shown in the 4th and 5th rows of "Value (estimated input values)" column of Table 4-21. Micro cracks developed and the time dependent variations in the load, which is exerted on the specimen through conical platens, during the iteration process as a result of which the actual model parameters are obtained, are shown in Figure 4-55.

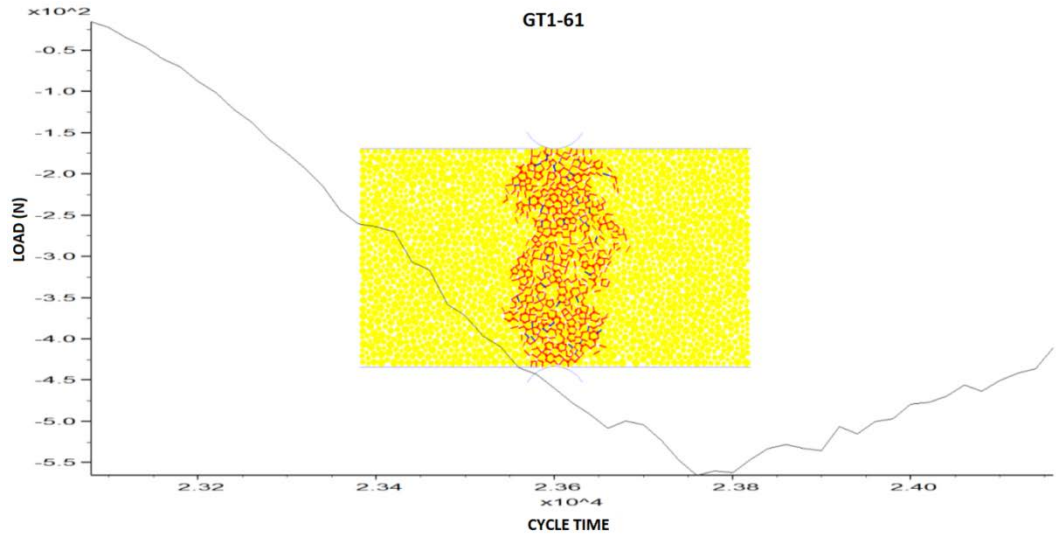

Figure 4-55 Field PL Model of CS GT1-61

According to the graph, failure load is said to be around 568N and this indicates that the iteration process was successfully completed for the specimen.

The results obtained from the model, which was constructed by using the input parameters of the last iteration for UCS test, and those obtained from the model, which was constructed by successive iterations to represent the PL test applied under field conditions, are compared in Table 4-22.

Table 4-23 Field PL Model vs. UCS Calibrated PL Model - CS GT1-61

No	Parameter	Field PL Model	UCS Calibrated PL Model	Ratio	Description
1	P (N)	568	426,000	750	Failure load
2	PB EM (GPa)	0.0045	0.4652	103	Parallel bond elasticity modulus
3	PB NS (MPa)	0.00565	29.645	5247	Parallel bond normal strength
4	D_e (mm)	51.3878		-	Equivalent specimen diameter
5	D_e^2 (mm)	2,640.7010		-	
6	I_S (MPa)	0.2151	161.3208	750	PL index
7	F	1.0124		-	Correction factor
8	I_{S50} (MPa)	0.2178	163.3205	750	PL index for a specimen with a diameter of 50 mm
9	UCS (MPa)	4.81		-	Result of the laboratory test
10	Conversion factor	22.09	0.03	0.001	Ratio of lab. UCS test result to PL indexes obtained from PL and UCS iterations

According to the results, the conversion factor, which was obtained at the end of the iteration process for which the input parameters of the last iteration for the matched UCS test model were used, is 0.03 and it is not a realistic value. On the other hand, conversion factor obtained at the end of the iteration process, which was continued until the same result of the field PL test was attained, is 22.09 and it is close to the conversion factor of 17.1, which is given in Table 3-19 for claystone.

4.4.1.2 Numerical Modeling of PL Test for CS GT1-63

PL test applied on the specimen GT1-63 under field conditions was matched with the laboratory UCS test specimen GT1-908 and it was numerically modeled in PFC and the results were compared to each other. Parameters given in Table 4-23 were used for numerical modeling.

Table 4-24 Parameters of CS GT1-63

No	Parameter	Value (input parameters of the last UCS iteration)	Value (estimated input values)
1	Particle density (kg/m^3)	2050	2050
2	Particle elasticity modulus (Pa)	0.16E+09	0.16E+09
3	Particle friction coefficient	0.90	0.90
4	Parallel bond elasticity modulus (Pa)	1.65905E+06	Iteration input
5	Parallel bond normal strength (Pa)	7.7500E+07	Iteration input
6	Length (m)	45.00E-03	45.00E-03
7	Width (m)	61.00E-03	61.00E-03

The first numerical model was constructed by using the parameters that were used as the inputs for the last iteration of the UCS test with which this PL test is matched and to which a relationship is to be established. These parameters are given in the 4th and 5th rows of the "Value (input parameters of the last UCS iteration)" column of Table 4-23. Micro cracks and the time dependent variations in the load, which is exerted on the specimen through the conical platens in the PFC model, are given in Figure 4-56.

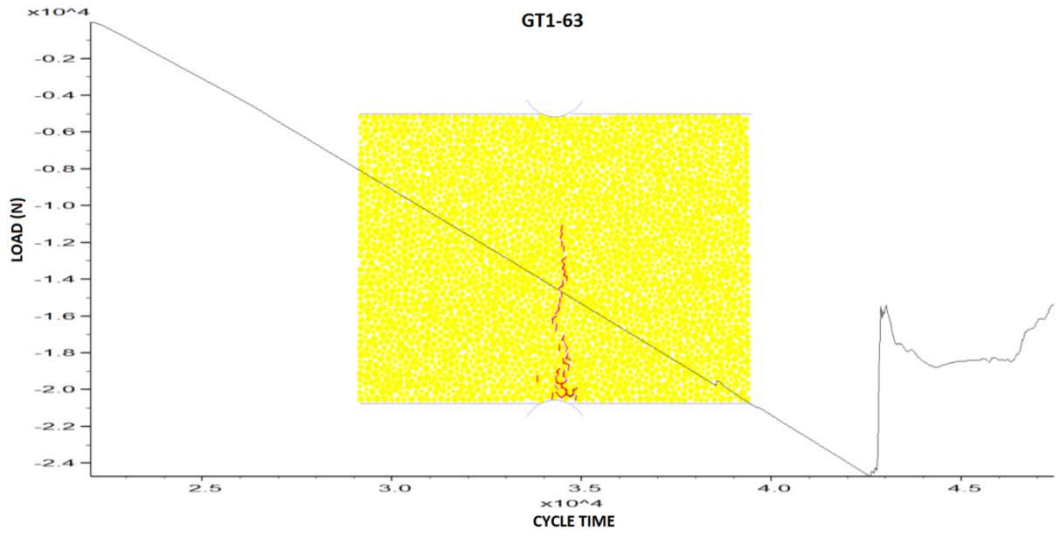

Figure 4-56 UCS Calibrated PL Model of CS GT1-63

At the end of PL test, only failure load is obtained. Failure load found as a result of the field PL test is 341N. However, this load was read as 25,000N from the graph shown in Figure 4-56 given for the numerical modeling study, which was carried out by using the input parameters of the last iteration for the matched UCS test. The ratio between the two failure loads is 73. Consequently, it can be said that the PL test model that was calibrated by using UCS parameters cannot yield the correct PL failure load value. Therefore, in order to find the actual model parameters and represent the PL test applied under field conditions, PL numerical modeling study was performed by changing iteration input parameters shown in the 4th and 5th rows of "Value (estimated input values)" column of Table 4-23. Micro cracks developed and the time dependent variations in the load, which is exerted on the specimen through conical platens, during the iteration process as a result of which the actual model parameters are obtained, are shown in Figure 4-57.

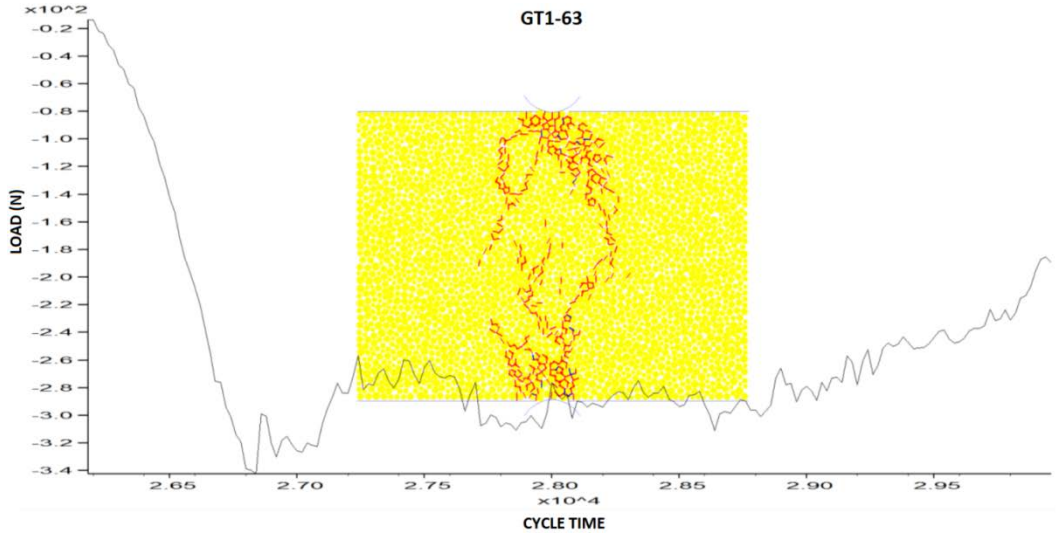

Figure 4-57 Field PL Model of CS GT1-63

According to the graph, failure load is said to be around 341N and this indicates that the iteration process was successfully completed for the specimen.

The results obtained from the model, which was constructed by using the input parameters of the last iteration for UCS test, and those obtained from the model,

which was constructed by successive iterations to represent the PL test applied under field conditions, are compared in Table 4-24.

Table 4-25 Field PL Model vs. UCS Calibrated PL Model - CS GT1-63

No	Parameter	Field PL Model	UCS Calibrated PL Model	Ratio	Description
1	P (N)	341	25,000	73	Failure load
2	PB EM (GPa)	7.00E-03	7.75E-02	11	Parallel bond elasticity modulus
3	PB NS (MPa)	0.017004	1.65905	98	Parallel bond normal strength
4	D_e (mm)	59.1189		-	Equivalent specimen diameter
5	D_e^2 (mm)	3,495.0455		-	
6	I_S (MPa)	0.0975	7.1530	73	PL index
7	F	1.0783		-	Correction factor
8	I_{S50} (MPa)	0.1051	7.7131	73	PL index for a specimen with a diameter of 50 mm
9	UCS (MPa)	2.88		-	Result of the laboratory test
10	Conversion factor	27.40	0.37	0.014	Ratio of lab. UCS test result to PL indexes obtained from PL and UCS iterations

According to the results, the conversion factor, which was obtained at the end of the iteration process for which the input parameters of the last iteration for the matched UCS test model were used, is 0.37 and it is not a realistic value. On the other hand, conversion factor obtained at the end of the iteration process, which was continued until the same result of the field PL test was attained, is 27.40 and it is around the conversion factor of 17.1, which is given in Table 3-19 for claystone.

4.4.1.3 Numerical Modeling of PL Test for CS GT2-58

PL test applied on the specimen GT2-58 under field conditions was matched with the laboratory UCS test specimen GT2-698 and it was numerically modeled in PFC and the results were compared to each other. Parameters given in Table 4-25 were used for numerical modeling.

Table 4-26 Parameters of CS GT2-58

No	Parameter	Value (input parameters of the last UCS iteration)	Value (estimated input values)
1	Particle density (kg/m^3)	2130	2130
2	Particle elasticity modulus (Pa)	1.77E+09	1.77E+09
3	Particle friction coefficient	0.90	0.90
4	Parallel bond elasticity modulus (Pa)	1.0043545E+09	Iteration input
5	Parallel bond normal strength (Pa)	3.9100E+06	Iteration input
6	Length (m)	45.00E-03	45.00E-03
7	Width (m)	.61.50E-03	61.50E-03

The first numerical model was constructed by using the parameters that were used as the inputs for the last iteration of the UCS test with which this PL test is matched and to which a relationship is to be established. These parameters are given in the 4th and 5th rows of the "Value (input parameters of the last UCS iteration)" column of Table 4-25. Micro cracks and the time dependent variations in the load, which is exerted on the specimen through the conical platens in the PFC model, are given in Figure 4-58.

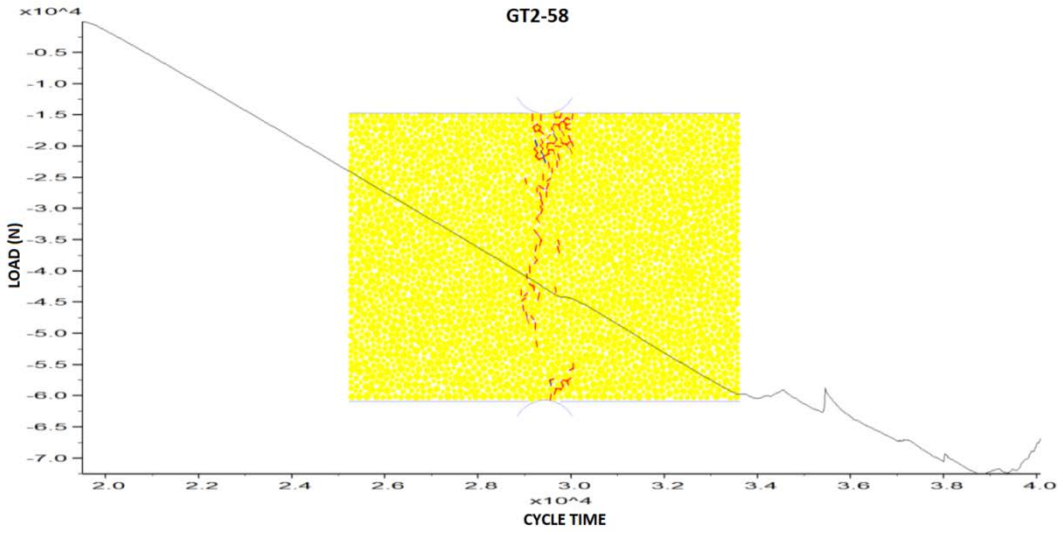

Figure 4-58 UCS Calibrated PL Model of CS GT2-58

At the end of PL test, only failure load is obtained. Failure load found as a result of the field PL test is 1,192N. However, this load was read as 72,600N from the graph shown in Figure 4-58 given for the numerical modeling study, which was carried out by using the input parameters of the last iteration for the matched UCS test. The ratio between the two failure loads is 61. Consequently, it can be said that the PL test model that was calibrated by using UCS parameters cannot yield the correct PL failure load value. Therefore, in order to find the actual model parameters and represent the PL test applied under field conditions, PL numerical modeling study was performed by changing iteration input parameters shown in the 4th and 5th rows of "Value (estimated input values)" column of Table 4-25. Micro cracks developed and the time dependent variations in the load, which is exerted on the specimen through conical platens, during the iteration process as a result of which the actual model parameters are obtained, are shown in Figure 4-59.

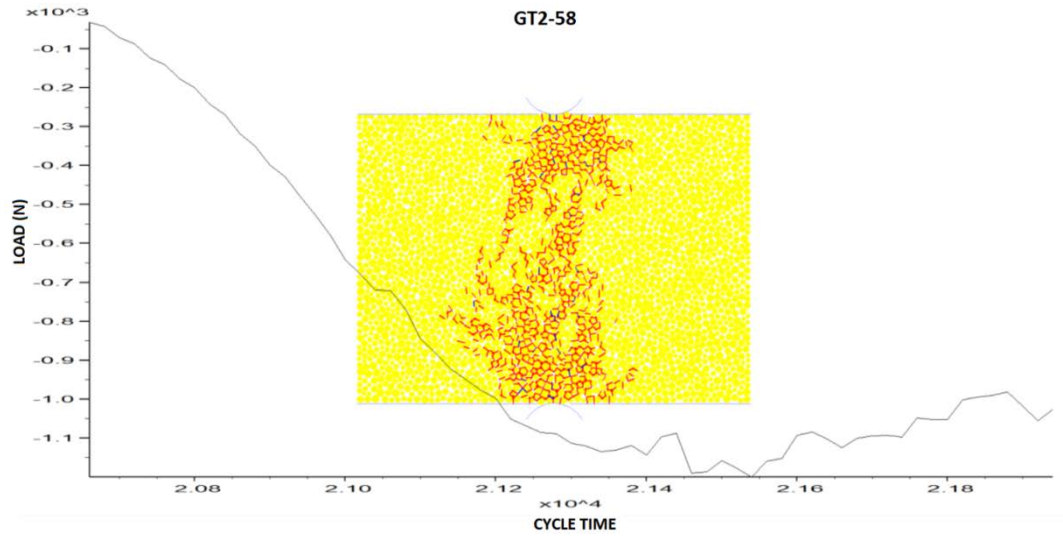

Figure 4-59 Field PL Model of CS GT2-58

According to the graph, failure load is said to be around 1,192N and this indicates that the iteration process was successfully completed for the specimen.

The results obtained from the model, which was constructed by using the input parameters of the last iteration for UCS test, and those obtained from the model,

which was constructed by successive iterations to represent the PL test applied under field conditions, are compared in Table 4-26.

Table 4-27 Field PL Model vs. UCS Calibrated PL Model - CS GT2-58

No	Parameter	Field PL Model	UCS Calibrated PL Model	Ratio	Description
1	P (N)	1,192	72,600	61	Failure load
2	PB EM (GPa)	0.09	1.0043545	11	Parallel bond elasticity modulus
3	PB NS (MPa)	0.0108	3.91	362	Parallel bond normal strength
4	D_e (mm)	59.3607		-	Equivalent specimen diameter
5	D_e^2 (mm)	3523.6934		-	
6	I_S (MPa)	0.3383	20.6034	61	PL index
7	F	1.0803		-	Correction factor
8	I_{S50} (MPa)	0.3654	22.2575	61	PL index for a specimen with a diameter of 50 mm
9	UCS (MPa)	6.61		-	Result of the laboratory test
10	Conversion factor	18.09	0.30	0.016	Ratio of lab. UCS test result to PL indexes obtained from PL and UCS iterations

According to the results, the conversion factor, which was obtained at the end of the iteration process for which the input parameters of the last iteration for the matched UCS test model were used, is 0.30 and it is not a realistic value. On the other hand, conversion factor obtained at the end of the iteration process, which was continued until the same result of the field PL test was attained, is 18.09 and it is very close to the conversion factor of 17.1, which is given in Table 3-19 for claystone.

4.4.1.4 Numerical Modeling of PL Test for CS GT2-79

PL test applied on the specimen GT2-79 under field conditions was matched with the laboratory UCS test specimen GT2-712 and it was numerically modeled in PFC and the results were compared to each other. Parameters given in Table 4-27 were used for numerical modeling.

Table 4-28 Parameters of CS GT2-79

No	Parameter	Value (input parameters of the last UCS iteration)	Value (estimated input values)
1	Particle density (kg/m^3)	2030	2030
2	Particle elasticity modulus (Pa)	0.64E+09	0.64E+09
3	Particle friction coefficient	1.43	1.43
4	Parallel bond elasticity modulus (Pa)	3.2400E+08	Iteration input
5	Parallel bond normal strength (Pa)	2.20002E+06	Iteration input
6	Length (m)	45.00E-03	45.00E-03
7	Width (m)	60.50E-03	60.50E-03

The first numerical model was constructed by using the parameters that were used as the inputs for the last iteration of the UCS test with which this PL test is matched and to which a relationship is to be established. These parameters are given in the 4th and 5th rows of the "Value (input parameters of the last UCS iteration)" column of Table 4-27. Micro cracks and the time dependent variations in the load, which is exerted on the specimen through the conical platens in the PFC model, are given in Figure 4-60.

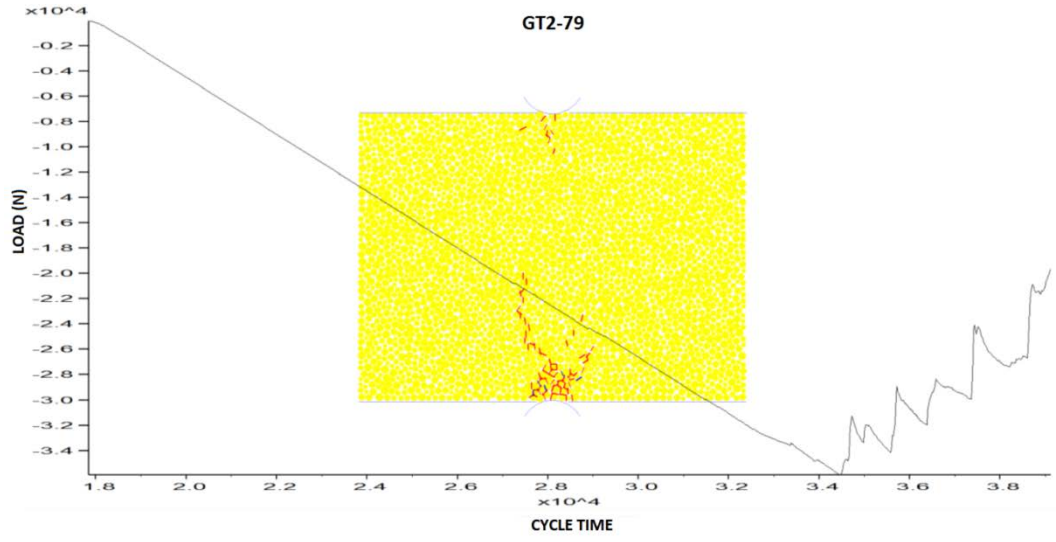

Figure 4-60 UCS Calibrated PL Model of CS GT2-79

At the end of PL test, only failure load is obtained. Failure load found as a result of the field PL test is 1,930N. However, this load was read as 35,900N from the graph shown in Figure 4-60 given for the numerical modeling study, which was carried out by using the input parameters of the last iteration for the matched UCS test. The ratio between the two failure loads is 19. Consequently, it can be said that the PL test model that was calibrated by using UCS parameters cannot yield the correct PL failure load value. Therefore, in order to find the actual model parameters and represent the PL test applied under field conditions, PL numerical modeling study was performed by changing iteration input parameters shown in the 4th and 5th rows of "Value (estimated input values)" column of Table 4-27. Micro cracks developed and the time dependent variations in the load, which is exerted on the specimen through conical platens, during the iteration process as a result of which the actual model parameters are obtained, are shown in Figure 4-61.

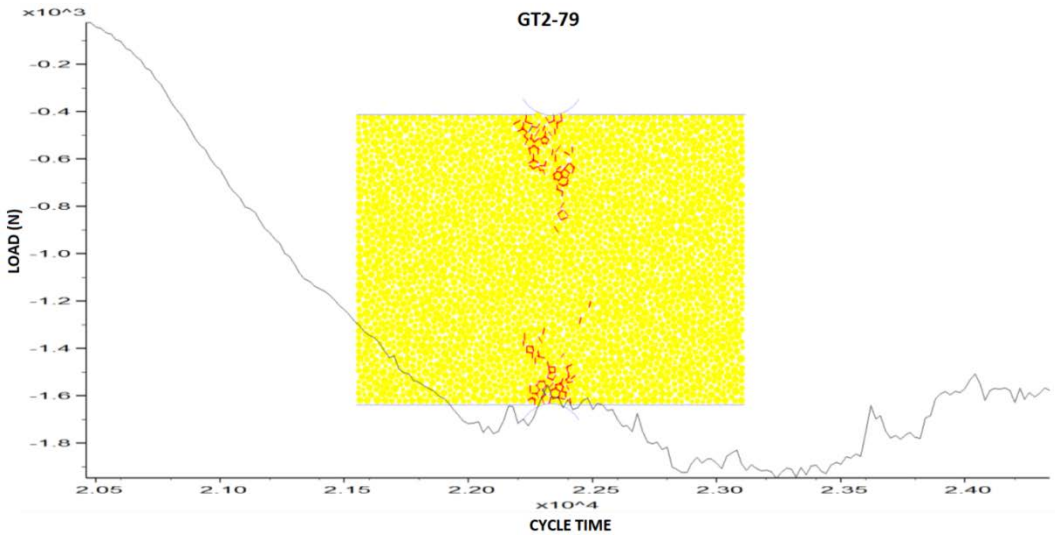

Figure 4-61 Field PL Model of CS GT2-79

According to the graph, failure load is said to be around 1,930N and this indicates that the iteration process was successfully completed for the specimen.

The results obtained from the model, which was constructed by using the input parameters of the last iteration for UCS test, and those obtained from the model,

which was constructed by successive iterations to represent the PL test applied under field conditions, are compared in Table 4-28.

Table 4-29 Field PL Model vs. UCS Calibrated PL Model - CS GT2-79

No	Parameter	Field PL Model	UCS Calibrated PL Model	Ratio	Description
1	P (N)	1,930	35,900	19	Failure load
2	PB EM (GPa)	3.20E-02	3.24E-01	10	Parallel bond elasticity modulus
3	PB NS (MPa)	0.1191	2.20002	18	Parallel bond normal strength
4	D_e (mm)	58.8761		-	Equivalent specimen diameter
5	D_e^2 (mm)	3,466.3976		-	
6	I_S (MPa)	0.5568	10.3566	19	PL index
7	F	1.0763		-	Correction factor
8	I_{S50} (MPa)	0.5993	11.1469	19	PL index for a specimen with a diameter of 50 mm
9	UCS (MPa)	3.80		-	Result of the laboratory test
10	Conversion factor	6.34	0.34	0.054	Ratio of lab. UCS test result to PL indexes obtained from PL and UCS iterations

According to the results, the conversion factor, which was obtained at the end of the iteration process for which the input parameters of the last iteration for the matched UCS test model were used, is 0.34 and it is not a realistic value. On the other hand, conversion factor obtained at the end of the iteration process, which was continued until the same result of the field PL test was attained, is 6.34 and it is around the conversion factor of 17.1, which is given in Table 3-19 for claystone.

4.4.2 Numerical Modeling of PL Tests for Bituminous Shale Specimens

Among the PL tests performed under the field conditions for bituminous shale, the specimens with the number of:

- GT1-8
- GT1-14
- GT2-14 and
- GT2-16

were numerically modeled. Modeling studies for these specimens are discussed in detail in the following sections.

4.4.2.1 Numerical Modeling of PL Test for BS GT1-8

PL test applied on the specimen GT1-8 under field conditions was matched with the laboratory UCS test specimen GT1-855 and it was numerically modeled in PFC and the results were compared to each other. Parameters given in Table 4-29 were used for numerical modeling.

Table 4-30 Parameters of BS GT1-8

No	Parameter	Value (input parameters of the last UCS iteration)	Value (estimated input values)
1	Particle density (kg/m^3)	2260	2260
2	Particle elasticity modulus (Pa)	1.77E+09	1.77E+09
3	Particle friction coefficient	0.98	0.98
4	Parallel bond elasticity modulus (Pa)	9.7700E+08	Iteration input
5	Parallel bond normal strength (Pa)	1.2635392E+07	Iteration input
6	Length (m)	40.00E-03	40.00E-03
7	Width (m)	60.00E-03	60.00E-03

The first numerical model was constructed by using the parameters that were used as the inputs for the last iteration of the UCS test with which this PL test is matched and to which a relationship is to be established. These parameters are given in the 4th and 5th rows of the "Value (input parameters of the last UCS iteration)" column of Table 4-29. Micro cracks and the time dependent variations in the load, which is exerted on the specimen through the conical platens in the PFC model, are given in Figure 4-62.

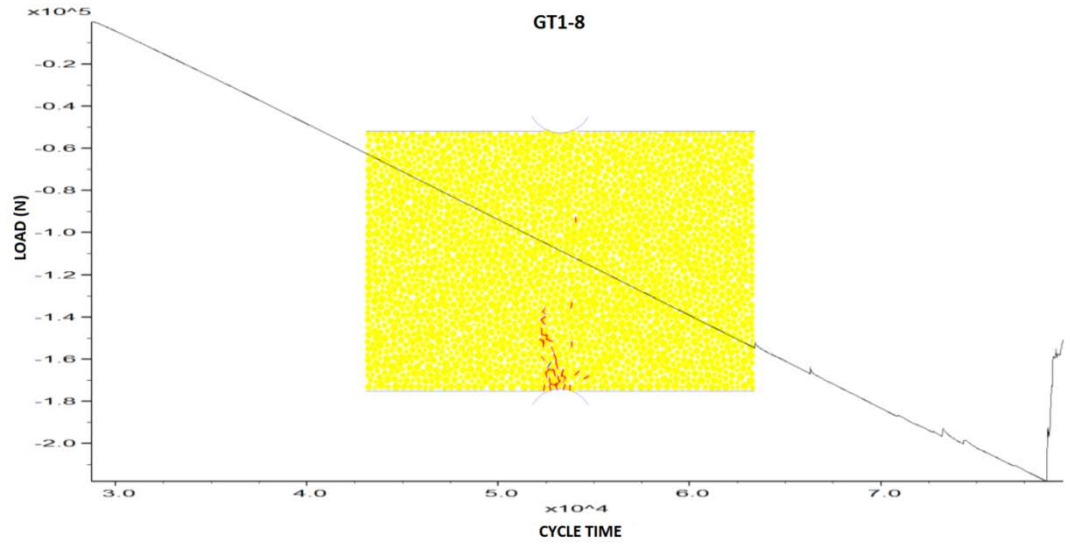

Figure 4-62 UCS Calibrated PL Model of BS GT1-8

At the end of PL test, only failure load is obtained. Failure load found as a result of the field PL test is 2,498N. However, this load was read as 215,000N from the graph shown in Figure 4-62 given for the numerical modeling study, which was carried out by using the input parameters of the last iteration for the matched UCS test. The ratio between the two failure loads is 86. Consequently, it can be said that the PL test model that was calibrated by using UCS parameters cannot yield the correct PL failure load value. Therefore, in order to find the actual model parameters and represent the PL test applied under field conditions, PL numerical modeling study was performed by changing iteration input parameters shown in the 4^{th} and 5^{th} rows of "Value (estimated input values)" column of Table 4-29. Micro cracks developed and the time dependent variations in the load, which is exerted on the specimen through conical platens, during the iteration process as a result of which the actual model parameters are obtained, are shown in Figure 4-63.

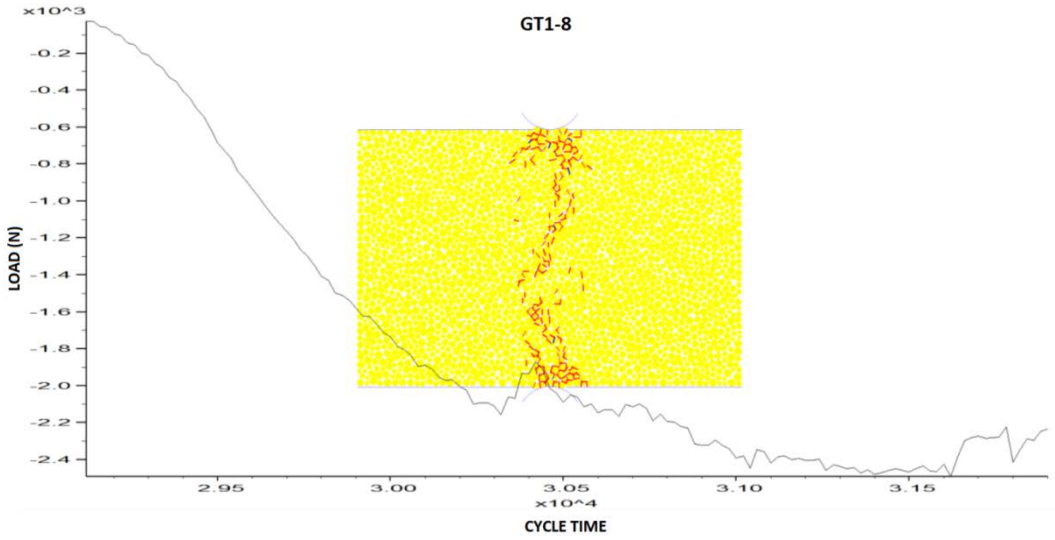

Figure 4-63 Field PL Model of BS GT1-8

According to the graph, failure load is said to be around 2,498N and this indicates that the iteration process was successfully completed for the specimen.

The results obtained from the model, which was constructed by using the input parameters of the last iteration for UCS test, and those obtained from the model, which was constructed by successive iterations to represent the PL test applied under field conditions, are compared in Table 4-30.

Table 4-31 Field PL Model vs. UCS Calibrated PL Model - BS GT1-8

No	Parameter	Field PL Model	UCS Calibrated PL Model	Ratio	Description
1	P (N)	2,498	215,000	86	Failure load
2	PB EM (GPa)	9.74E-02	9.77E-01	10	Parallel bond elasticity modulus
3	PB NS (MPa)	0.1	12.635392	126	Parallel bond normal strength
4	D_e (mm)	55.2791		-	Equivalent specimen diameter
5	D_e^2 (mm)	3,055.7775		-	
6	I_S (MPa)	0.8175	70.3585	86	PL index
7	F	1.0462		-	Correction factor
8	I_{S50} (MPa)	0.8552	73.6093	86	PL index for a specimen with a diameter of 50 mm
9	UCS (MPa)	20.18		-	Result of the laboratory test
10	Conversion factor	23.60	0.27	0.012	Ratio of lab. UCS test result to PL indexes obtained from PL and UCS iterations

According to the results, the conversion factor, which was obtained at the end of the iteration process for which the input parameters of the last iteration for the matched UCS test model were used, is 0.27 and it is not a realistic value. On the other hand, conversion factor obtained at the end of the iteration process, which was continued until the same result of the field PL test was attained, is 23.60 and it is close to the conversion factor of 26.9, which is given in Table 3-19 for bituminous shale.

4.4.2.2 Numerical Modeling of PL Test for BS GT1-14

PL test applied on the specimen GT1-14 under field conditions was matched with the laboratory UCS test specimen GT1-860 and it was numerically modeled in PFC and the results were compared to each other. Parameters given in Table 4-31 were used for numerical modeling.

Table 4-32 Parameters of BS GT1-14

No	Parameter	Value (input parameters of the last UCS iteration)	Value (estimated input values)
1	Particle density (kg/m^3)	2310	2310
2	Particle elasticity modulus (Pa)	5.44E+09	5.44E+09
3	Particle friction coefficient	0.98	0.98
4	Parallel bond elasticity modulus (Pa)	3.1050E+09	Iteration input
5	Parallel bond normal strength (Pa)	1.7470E+05	Iteration input
6	Length (m)	37.00E-03	37.00E-03
7	Width (m)	56.50E-03	56.50E-03

The first numerical model was constructed by using the parameters that were used as the inputs for the last iteration of the UCS test with which this PL test is matched and to which a relationship is to be established. These parameters are given in the 4th and 5th rows of the “Value (input parameters of the last UCS iteration)” column of Table 4-31. Micro cracks and the time dependent variations in the load, which is exerted on the specimen through the conical platens in the PFC model, are given in Figure 4-64.

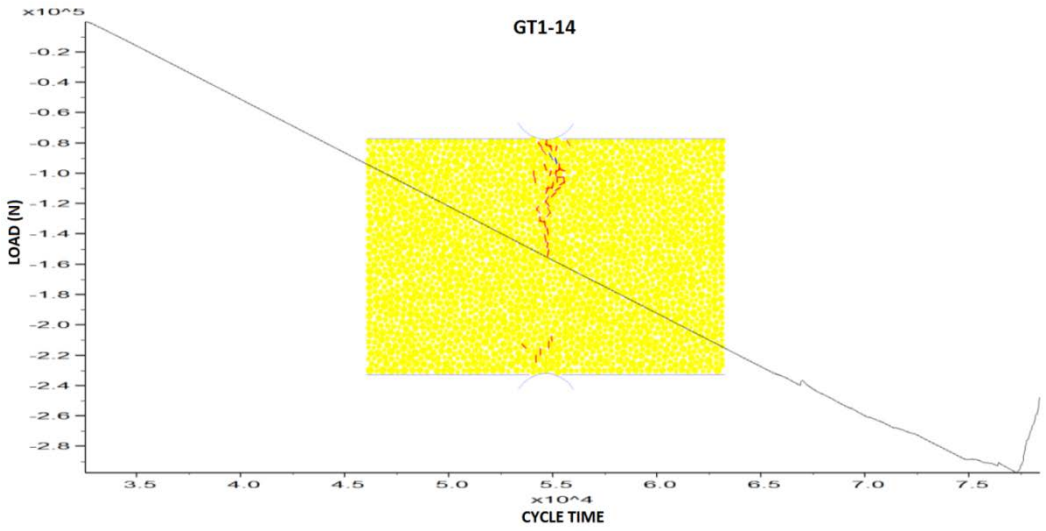

Figure 4-64 UCS Calibrated PL Model of BS GT1-14

At the end of PL test, only failure load is obtained. Failure load found as a result of the field PL test is 2,725N. However, this load was read as 288,000N from the graph shown in Figure 4-64 given for the numerical modeling study, which was carried out by using the input parameters of the last iteration for the matched UCS test. The ratio between the two failure loads is 106. Consequently, it can be said that the PL test model that was calibrated by using UCS parameters cannot yield the correct PL failure load value. Therefore, in order to find the actual model parameters and represent the PL test applied under field conditions, PL numerical modeling study was performed by changing iteration input parameters shown in the 4^{th} and 5^{th} rows of "Value (estimated input values)" column of Table 4-31. Micro cracks developed and the time dependent variations in the load, which is exerted on the specimen through conical platens, during the iteration process as a result of which the actual model parameters are obtained, are shown in Figure 4-65.

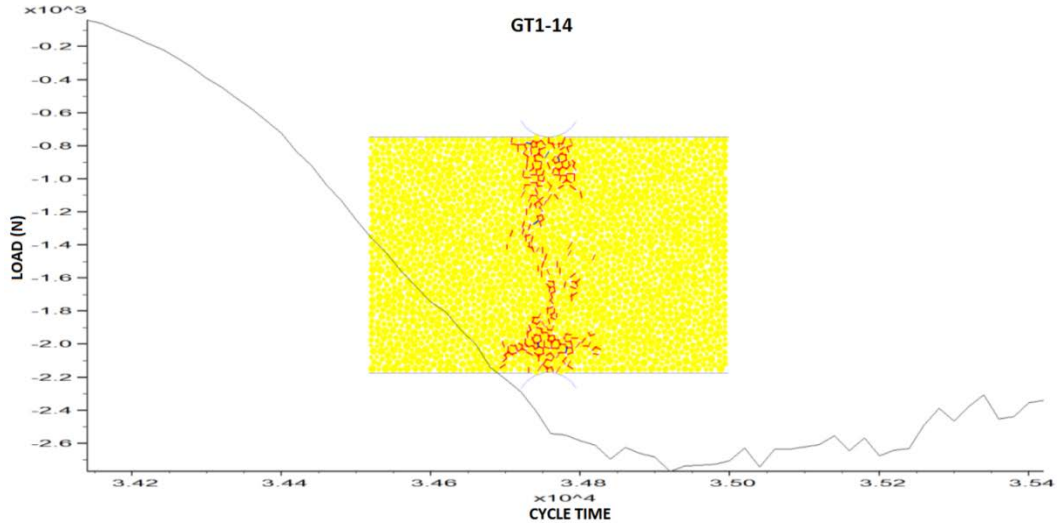

Figure 4-65 Field PL Model of BS GT1-14

According to the graph, failure load is said to be around 2,725N and this indicates that the iteration process was successfully completed for the specimen.

The results obtained from the model, which was constructed by using the input parameters of the last iteration for UCS test, and those obtained from the model, which was constructed by successive iterations to represent the PL test applied under field conditions, are compared in Table 4-32.

Table 4-33 Field PL Model vs. UCS Calibrated PL Model - BS GT1-14

No	Parameter	Field PL Model	UCS Calibrated PL Model	Ratio	Description
1	P (N)	2,725	288,000	106	Failure load
2	PB EM (GPa)	3.11E-01	3.11E+00	10	Parallel bond elasticity modulus
3	PB NS (MPa)	0.0717	17.47	244	Parallel bond normal strength
4	D_e (mm)	51.5918		-	Equivalent specimen diameter
5	D_e^2 (mm)	2,661.7095		-	
6	I_S (MPa)	1.0238	108.2011	106	PL index
7	F	1.0142		-	Correction factor
8	I_{S50} (MPa)	1.0383	109.7379	106	PL index for a specimen with a diameter of 50 mm
9	UCS (MPa)	28.44		-	Result of the laboratory test
10	Conversion factor	27.39	0.26	0.009	Ratio of lab. UCS test result to PL indexes obtained from PL and UCS iterations

According to the results, the conversion factor, which was obtained at the end of the iteration process for which the input parameters of the last iteration for the matched UCS test model were used, is 0.26 and it is not a realistic value. On the other hand, conversion factor obtained at the end of the iteration process, which was continued until the same result of the field PL test was attained, is 27.39 and it is close to the conversion factor of 26.9, which is given in Table 3-19 for bituminous shale.

4.4.2.3 Numerical Modeling of PL Test for BS GT2-14

PL test applied on the specimen GT2-14 under field conditions was matched with the laboratory UCS test specimen GT2-657 and it was numerically modeled in PFC and the results were compared to each other. Parameters given in Table 4-33 were used for numerical modeling.

Table 4-34 Parameters of BS GT2-14

No	Parameter	Value (input parameters of the last UCS iteration)	Value (estimated input values)
1	Particle density (kg/m^3)	2160	2160
2	Particle elasticity modulus (Pa)	2.87E+09	2.87E+09
3	Particle friction coefficient	0.47	0.47
4	Parallel bond elasticity modulus (Pa)	1.8090E+09	Iteration input
5	Parallel bond normal strength (Pa)	1.8999E+07	Iteration input
6	Length (m)	45.00E-03	45.00E-03
7	Width (m)	61.00E-03	61.00E-03

The first numerical model was constructed by using the parameters that were used as the inputs for the last iteration of the UCS test with which this PL test is matched and to which a relationship is to be established. These parameters are given in the 4th and 5th rows of the "Value (input parameters of the last UCS iteration)" column of Table 4-33. Micro cracks and the time dependent variations in the load, which is exerted on the specimen through the conical platens in the PFC model, are given in Figure 4-66.

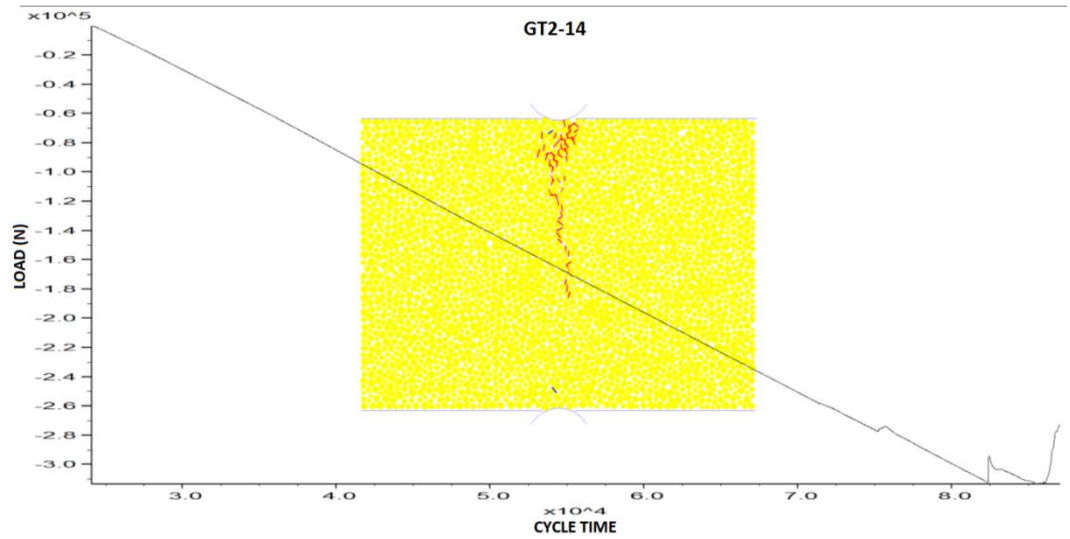

Figure 4-66 UCS Calibrated PL Model of BS GT2-14

At the end of PL test, only failure load is obtained. Failure load found as a result of the field PL test is 2,044N. However, this load was read as 312,000N from the graph shown in Figure 4-66 given for the numerical modeling study, which was carried out by using the input parameters of the last iteration for the matched UCS test. The ratio between the two failure loads is 153. Consequently, it can be said that the PL test model that was calibrated by using UCS parameters cannot yield the correct PL failure load value. Therefore, in order to find the actual model parameters and represent the PL test applied under field conditions, PL numerical modeling study was performed by changing iteration input parameters shown in the 4^{th} and 5^{th} rows of "Value (estimated input values)" column of Table 4-33. Micro cracks developed and the time dependent variations in the load, which is exerted on the specimen through conical platens, during the iteration process as a result of which the actual model parameters are obtained, are shown in Figure 4-67.

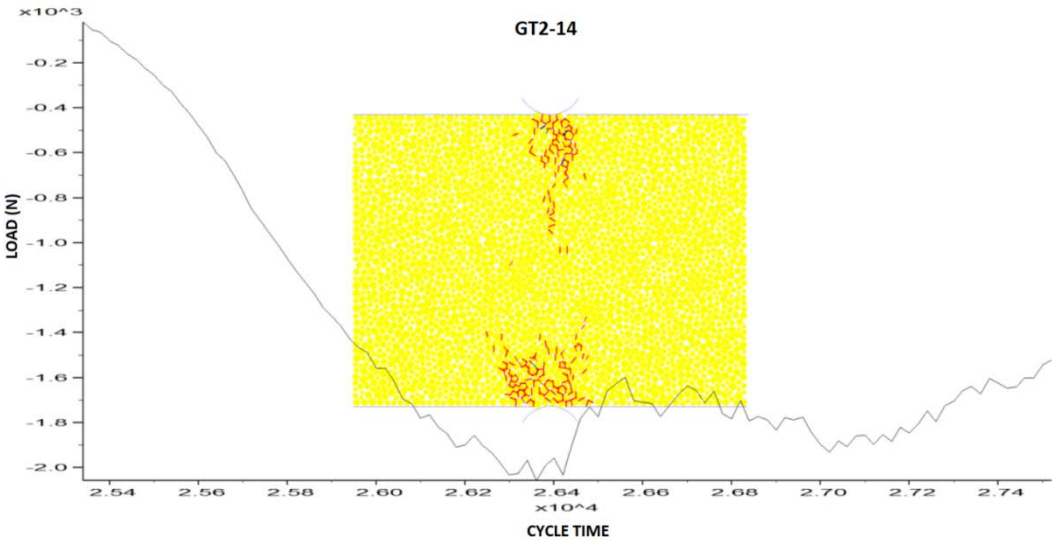

Figure 4-67 Field PL Model of BS GT2-14

According to the graph, failure load is said to be around 2,044N and this indicates that the iteration process was successfully completed for the specimen.

The results obtained from the model, which was constructed by using the input parameters of the last iteration for UCS test, and those obtained from the model, which was constructed by successive iterations to represent the PL test applied under field conditions, are compared in Table 4-34.

Table 4-35 Field PL Model vs. UCS Calibrated PL Model - BS GT2-14

No	Parameter	Field PL Model	UCS Calibrated PL Model	Ratio	Description
1	P (N)	2,044	312,000	153	Failure load
2	PB EM (GPa)	1.80E-01	1.81E+00	10	Parallel bond elasticity modulus
3	PB NS (MPa)	8.20E-02	18.999	232	Parallel bond normal strength
4	D_e (mm)	59.1189		-	Equivalent specimen diameter
5	D_e^2 (mm)	3,495.0455		-	
6	I_S (MPa)	0.5848	89.2692	153	PL index
7	F	1.0783		-	Correction factor
8	I_{S50} (MPa)	0.6306	96.2592	153	PL index for a specimen with a diameter of 50 mm
9	UCS (MPa)	28.14		-	Result of the laboratory test
10	Conversion factor	44.62	0.29	0.007	Ratio of lab. UCS test result to PL indexes obtained from PL and UCS iterations

According to the results, the conversion factor, which was obtained at the end of the iteration process for which the input parameters of the last iteration for the matched UCS test model were used, is 0.29 and it is not a realistic value. On the other hand, conversion factor obtained at the end of the iteration process, which was continued until the same result of the field PL test was attained, is 44.62 and it is around the conversion factor of 26.9, which is given in Table 3-19 for bituminous shale.

4.4.2.4 Numerical Modeling of PL Test for BS GT2-16

PL test applied on the specimen GT2-16 under field conditions was matched with the laboratory UCS test specimen GT2-659 and it was numerically modeled in PFC and the results were compared to each other. Parameters given in Table 4-35 were used for numerical modeling.

Table 4-36 Parameters of BS GT2-16

No	Parameter	Value (input parameters of the last UCS iteration)	Value (estimated input values)
1	Particle density (kg/m^3)	2180	2180
2	Particle elasticity modulus (Pa)	2.84E+09	2.84E+09
3	Particle friction coefficient	0.47	0.47
4	Parallel bond elasticity modulus (Pa)	1.7950E+09	Iteration input
5	Parallel bond normal strength (Pa)	1.3810E+07	Iteration input
6	Length (m)	50.00E-03	50.00E-03
7	Width (m)	60.00E-03	60.00E-03

The first numerical model was constructed by using the parameters that were used as the inputs for the last iteration of the UCS test with which this PL test is matched and to which a relationship is to be established. These parameters are given in the 4th and 5th rows of the “Value (input parameters of the last UCS iteration)” column of Table 4-35. Micro cracks and the time dependent variations in the load, which is exerted on the specimen through the conical platens in the PFC model, are given in Figure 4-68.

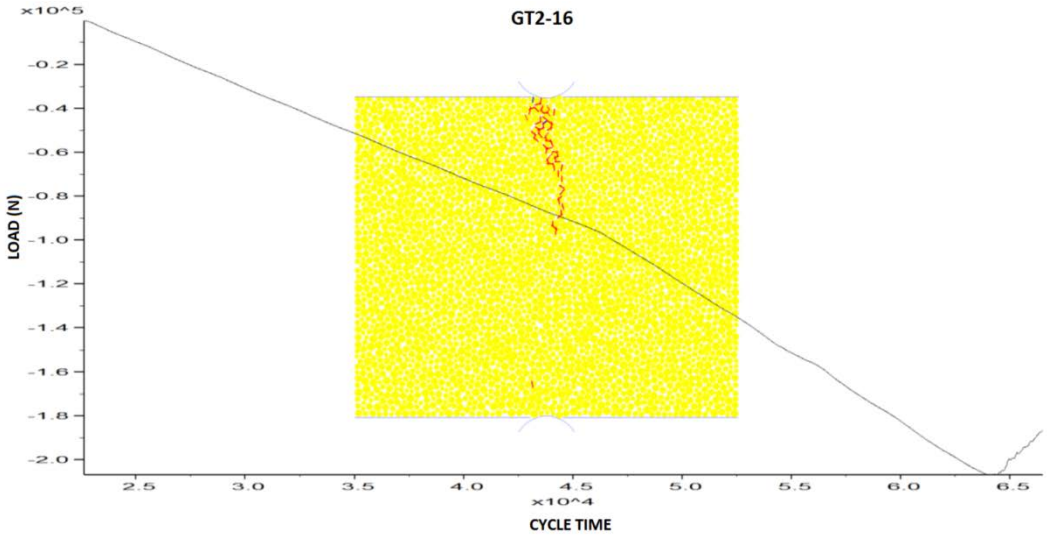

Figure 4-68 UCS Calibrated PL Model of BS GT2-16

At the end of PL test, only failure load is obtained. Failure load found as a result of the field PL test is 2,044N. However, this load was read as 205,000N from the graph shown in Figure 4-68 given for the numerical modeling study, which was carried out by using the input parameters of the last iteration for the matched UCS test. The ratio between the two failure loads is 100. Consequently, it can be said that the PL test model that was calibrated by using UCS parameters cannot yield the correct PL failure load value. Therefore, in order to find the actual model parameters and represent the PL test applied under field conditions, PL numerical modeling study was performed by changing iteration input parameters shown in the 4^{th} and 5^{th} rows of "Value (estimated input values)" column of Table 4-35. Micro cracks developed and the time dependent variations in the load, which is exerted on the specimen through conical platens, during the iteration process as a result of which the actual model parameters are obtained, are shown in Figure 4-69.

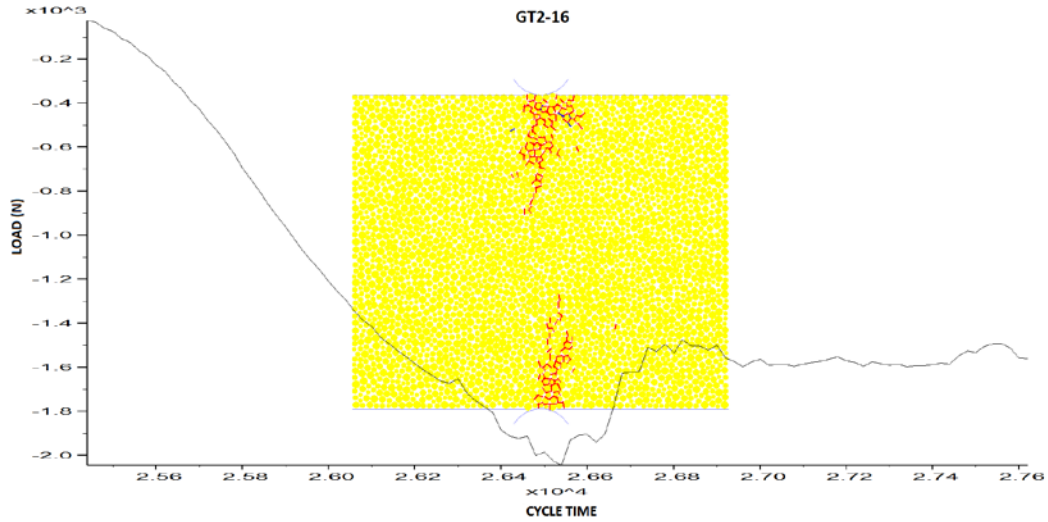

Figure 4-69 Field PL Model of BS GT2-16

According to the graph, failure load is said to be around 2,044N and this indicates that the iteration process was successfully completed for the specimen.

The results obtained from the model, which was constructed by using the input parameters of the last iteration for UCS test, and those obtained from the model, which was constructed by successive iterations to represent the PL test applied under field conditions, are compared in Table 4-36.

Table 4-37 Field PL Model vs. UCS Calibrated PL Model - BS GT2-16

No	Parameter	Field PL Model	UCS Calibrated PL Model	Ratio	Description
1	P (N)	2,044	205,000	100	Failure load
2	PB EM (GPa)	1.60E-01	1.80E+00	11	Parallel bond elasticity modulus
3	PB NS (MPa)	9.80E-02	13.81	141	Parallel bond normal strength
4	D_e (mm)	61.8039		-	Equivalent specimen diameter
5	D_e^2 (mm)	3,819.7219		-	
6	I_S (MPa)	0.5351	53.6688	100	PL index
7	F	1.1001		-	Correction factor
8	I_{S50} (MPa)	0.5887	59.0395	100	PL index for a specimen with a diameter of 50 mm
9	UCS (MPa)	21.56		-	Result of the laboratory test
10	Conversion factor	36.63	0.37	0.010	Ratio of lab. UCS test result to PL indexes obtained from PL and UCS iterations

According to the results, the conversion factor, which was obtained at the end of the iteration process for which the input parameters of the last iteration for the matched UCS test model were used, is 0.37 and it is not a realistic value. On the other hand, conversion factor obtained at the end of the iteration process, which was continued until the same result of the field PL test was attained, is 36.63 and it is around the conversion factor of 26.9, which is given in Table 3-19 for bituminous shale.

4.4.3 Numerical Modeling of PL Tests for Upper Trona Specimens

Among the PL tests performed under the field conditions for upper trona, the specimens with the number of:

- GT1-27
- GT1-28
- GT2-36 and
- GT2-39

were numerically modeled. Modeling studies for these specimens are discussed in detail in the following sections.

4.4.3.1 Numerical Modeling of PL Test for UT GT1-27

PL test applied on the specimen GT1-27 under field conditions was matched with the laboratory UCS test specimen GT1-874 and it was numerically modeled in PFC and the results were compared to each other. Parameters given in Table 4-37 were used for numerical modeling.

Table 4-38 Parameters of UT GT1-27

No	Parameter	Value (input parameters of the last UCS iteration)	Value (estimated input values)
1	Particle density (kg/m^3)	2040	2040
2	Particle elasticity modulus (Pa)	4.82E+09	4.82E+09
3	Particle friction coefficient	0.91	0.91
4	Parallel bond elasticity modulus (Pa)	2.8710E+09	Iteration input
5	Parallel bond normal strength (Pa)	6.8467E+07	Iteration input
6	Length (m)	32.00E-03	32.00E-03
7	Width (m)	60.00E-03	60.00E-03

The first numerical model was constructed by using the parameters that were used as the inputs for the last iteration of the UCS test with which this PL test is matched and to which a relationship is to be established. These parameters are given in the 4th and 5th rows of the "Value (input parameters of the last UCS iteration)" column of Table 4-37. Micro cracks and the time dependent variations in the load, which is exerted on the specimen through the conical platens in the PFC model, are given in Figure 4-70.

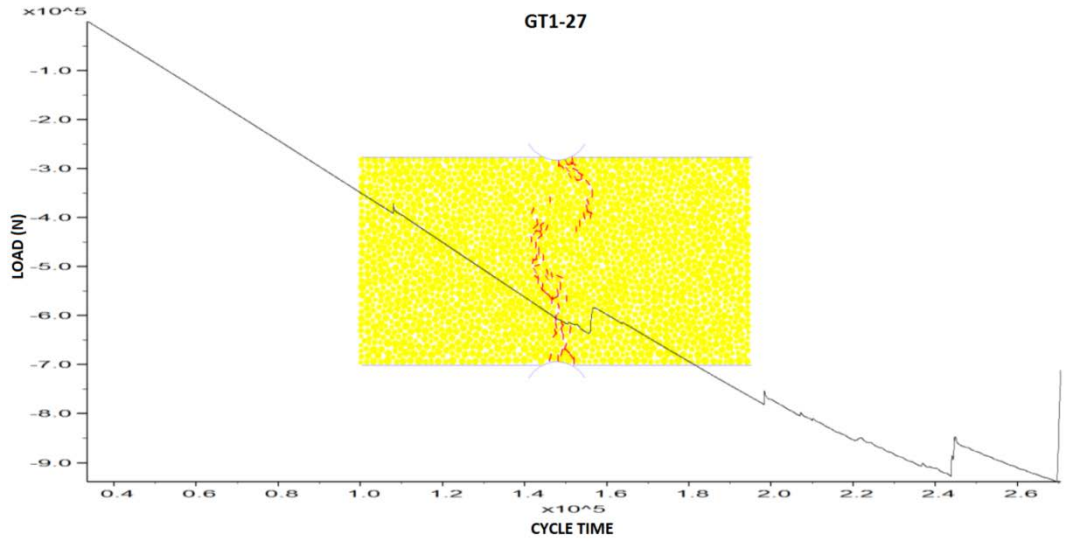

Figure 4-70 UCS Calibrated PL Model of UT GT1-27

At the end of PL test, only failure load is obtained. Failure load found as a result of the field PL test is 3,975N. However, this load was read as 935,000N from the graph shown in Figure 4-70 given for the numerical modeling study, which was carried out by using the input parameters of the last iteration for the matched UCS test. The ratio between the two failure loads is 235. Consequently, it can be said that the PL test model that was calibrated by using UCS parameters cannot yield the correct PL failure load value. Therefore, in order to find the actual model parameters and represent the PL test applied under field conditions, PL numerical modeling study was performed by changing iteration input parameters shown in the 4th and 5th rows of "Value (estimated input values)" column of Table 4-37. Micro cracks developed and the time dependent variations in the load, which is exerted on the specimen through conical platens, during the iteration process as a result of which the actual model parameters are obtained, are shown in Figure 4-71.

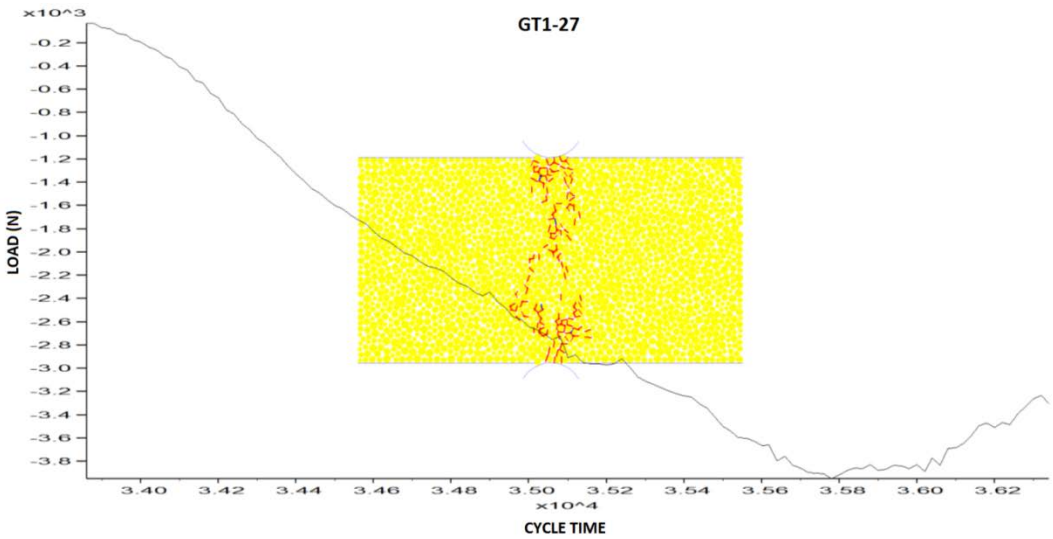

Figure 4-71 Field PL Model of UT GT1-27

According to the graph, failure load is said to be around 3,975N and this indicates that the iteration process was successfully completed for the specimen.

The results obtained from the model, which was constructed by using the input parameters of the last iteration for UCS test, and those obtained from the model,

which was constructed by successive iterations to represent the PL test applied under field conditions, are compared in Table 4-38.

Table 4-39 Field PL Model vs. UCS Calibrated PL Model - UT GT1-27

No	Parameter	Field PL Model	UCS Calibrated PL Model	Ratio	Description
1	P (N)	3,975	935,000	235	Failure load
2	PB EM (GPa)	2.75E-01	2.87E+00	10	Parallel bond elasticity modulus
3	PB NS (MPa)	1.65E-01	68.467	415	Parallel bond normal strength
4	D_e (mm)	49.4431		-	Equivalent specimen diameter
5	D_e^2 (mm)	2,444.6220		-	
6	I_S (MPa)	1.6260	382.4722	235	PL index
7	F	0.9950		-	Correction factor
8	I_{S50} (MPa)	1.6178	380.5494	235	PL index for a specimen with a diameter of 50 mm
9	UCS (MPa)	11.17		-	Result of the laboratory test
10	Conversion factor	6.90	0.03	0.004	Ratio of lab. UCS test result to PL indexes obtained from PL and UCS iterations

According to the results, the conversion factor, which was obtained at the end of the iteration process for which the input parameters of the last iteration for the matched UCS test model were used, is 0.03 and it is not a realistic value. On the other hand, conversion factor obtained at the end of the iteration process, which was continued until the same result of the field PL test was attained, is 6.90 and it is around the conversion factor of 14.2, which is given in Table 3-19 for upper trona.

4.4.3.2 Numerical Modeling of PL Test for UT GT1-28

PL test applied on the specimen GT1-28 under field conditions was matched with the laboratory UCS test specimen GT1-875 and it was numerically modeled in PFC and the results were compared to each other. Parameters given in Table 4-39 were used for numerical modeling.

Table 4-40 Parameters of UT GT1-28

No	Parameter	Value (input parameters of the last UCS iteration)	Value (estimated input values)
1	Particle density (kg/m^3)	1980	1980
2	Particle elasticity modulus (Pa)	4.64E+09	4.64E+09
3	Particle friction coefficient	0.91	0.91
4	Parallel bond elasticity modulus (Pa)	2.7443E+09	Iteration input
5	Parallel bond normal strength (Pa)	9.8980E+06	Iteration input
6	Length (m)	30.00E-03	30.00E-03
7	Width (m)	60.00E-03	60.00E-03

The first numerical model was constructed by using the parameters that were used as the inputs for the last iteration of the UCS test with which this PL test is matched and to which a relationship is to be established. These parameters are given in the 4th and 5th rows of the "Value (input parameters of the last UCS iteration)" column of Table 4-39. Micro cracks and the time dependent variations in the load, which is exerted on the specimen through the conical platens in the PFC model, are given in Figure 4-72.

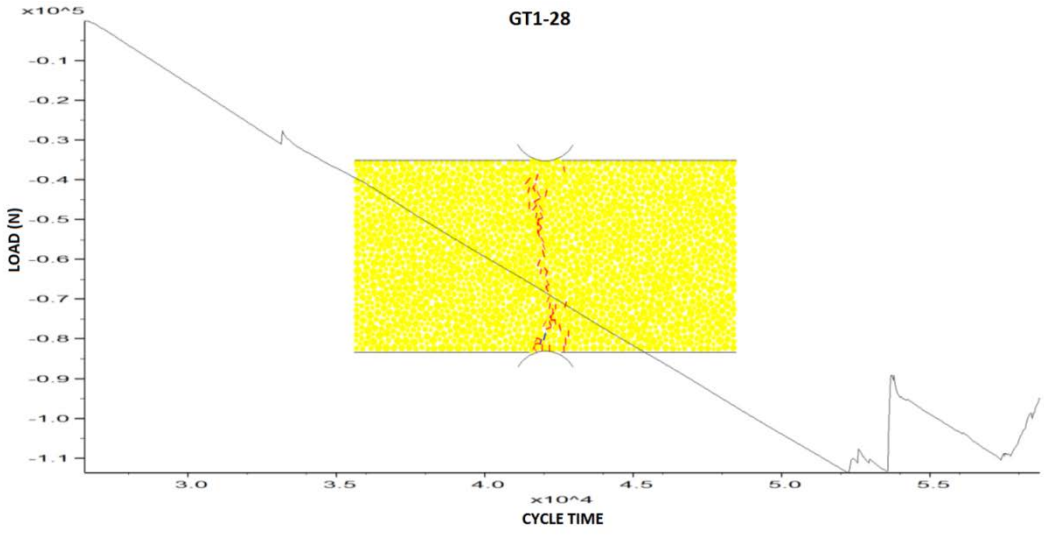

Figure 4-72 UCS Calibrated PL Model of UT GT1-28

At the end of PL test, only failure load is obtained. Failure load found as a result of the field PL test is 4,315N. However, this load was read as 114,000N from the graph shown in Figure 4-72 given for the numerical modeling study, which was carried out by using the input parameters of the last iteration for the matched UCS test. The ratio between the two failure loads is 26. Consequently, it can be said that the PL test model that was calibrated by using UCS parameters cannot yield the correct PL failure load value. Therefore, in order to find the actual model parameters and represent the PL test applied under field conditions, PL numerical modeling study was performed by changing iteration input parameters shown in the 4th and 5th rows of "Value (estimated input values)" column of Table 4-39. Micro cracks developed and the time dependent variations in the load, which is exerted on the specimen through conical platens, during the iteration process as a result of which the actual model parameters are obtained, are shown in Figure 4-73.

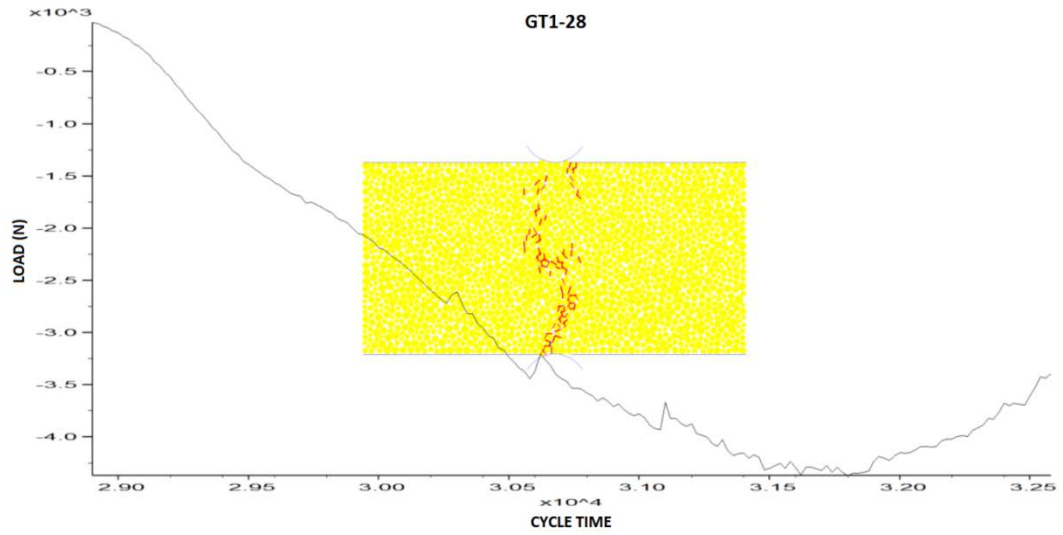

Figure 4-73 Field PL Model of UT GT1-28

According to the graph, failure load is said to be around 4,315N and this indicates that the iteration process was successfully completed for the specimen.

The results obtained from the model, which was constructed by using the input parameters of the last iteration for UCS test, and those obtained from the model,

which was constructed by successive iterations to represent the PL test applied under field conditions, are compared in Table 4-40.

Table 4-41 Field PL Model vs. UCS Calibrated PL Model - UT GT1-28

No	Parameter	Field PL Model	UCS Calibrated PL Model	Ratio	Description
1	P (N)	4,315	114,000	26	Failure load
2	PB EM (GPa)	2.75E-01	2.74E+00	10	Parallel bond elasticity modulus
3	PB NS (MPa)	2.70E-01	9.898	37	Parallel bond normal strength
4	D_e (mm)	47.8731		-	Equivalent specimen diameter
5	D_e^2 (mm)	2,291.8331		-	
6	I_S (MPa)	1.8828	49.7418	26	PL index
7	F	0.9806		-	Correction factor
8	I_{S50} (MPa)	1.8463	48.7783	26	PL index for a specimen with a diameter of 50 mm
9	UCS (MPa)	15.45		-	Result of the laboratory test
10	Conversion factor	8.37	0.32	0.038	Ratio of lab. UCS test result to PL indexes obtained from PL and UCS iterations

According to the results, the conversion factor, which was obtained at the end of the iteration process for which the input parameters of the last iteration for the matched UCS test model were used, is 0.32 and it is not a realistic value. On the other hand, conversion factor obtained at the end of the iteration process, which was continued until the same result of the field PL test was attained, is 8.37 and it is around the conversion factor of 14.2, which is given in Table 3-19 for upper trona.

4.4.3.3 Numerical Modeling of PL Test for UT GT2-36

PL test applied on the specimen GT2-36 under field conditions was matched with the laboratory UCS test specimen GT2-674 and it was numerically modeled in PFC and the results were compared to each other. Parameters given in Table 4-41 were used for numerical modeling.

Table 4-42 Parameters of UT GT2-36

No	Parameter	Value (input parameters of the last UCS iteration)	Value (estimated input values)
1	Particle density (kg/m^3)	2070	2070
2	Particle elasticity modulus (Pa)	7.50E+09	7.50E+09
3	Particle friction coefficient	0.68	0.68
4	Parallel bond elasticity modulus (Pa)	4.5800E+09	Iteration input
5	Parallel bond normal strength (Pa)	1.1698E+07	Iteration input
6	Length (m)	40.00E-03	40.00E-03
7	Width (m)	60.00E-03	60.00E-03

The first numerical model was constructed by using the parameters that were used as the inputs for the last iteration of the UCS test with which this PL test is matched and to which a relationship is to be established. These parameters are given in the 4th and 5th rows of the "Value (input parameters of the last UCS iteration)" column of Table 4-41. Micro cracks and the time dependent variations in the load, which is exerted on the specimen through the conical platens in the PFC model, are given in Figure 4-74.

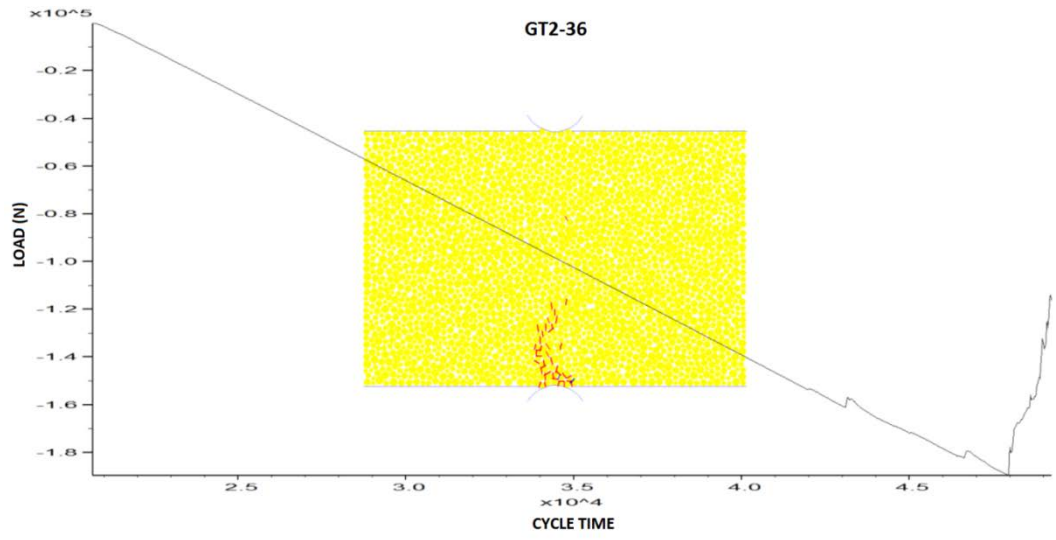

Figure 4-74 UCS Calibrated PL Model of UT GT2-36

At the end of PL test, only failure load is obtained. Failure load found as a result of the field PL test is 5,225N. However, this load was read as 189,000N from the graph shown in Figure 4-74 given for the numerical modeling study, which was carried out by using the input parameters of the last iteration for the matched UCS test. The ratio between the two failure loads is 36. Consequently, it can be said that the PL test model that was calibrated by using UCS parameters cannot yield the correct PL failure load value. Therefore, in order to find the actual model parameters and represent the PL test applied under field conditions, PL numerical modeling study was performed by changing iteration input parameters shown in the 4th and 5th rows of "Value (estimated input values)" column of Table 4-41. Micro cracks developed and the time dependent variations in the load, which is exerted on the specimen through conical platens, during the iteration process as a result of which the actual model parameters are obtained, are shown in Figure 4-75.

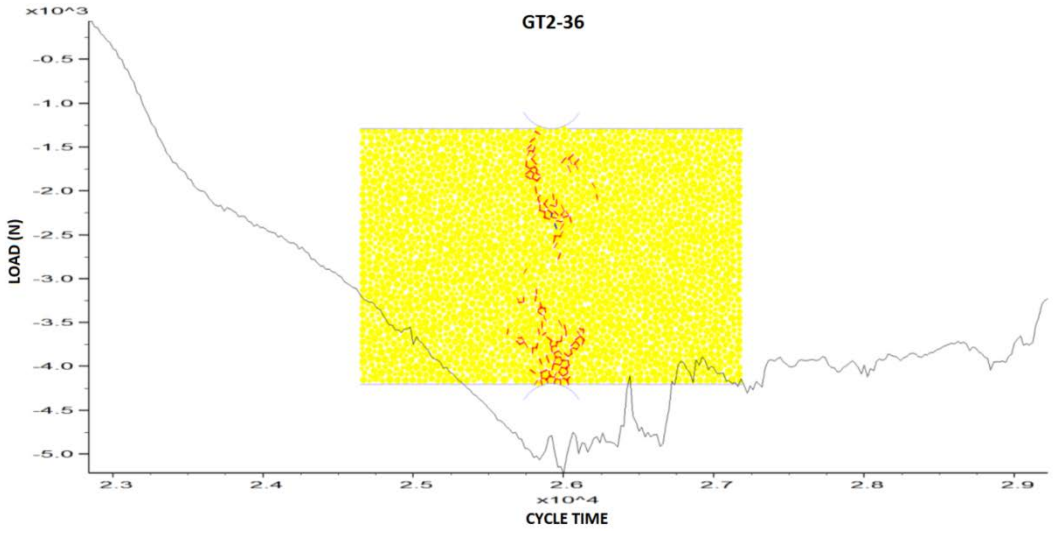

Figure 4-75 Field PL Model of UT GT2-36

According to the graph, failure load is said to be around 5,225N and this indicates that the iteration process was successfully completed for the specimen.

The results obtained from the model, which was constructed by using the input parameters of the last iteration for UCS test, and those obtained from the model,

which was constructed by successive iterations to represent the PL test applied under field conditions, are compared in Table 4-42.

Table 4-43 Field PL Model vs. UCS Calibrated PL Model - UT GT2-36

No	Parameter	Field PL Model	UCS Calibrated PL Model	Ratio	Description
1	P (N)	5,225	189,000	36	Failure load
2	PB EM (GPa)	1.25E-01	4.58E+00	37	Parallel bond elasticity modulus
3	PB NS (MPa)	2.65E-01	11.698	44	Parallel bond normal strength
4	D_e (mm)	55.2791		-	Equivalent specimen diameter
5	D_e^2 (mm)	3,055.7775		-	
6	I_S (MPa)	1.7099	61.8501	36	PL index
7	F	1.0462		-	Correction factor
8	I_{S50} (MPa)	1.7889	64.7077	36	PL index for a specimen with a diameter of 50 mm
9	UCS (MPa)	18.90		-	Result of the laboratory test
10	Conversion factor	10.57	0.29	0.028	Ratio of lab. UCS test result to PL indexes obtained from PL and UCS iterations

According to the results, the conversion factor, which was obtained at the end of the iteration process for which the input parameters of the last iteration for the matched UCS test model were used, is 0.29 and it is not a realistic value. On the other hand, conversion factor obtained at the end of the iteration process, which was continued until the same result of the field PL test was attained, is 10.57 and it is around the conversion factor of 14.2, which is given in Table 3-19 for upper trona.

4.4.3.4 Numerical Modeling of PL Test for UT GT2-39

PL test applied on the specimen GT2-39 under field conditions was matched with the laboratory UCS test specimen GT2-679 and it was numerically modeled in PFC and the results were compared to each other. Parameters given in Table 4-43 were used for numerical modeling.

Table 4-44 Parameters of UT GT2-39

No	Parameter	Value (input parameters of the last UCS iteration)	Value (estimated input values)
1	Particle density (kg/m^3)	2020	2020
2	Particle elasticity modulus (Pa)	12.94E+09	12.94E+09
3	Particle friction coefficient	0.49	0.49
4	Parallel bond elasticity modulus (Pa)	8.71524E+09	Iteration input
5	Parallel bond normal strength (Pa)	7.7109E+09	Iteration input
6	Length (m)	40.00E-03	40.00E-03
7	Width (m)	59.00E-03	59.00E-03

The first numerical model was constructed by using the parameters that were used as the inputs for the last iteration of the UCS test with which this PL test is matched and to which a relationship is to be established. These parameters are given in the 4th and 5th rows of the "Value (input parameters of the last UCS iteration)" column of Table 4-43. Micro cracks and the time dependent variations in the load, which is exerted on the specimen through the conical platens in the PFC model, are given in Figure 4-76.

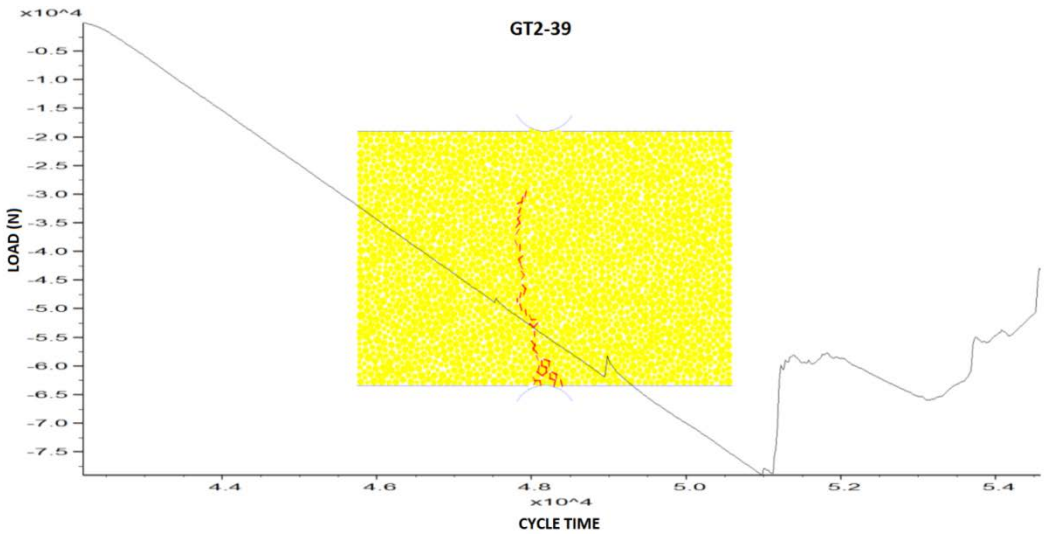

Figure 4-76 UCS Calibrated PL Model of UT GT2-39

At the end of PL test, only failure load is obtained. Failure load found as a result of the field PL test is 3,520N. However, this load was read as 78,200N from the graph shown in Figure 4-76 given for the numerical modeling study, which was carried out by using the input parameters of the last iteration for the matched UCS test. The ratio between the two failure loads is 22. Consequently, it can be said that the PL test model that was calibrated by using UCS parameters cannot yield the correct PL failure load value. Therefore, in order to find the actual model parameters and represent the PL test applied under field conditions, PL numerical modeling study was performed by changing iteration input parameters shown in the 4th and 5th rows of "Value (estimated input values)" column of Table 4-43. Micro cracks developed and the time dependent variations in the load, which is exerted on the specimen through conical platens, during the iteration process as a result of which the actual model parameters are obtained, are shown in Figure 4-77.

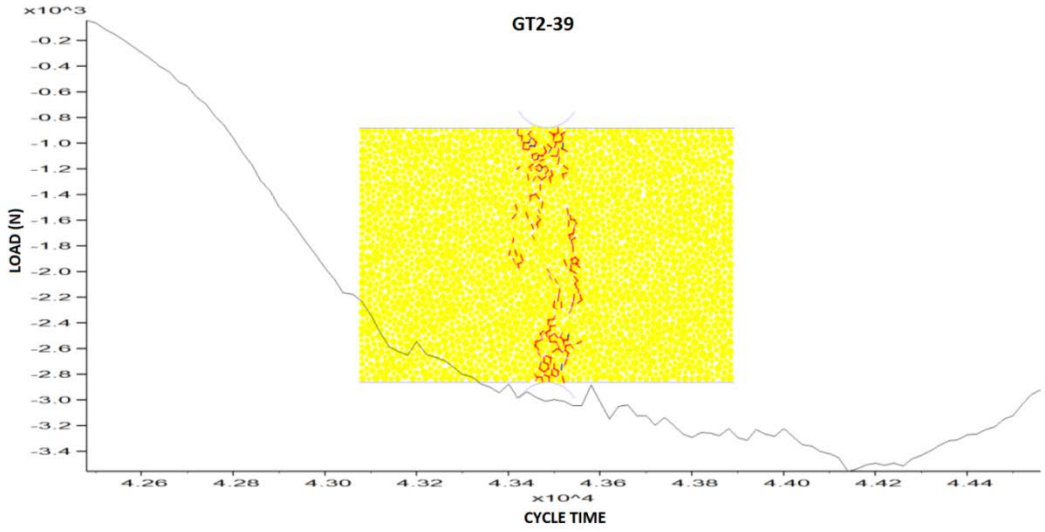

Figure 4-77 Field PL Model of UT GT2-39

According to the graph, failure load is said to be around 3,520N and this indicates that the iteration process was successfully completed for the specimen.

The results obtained from the model, which was constructed by using the input parameters of the last iteration for UCS test, and those obtained from the model,

which was constructed by successive iterations to represent the PL test applied under field conditions, are compared in Table 4-44.

Table 4-45 Field PL Model vs. UCS Calibrated PL Model - UT GT2-39

No	Parameter	Field PL Model	UCS Calibrated PL Model	Ratio	Description
1	P (N)	3,520	78,200	22	Failure load
2	PB EM (GPa)	8.70E-01	8.72E+00	10	Parallel bond elasticity modulus
3	PB NS (MPa)	1.86E-01	7.7109	41	Parallel bond normal strength
4	D_e (mm)	54.8165		-	Equivalent specimen diameter
5	D_e^2 (mm)	3,004.8479		-	
6	I_S (MPa)	1.1714	26.0246	22	PL index
7	F	1.0423		-	Correction factor
8	I_{S50} (MPa)	1.2209	27.1243	22	PL index for a specimen with a diameter of 50 mm
9	UCS (MPa)	12.30		-	Result of the laboratory test
10	Conversion factor	10.07	0.45	0.045	Ratio of lab. UCS test result to PL indexes obtained from PL and UCS iterations

According to the results, the conversion factor, which was obtained at the end of the iteration process for which the input parameters of the last iteration for the matched UCS test model were used, is 0.45 and it is not a realistic value. On the other hand, conversion factor obtained at the end of the iteration process, which was continued until the same result of the field PL test was attained, is 10.07 and it is around the conversion factor of 14.2, which is given in Table 3-19 for upper trona.

4.4.4 Numerical Modeling of PL Tests for Lower Trona Specimens

Among the PL tests performed under the field conditions for lower trona, the specimens with the number of:

- GT2-84
- GT2-92
- GT2-100 and
- GT2-114

were numerically modeled. Modeling studies for these specimens are discussed in detail in the following sections.

4.4.4.1 Numerical Modeling of PL Test for LT GT2-84

PL test applied on the specimen GT2-84 under field conditions was matched with the laboratory UCS test specimen GT2-708 and it was numerically modeled in PFC and the results were compared to each other. Parameters given in Table 4-45 were used for numerical modeling.

Table 4-46 Parameters of LT GT2-84

No	Parameter	Value (input parameters of the last UCS iteration)	Value (estimated input values)
1	Particle density (kg/m^3)	2020	2020
2	Particle elasticity modulus (Pa)	1.01E+09	1.01E+09
3	Particle friction coefficient	1.23	1.23
4	Parallel bond elasticity modulus (Pa)	5.2100E+08	Iteration input
5	Parallel bond normal strength (Pa)	4.0850E+06	Iteration input
6	Length (m)	30.00E-03	30.00E-03
7	Width (m)	60.00E-03	60.00E-03

The first numerical model was constructed by using the parameters that were used as the inputs for the last iteration of the UCS test with which this PL test is matched and to which a relationship is to be established. These parameters are given in the 4th and 5th rows of the "Value (input parameters of the last UCS iteration)" column of Table 4-45. Micro cracks and the time dependent variations in the load, which is exerted on the specimen through the conical platens in the PFC model, are given in Figure 4-78.

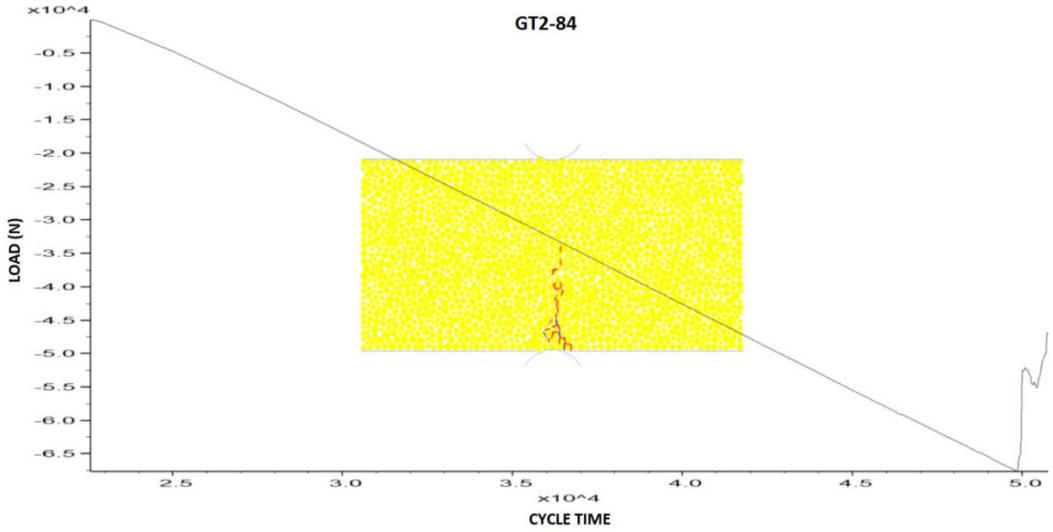

Figure 4-78 UCS Calibrated PL Model of LT GT2-84

At the end of PL test, only failure load is obtained. Failure load found as a result of the field PL test is 1,817N. However, this load was read as 67,500N from the graph shown in Figure 4-78 given for the numerical modeling study, which was carried out by using the input parameters of the last iteration for the matched UCS test. The ratio between the two failure loads is 37. Consequently, it can be said that the PL test model that was calibrated by using UCS parameters cannot yield the correct PL failure load value. Therefore, in order to find the actual model parameters and represent the PL test applied under field conditions, PL numerical modeling study was performed by changing iteration input parameters shown in the 4^{th} and 5^{th} rows of "Value (estimated input values)" column of Table 4-45. Micro cracks developed and the time dependent variations in the load, which is exerted on the specimen through conical platens, during the iteration process as a result of which the actual model parameters are obtained, are shown in Figure 4-79.

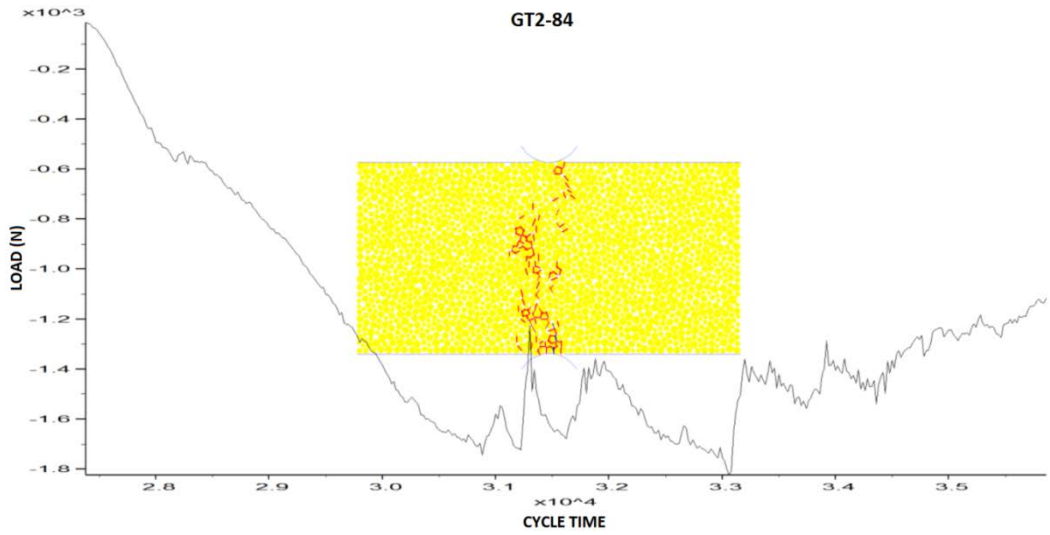

Figure 4-79 Field PL Model of LT GT2-84

According to the graph, failure load is said to be around 1,817N and this indicates that the iteration process was successfully completed for the specimen.

The results obtained from the model, which was constructed by using the input parameters of the last iteration for UCS test, and those obtained from the model, which was constructed by successive iterations to represent the PL test applied under field conditions, are compared in Table 4-46.

Table 4-47 Field PL Model vs. UCS Calibrated PL Model - LT GT2-84

No	Parameter	Field PL Model	UCS Calibrated PL Model	Ratio	Description
1	P (N)	1,817	67,500	37	Failure load
2	PB EM (GPa)	1.40E-02	5.21E-01	37	Parallel bond elasticity modulus
3	PB NS (MPa)	1.02E-01	4.085	40	Parallel bond normal strength
4	D_e (mm)	47.8731		-	Equivalent specimen diameter
5	D_e^2 (mm)	2,291.8331		-	
6	I_S (MPa)	0.7928	29.4524	37	PL index
7	F	0.9806		-	Correction factor
8	I_{S50} (MPa)	0.7775	28.8819	37	PL index for a specimen with a diameter of 50 mm
9	UCS (MPa)	7.33		-	Result of the laboratory test
10	Conversion factor	9.43	0.25	0.027	Ratio of lab. UCS test result to PL indexes obtained from PL and UCS iterations

According to the results, the conversion factor, which was obtained at the end of the iteration process for which the input parameters of the last iteration for the matched UCS test model were used, is 0.25 and it is not a realistic value. On the other hand, conversion factor obtained at the end of the iteration process, which was continued until the same result of the field PL test was attained, is 9.43 and it is so close to the conversion factor of 9.3, which is given in Table 3-19 for lower trona.

4.4.4.2 Numerical Modeling of PL Test for LT GT2-92

PL test applied on the specimen GT2-92 under field conditions was matched with the laboratory UCS test specimen GT2-719 and it was numerically modeled in PFC and the results were compared to each other. Parameters given in Table 4-47 were used for numerical modeling.

Table 4-48 Parameters of LT GT2-92

No	Parameter	Value (input parameters of the last UCS iteration)	Value (estimated input values)
1	Particle density (kg/m^3)	2070	2070
2	Particle elasticity modulus (Pa)	1.86E+09	1.86E+09
3	Particle friction coefficient	0.71	0.71
4	Parallel bond elasticity modulus (Pa)	1.0600E+09	Iteration input
5	Parallel bond normal strength (Pa)	4.0650E+06	Iteration input
6	Length (m)	33.00E-03	33.00E-03
7	Width (m)	58.00E-03	58.00E-03

The first numerical model was constructed by using the parameters that were used as the inputs for the last iteration of the UCS test with which this PL test is matched and to which a relationship is to be established. These parameters are given in the 4th and 5th rows of the "Value (input parameters of the last UCS iteration)" column of Table 4-47. Micro cracks and the time dependent variations in the load, which is exerted on the specimen through the conical platens in the PFC model, are given in Figure 4-80.

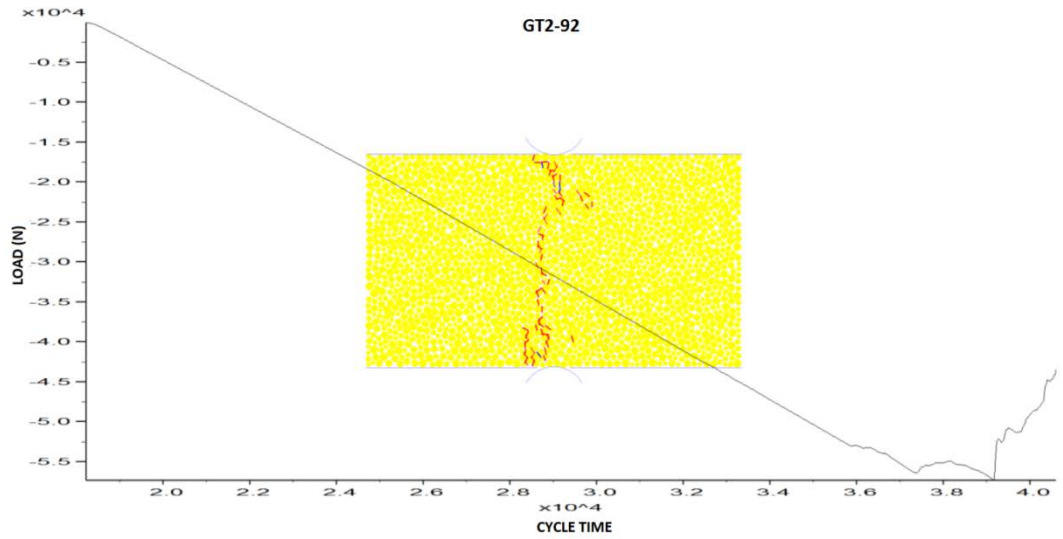

Figure 4-80 UCS Calibrated PL Model of LT GT2-92

At the end of PL test, only failure load is obtained. Failure load found as a result of the field PL test is 1,589N. However, this load was read as 57,000N from the graph shown in Figure 4-80 given for the numerical modeling study, which was carried out by using the input parameters of the last iteration for the matched UCS test. The ratio between the two failure loads is 36. Consequently, it can be said that the PL test model that was calibrated by using UCS parameters cannot yield the correct PL failure load value. Therefore, in order to find the actual model parameters and represent the PL test applied under field conditions, PL numerical modeling study was performed by changing iteration input parameters shown in the 4^{th} and 5^{th} rows of "Value (estimated input values)" column of Table 4-47. Micro cracks developed and the time dependent variations in the load, which is exerted on the specimen through conical platens, during the iteration process as a result of which the actual model parameters are obtained, are shown in Figure 4-81.

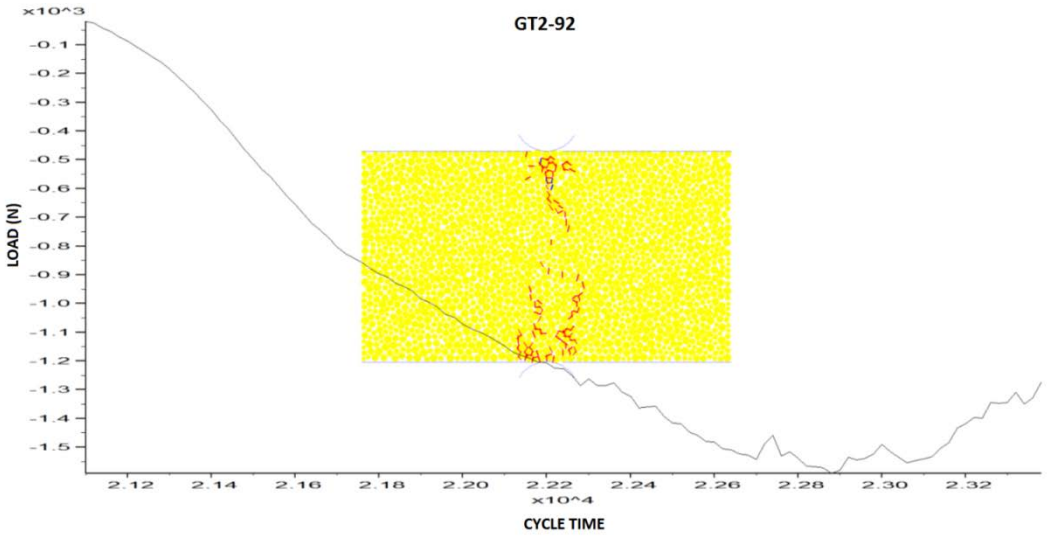

Figure 4-81 Field PL Model of LT GT2-92

According to the graph, failure load is said to be around 1,589N and this indicates that the iteration process was successfully completed for the specimen.

The results obtained from the model, which was constructed by using the input parameters of the last iteration for UCS test, and those obtained from the model, which was constructed by successive iterations to represent the PL test applied under field conditions, are compared in Table 4-48.

Table 4-49 Field PL Model vs. UCS Calibrated PL Model - LT GT2-92

No	Parameter	Field PL Model	UCS Calibrated PL Model	Ratio	Description
1	P (N)	1,589	57,000	36	Failure load
2	PB EM (GPa)	9.00E-02	1.06E+00	12	Parallel bond elasticity modulus
3	PB NS (MPa)	7.12E-02	4.065	57	Parallel bond normal strength
4	D_e (mm)	49.3658		-	Equivalent specimen diameter
5	D_e^2 (mm)	2,436.9825		-	
6	I_S (MPa)	0.6520	23.3896	36	PL index
7	F	0.9943		-	Correction factor
8	I_{S50} (MPa)	0.6483	23.2556	36	PL index for a specimen with a diameter of 50 mm
9	UCS (MPa)	6.90		-	Result of the laboratory test
10	Conversion factor	10.64	0.30	0.028	Ratio of lab. UCS test result to PL indexes obtained from PL and UCS iterations

According to the results, the conversion factor, which was obtained at the end of the iteration process for which the input parameters of the last iteration for the matched UCS test model were used, is 0.30 and it is not a realistic value. On the other hand, conversion factor obtained at the end of the iteration process, which was continued until the same result of the field PL test was attained, is 10.64 and it is so close to the conversion factor of 9.3, which is given in Table 3-19 for lower trona.

4.4.4.3 Numerical Modeling of PL Test for LT GT2-100

PL test applied on the specimen GT2-100 under field conditions was matched with the laboratory UCS test specimen GT2-723 and it was numerically modeled in PFC and the results were compared to each other. Parameters given in Table 4-49 were used for numerical modeling.

Table 4-50 Parameters of LT GT2-100

No	Parameter	Value (input parameters of the last UCS iteration)	Value (estimated input values)
1	Particle density (kg/m^3)	2080	2080
2	Particle elasticity modulus (Pa)	2.74E+09	2.74E+09
3	Particle friction coefficient	0.71	0.71
4	Parallel bond elasticity modulus (Pa)	1.5886E+09	Iteration input
5	Parallel bond normal strength (Pa)	4.3568E+06	Iteration input
6	Length (m)	30.00E-03	30.00E-03
7	Width (m)	58.50E-03	58.50E-03

The first numerical model was constructed by using the parameters that were used as the inputs for the last iteration of the UCS test with which this PL test is matched and to which a relationship is to be established. These parameters are given in the 4th and 5th rows of the “Value (input parameters of the last UCS iteration)” column of Table 4-49. Micro cracks and the time dependent variations in the load, which is exerted on the specimen through the conical platens in the PFC model, are given in Figure 4-82.

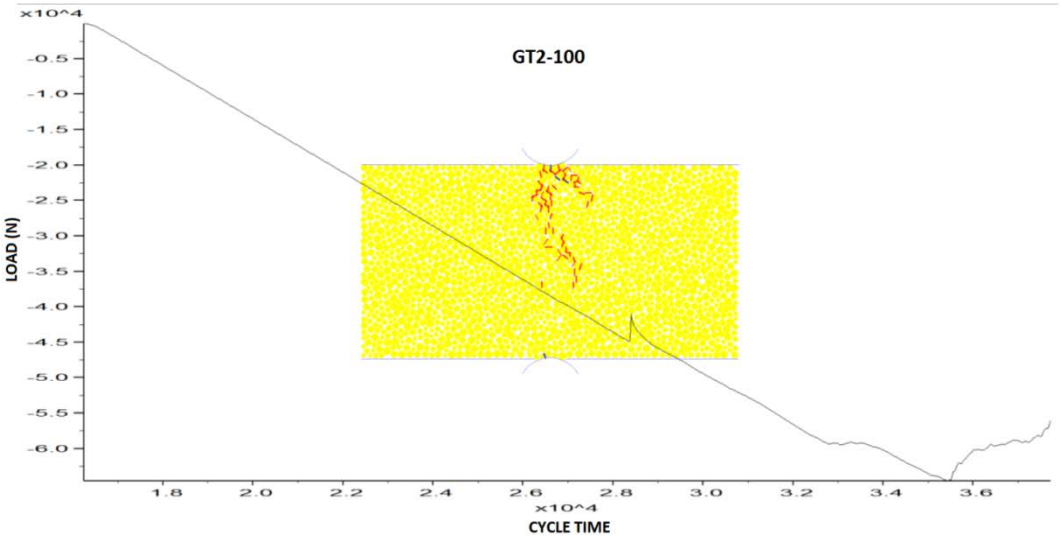

Figure 4-82 UCS Calibrated PL Model of LT GT2-100

At the end of PL test, only failure load is obtained. Failure load found as a result of the field PL test is 1,760N. However, this load was read as 64,000N from the graph shown in Figure 4-82 given for the numerical modeling study, which was carried out by using the input parameters of the last iteration for the matched UCS test. The ratio between the two failure loads is 36. Consequently, it can be said that the PL test model that was calibrated by using UCS parameters cannot yield the correct PL failure load value. Therefore, in order to find the actual model parameters and represent the PL test applied under field conditions, PL numerical modeling study was performed by changing iteration input parameters shown in the 4^{th} and 5^{th} rows of "Value (estimated input values)" column of Table 4-49. Micro cracks developed and the time dependent variations in the load, which is exerted on the specimen through conical platens, during the iteration process as a result of which the actual model parameters are obtained, are shown in Figure 4-83.

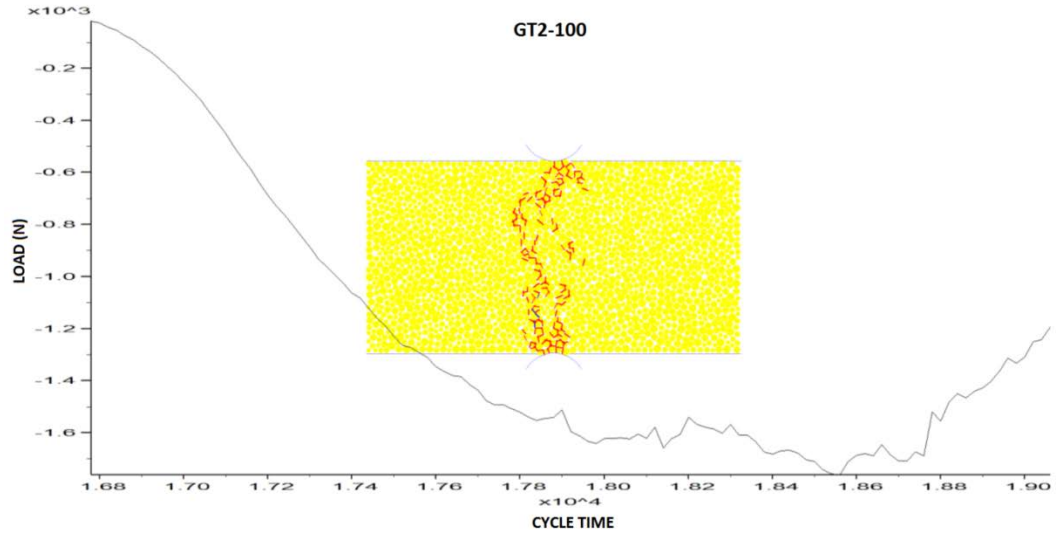

Figure 4-83 Field PL Model of LT GT2-100

According to the graph, failure load is said to be around 1,760N and this indicates that the iteration process was successfully completed for the specimen.

The results obtained from the model, which was constructed by using the input parameters of the last iteration for UCS test, and those obtained from the model, which was constructed by successive iterations to represent the PL test applied under field conditions, are compared in Table 4-50.

Table 4-51 Field PL Model vs. UCS Calibrated PL Model - LT GT2-100

No	Parameter	Field PL Model	UCS Calibrated PL Model	Ratio	Description
1	P (N)	1,760	64,000	36	Failure load
2	PB EM (GPa)	1.50E-01	1.59E+00	11	Parallel bond elasticity modulus
3	PB NS (MPa)	8.20E-02	4.3568	53	Parallel bond normal strength
4	D_e (mm)	47.2709		-	Equivalent specimen diameter
5	D_e^2 (mm)	2,234.5373		-	
6	I_S (MPa)	0.7876	28.6413	36	PL index
7	F	0.9751		-	Correction factor
8	I_{S50} (MPa)	0.7680	27.9269	36	PL index for a specimen with a diameter of 50 mm
9	UCS (MPa)	7.32		-	Result of the laboratory test
10	Conversion factor	9.53	0.26	0.028	Ratio of lab. UCS test result to PL indexes obtained from PL and UCS iterations

According to the results, the conversion factor, which was obtained at the end of the iteration process for which the input parameters of the last iteration for the matched UCS test model were used, is 0.26 and it is not a realistic value. On the other hand, conversion factor obtained at the end of the iteration process, which was continued until the same result of the field PL test was attained, is 9.53 and it is very close to the conversion factor of 9.3, which is given in Table 3-19 for lower trona.

4.4.4.4 Numerical Modeling of PL Test for LT GT2-114

PL test applied on the specimen GT2-114 under field conditions was matched with the laboratory UCS test specimen GT2-733 and it was numerically modeled in PFC and the results were compared to each other. Parameters given in Table 4-51 were used for numerical modeling.

Table 4-52 Parameters of LT GT2-114

No	Parameter	Value (input parameters of the last UCS iteration)	Value (estimated input values)
1	Particle density (kg/m^3)	2090	2090
2	Particle elasticity modulus (Pa)	8.80E+09	8.80E+09
3	Particle friction coefficient	1.25	1.25
4	Parallel bond elasticity modulus (Pa)	4.8271E+09	Iteration input
5	Parallel bond normal strength (Pa)	1.13455E+07	Iteration input
6	Length (m)	35.00E-03	35.00E-03
7	Width (m)	60.00E-03	60.00E-03

The first numerical model was constructed by using the parameters that were used as the inputs for the last iteration of the UCS test with which this PL test is matched and to which a relationship is to be established. These parameters are given in the 4th and 5th rows of the “Value (input parameters of the last UCS iteration)” column of Table 4-51. Micro cracks and the time dependent variations in the load, which is exerted on the specimen through the conical platens in the PFC model, are given in Figure 4-84.

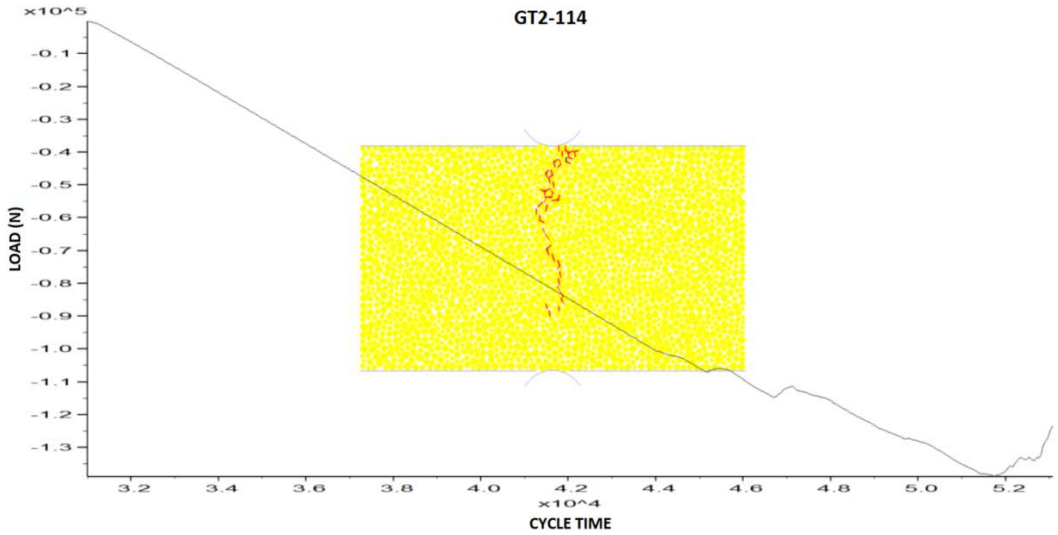

Figure 4-84 UCS Calibrated PL Model of LT GT2-114

At the end of PL test, only failure load is obtained. Failure load found as a result of the field PL test is 5,790N. However, this load was read as 139,000N from the graph shown in Figure 4-84 given for the numerical modeling study, which was carried out by using the input parameters of the last iteration for the matched UCS test. The ratio between the two failure loads is 24. Consequently, it can be said that the PL test model that was calibrated by using UCS parameters cannot yield the correct PL failure load value. Therefore, in order to find the actual model parameters and represent the PL test applied under field conditions, PL numerical modeling study was performed by changing iteration input parameters shown in the 4th and 5th rows of "Value (estimated input values)" column of Table 4-51. Micro cracks developed and the time dependent variations in the load, which is exerted on the specimen through conical platens, during the iteration process as a result of which the actual model parameters are obtained, are shown in Figure 4-85.

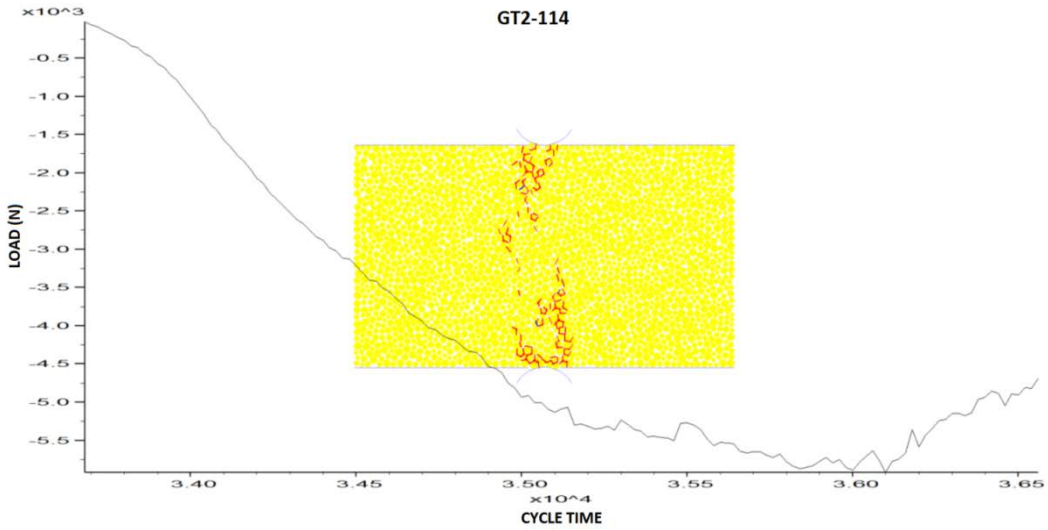

Figure 4-85 Field PL Model of LT GT2-114

According to the graph, failure load is said to be around 5,790N and this indicates that the iteration process was successfully completed for the specimen.

The results obtained from the model, which was constructed by using the input parameters of the last iteration for UCS test, and those obtained from the model, which was constructed by successive iterations to represent the PL test applied under field conditions, are compared in Table 4-52.

Table 4-53 Field PL Model vs. UCS Calibrated PL Model - LT GT2-114

No	Parameter	Field PL Model	UCS Calibrated PL Model	Ratio	Description
1	P (N)	5,790	139,000	24	Failure load
2	PB EM (GPa)	4.80E-01	4.83E+00	10	Parallel bond elasticity modulus
3	PB NS (MPa)	2.61E-01	11.3455	43	Parallel bond normal strength
4	D_e (mm)	51.7089		-	Equivalent specimen diameter
5	D_e^2 (mm)	2,673.8053		-	
6	I_S (MPa)	2.1655	51.9858	24	PL index
7	F	1.0152		-	Correction factor
8	I_{S50} (MPa)	2.1984	52.7780	24	PL index for a specimen with a diameter of 50 mm
9	UCS (MPa)	18.67		-	Result of the laboratory test
10	Conversion factor	8.49	0.35	0.042	Ratio of lab. UCS test result to PL indexes obtained from PL and UCS iterations

According to the results, the conversion factor, which was obtained at the end of the iteration process for which the input parameters of the last iteration for the matched UCS test model were used, is 0.35 and it is not a realistic value. On the other hand, conversion factor obtained at the end of the iteration process, which was continued until the same result of the field PL test was attained, is 8.49 and it is very close to the conversion factor of 9.3, which is given in Table 3-19 for lower trona.

4.4.5 Material Properties Obtained From Iterations for PL Tests

The first iteration of each PL model was carried out by using the UCS calibrated input parameters, which are given in Table 4-53 and by which the correct output values for UCS and elasticity modulus were obtained. Table 4-53 shows the details of the first PL test model parameters of 16 specimens.

Table 4-54 Material Properties Obtained From Iterations of UCS Calibrated PL Models

No	Lith.	Hole ID	Spec. No.	Parallel Bond Normal Strength (MPa) (input)	Parallel Bond EM (GPa) (input)	# of Iterations	# of Particles	Failure Load (test result) (N)	UCS Calibrated Failure Load (iterated) (N) (output)	Ratio of Iterated to Actual Failure Load
1	CS	GT1	61	29.645	0.4652	1	1,946	568	426,000	750
2	CS	GT1	63	1.65905	0.0775	1	2,576	341	25,000	73
3	CS	GT2	58	3.910	1.0043545	1	2,597	1,192	72,600	61
4	CS	GT2	79	2.20002	0.324	1	2,555	1,930	35,900	19
5	BS	GT1	8	12.635392	0.977	1	2,251	2,498	215,000	86
6	BS	GT1	14	17.470	3.105	1	1,959	2,725	288,000	106
7	BS	GT2	14	18.999	1.809	1	2,576	2,044	312,000	153
8	BS	GT2	16	13.810	1.795	1	2,815	2,044	205,000	100
9	UT	GT1	27	68.467	2.871	1	1,800	3,975	935,000	235
10	UT	GT1	28	9.898	2.7443	1	1,714	4,315	114,000	26
11	UT	GT2	36	11.698	4.580	1	2,251	5,225	189,000	36
12	UT	GT2	39	7.7109	8.71524	1	2,201	3,520	78,200	22
13	LT	GT2	84	4.085	0.521	1	1,689	1,817	67,500	37
14	LT	GT2	92	4.065	1.060	1	2,213	1,589	57,000	36
15	LT	GT2	100	4.3568	1.5886	1	1,646	1,760	64,000	36
16	LT	GT2	114	11.3455	4.8271	1	1,970	5,790	139,000	24
					TOTAL	16				

Values under the column “UCS Calibrated Failure Load (iterated) (N) (output)” are the failure loads obtained at the end of the first iteration of each modeling and those under the column “Failure Load (test result) (N)” are the failure loads read at the end of field PL tests. It is concluded from these figures that PL test models that were calibrated by using UCS parameters cannot yield the correct PL failure load values. Failure load values found as a result of the first iterations are higher than the actual failure load values for all numerical models constructed and the ratios of iterated failure load to actual one range from 19 to 750. The overestimation of the PL/Brazilian tensile strength is in accordance with the findings of Potyondy & Cundall (2004).

In order to find the actual model parameters and represent the PL test applied under field conditions, PL numerical modeling study was performed by changing iteration input parameters of “Parallel bond elasticity modulus” and “Parallel bond normal strength”. Values obtained as a result of the PL iterations are given in Table 4-54.

Table 4-55 Material Properties Obtained From Iterations of Field PL Models

No	Lith.	Hole ID	Spec. No.	Parallel Bond Normal Strength (MPa) (input)	Parallel Bond EM (GPa) (input)	# of Iterations	# of Particles	Failure Load (test result) (N)	Failure Load (iterated) (N) (output)
1	CS	GT1	61	0.0057	0.0045	11	1,946	568	568
2	CS	GT1	63	0.017004	0.0070	9	2,576	341	341
3	CS	GT2	58	0.01080	0.0900	10	2,597	1,192	1192
4	CS	GT2	79	0.1191	0.0320	5	2,555	1,930	1930
5	BS	GT1	8	0.1000	0.0974	12	2,251	2,498	2498
6	BS	GT1	14	0.0717	0.3105	5	1,959	2,725	2725
7	BS	GT2	14	0.0820	0.1800	5	2,576	2,044	2044
8	BS	GT2	16	0.0980	0.1600	15	2,815	2,044	2044
9	UT	GT1	27	0.1650	0.2750	4	1,800	3,975	3975
10	UT	GT1	28	0.2700	0.2750	4	1,714	4,315	4315
11	UT	GT2	36	0.2650	0.1250	5	2,251	5,225	5225
12	UT	GT2	39	0.1860	0.8700	5	2,201	3,520	3520
13	LT	GT2	84	0.1020	0.0140	4	1,689	1,817	1817
14	LT	GT2	92	0.0712	0.0900	15	2,213	1,589	1589
15	LT	GT2	100	0.0820	0.1500	6	1,646	1,760	1760
16	LT	GT2	114	0.2610	0.4800	5	1,970	5,790	5790
					TOTAL	120			

4.5 Interpretation for Numerical Modeling of UCS and PL Tests

As stated in Section 4.3 and 4.4, 16 UCS and 16 PL tests were numerically modeled in PFC. A total of 283 iterations for UCS tests and 136 iterations for PL tests were carried out.

The behavior of rock specimens were also observed in these UCS and PL iterations by using the video files created by PFC. In contrast to the UCS test, which relies on inducing shear stress by a compressive force application, PL test relies on the principle of inducing tensile stress into the body by the application of a compressive force and it is stated in the literature that rock specimens show different behaviors under different loading conditions. The damage processes of intact rock differ under compressive or tensile loading conditions (Meredith, 1990). Under slowly increasing compressive loading in Brazilian tests, numerous microcracks nucleate and propagate primarily as tensile (mode I) cracks in a direction parallel to the compression axis (Potyondy, 2014). This behavior was also observed in the PFC generated video files. While, in UCS modeling, cracking starts to develop throughout the specimen, in PL modeling it starts to develop on the contact points of conical platens and the specimens and cracks grow towards the center of the specimen until the specimen fails. The macroscopic failure mode is axial splitting through a major tensile fracture in the center of the specimen.

Median cracks, which are observed in brittle materials, developed during PL tests that were modeled by using the input parameters of UCS tests. However, crushing based failure, which is specific for softer materials, was observed during the PL models representing the actual field PL tests.

4.6 Comparison of PL and UCS Tests Modeled in PFC

Results from both types of tests are compared in this section. Input values found in different modeling studies for the same rock type can be seen in Table 4-55. In Table 4-55 pb_Ec represents elasticity modulus between parallel bonds and pb_sn

represents mean normal strength between parallel bonds. As seen in the table, although the material is the same, each test yields different pb_Ec and pb_sn values for its own calibration. This shows that UCS test calibration values, which are based on compressing, are different from PL test calibration values, which are based on tensioning. Ratios of elasticity modulus between parallel bonds of UCS to that of PL range from 10 to 103 and ratios of mean normal strength between parallel bonds of UCS to that of PL range from 18 to 5,247. In the literature it is verified that different calibration values are found for the same material during tensile (Brazilian) and compressive calibration of the materials, which are represented by parallel bonds (Cho et al., 2007; Kazerani & Zhao, 2010).

Table 4-56 Comparison of UCS and PL Modeling Results in Terms of Parallel Bond

No	Lith.	Hole ID	UCS Spec. No.	PL Spec. No.	UCS		PL		Ratio (UCS/PL)	
					pb_Ec (GPa)	pb_sn (MPa)	pb_Ec (GPa)	pb_sn (MPa)	pb_Ec	pb_sn
1	CS	GT1	904	61	0.4652	29.6450	0.0045	0.0057	103	5,247
2	CS	GT1	908	63	0.0775	1.65905	0.0070	0.017004	11	98
3	CS	GT2	698	58	1.0043545	3.9100	0.0900	0.0108	11	362
4	CS	GT2	712	79	0.3240	2.20002	0.0320	0.1191	10	18
5	BS	GT1	855	8	0.9770	12.635392	0.0974	0.1000	10	126
6	BS	GT1	860	14	3.1050	17.4700	0.3105	0.0717	10	244
7	BS	GT2	657	14	1.8090	18.9990	0.1800	0.0820	10	232
8	BS	GT2	659	16	1.7950	13.8100	0.1600	0.0980	11	141
9	UT	GT1	874	27	2.8710	68.4670	0.2750	0.1650	10	415
10	UT	GT1	875	28	2.7443	9.8980	0.2750	0.2700	10	37
11	UT	GT2	674	36	4.5800	11.6980	0.1250	0.2650	37	44
12	UT	GT2	679	39	8.7152	7.7109	0.8700	0.1860	10	41
13	LT	GT2	708	84	0.5210	4.0850	0.0140	0.1020	37	40
14	LT	GT2	719	92	1.0600	4.0650	0.0900	0.0712	12	57
15	LT	GT2	723	100	1.5886	4.3568	0.1500	0.0820	11	53
16	LT	GT2	733	114	4.8271	11.3455	0.4800	0.2610	10	43

In order to find conversion factors from PL to UCS for numerical models, the load exerted through conical platens was converted to I_{S50} and Table 4-56 was prepared for a comparison with UCS. In Table 4-56, the figures under the column "PFC PL I_{S50} (first iteration) (MPa)" are the I_{S50} values calculated by using the failure loads obtained as a result of the first iterations, which were carried out by using input parameters of UCS tests, and the figures under the column "PFC Conversion Factor (first iteration)" are the conversion factor values calculated by using these I_{S50} values. These conversion factors are very low since the failure loads from the first iterations that were carried out by using input parameters of UCS tests were overestimated. This indicates that calibration parameters obtained from UCS tests can be used as input parameters only for the tests that show compressive based failure behavior.

The figures under the column "PFC PL I_{S50} (final iteration) (MPa)" are the I_{S50} values calculated by using the failure loads obtained as a result of the final iterations, which yielded the correct value for failure loads, and the figures under the column "PFC Conversion Factor (final iteration)" are the conversion factor values calculated by using these I_{S50} values. These conversion factors are almost the same as the ones obtained as a result of the real tests and this shows that iteration processes were successfully completed for PL models.

Table 4-57 Comparison of Conversion Factors from Modeling and Test Results

No	Lith.	Hole ID	UCS Spec. No.	PL Spec. No.	PFC UCS (MPa)	PFC PL I_{S50} (first iteration) (MPa)	PFC Conversion Factor (first iteration)	PFC PL I_{S50} (final iteration) (MPa)	PFC Conversion Factor (final iteration)
1	CS	GT1	904	61	4.81	163.32	0.03	0.22	22.08
2	CS	GT1	908	63	2.88	7.71	0.37	0.11	27.40
3	CS	GT2	698	58	6.61	22.26	0.30	0.37	18.09
4	CS	GT2	712	79	3.80	11.15	0.34	0.60	6.34
5	BS	GT1	855	8	20.18	73.61	0.27	0.86	23.60
6	BS	GT1	860	14	28.44	108.20	0.26	1.02	27.78
7	BS	GT2	657	14	28.14	96.26	0.29	0.63	44.62
8	BS	GT2	659	16	21.56	59.04	0.37	0.59	36.62
9	UT	GT1	874	27	11.17	380.55	0.03	1.62	6.90
10	UT	GT1	875	28	15.45	48.78	0.32	1.85	8.37
11	UT	GT2	674	36	18.90	64.71	0.29	1.79	10.57
12	UT	GT2	679	39	12.30	27.12	0.45	1.22	10.07
13	LT	GT2	708	84	7.33	28.88	0.25	0.78	9.43
14	LT	GT2	719	92	6.90	23.26	0.30	0.65	10.64
15	LT	GT2	723	100	7.32	27.93	0.26	0.77	9.53
16	LT	GT2	733	114	18.67	52.78	0.35	2.20	8.49

CHAPTER 5

CONCLUSIONS AND RECOMMENDATIONS

The objectives of this thesis are to determine conversion factors from point load (PL) index to uniaxial compressive strength (UCS) for trona and interburden rocks and to numerically model the selected tests. For this purpose, PL tests were performed at the field and UCS tests were performed in the laboratory and regression analyses were carried out by using the results of these tests to determine conversion factors for the aforementioned rocks. Afterwards, 16 PL and 16 UCS tests were numerically modeled by using the 2-dimensional Particle Flow Code (PFC2D, ItascaTM, 2008) and PL test models were analyzed in detail in terms of crack development.

Main conclusions from this thesis are as follows:

i. In order to suggest conversion factors for trona and interburden rocks, regression analyses were carried out by using the results of the corresponding PL and UCS tests. In order to find conversion factors, obtained linear regression equations were forced to pass through the origin as UCS of a specimen should be zero when its PL index is zero. Determined conversion factors are as follows:

No	Lithological Unit	Conversion Factor
1	Claystone	17.1
2	Bituminous Shale	26.9
3	Claystone + Bituminous Shale	19.9
4	Upper Trona	14.2
5	Lower Trona	9.3
6	Trona (upper + lower)	13.6

While this research was underway, the mining company was using a conversion factor of 21 for all the units. They were overestimating the UCS of rocks. So, they need to correct the UCS results based on these factors.

ii. Out of 54 test pairs, 16 UCS tests were numerically modeled based on the parallel bond model by using the existing code of PFC. 4 specimens from each lithological unit, namely claystone, bituminous shale, upper trona and lower trona, were selected and a total of 283 iterations were performed. Model input parameters were duly determined and explained in detail for each numerical model. Fracture models developed during modeling studies and resultant stress-strain relationships were given.

iii. Parallel bond normal strength and parallel bond elasticity modulus parameters are the iteration inputs, which were estimated for the subsequent iteration process. Final values for these parameters were summarized in Table 4-19. Parallel bond normal strength ranges from 1.66MPa to 68.47MPa and parallel bond elasticity modulus changes between 0.08GPa to 8.72GPa. These values can help future researchers while modeling their problem (excavation, slope etc.) in PFC for calibration of their models in compression for the specified rock types.

iv. Out of 54 test pairs, 16 PL tests were numerically modeled based on the parallel bond model by developing a new routine in coding language called FISH in PFC. Four specimens from each lithological unit, namely claystone, bituminous shale, upper trona and lower trona, were selected and a total of 136 iterations were carried out. Constraining wall conditions were duly specified and model input parameters were duly determined and explained in detail for each numerical model.

v. The first iterations for PL tests were carried out by using the input parameters of the final UCS iterations, as a result of which the correct

values for UCS and elasticity modulus were obtained. Fracture models developed during modeling studies and resultant failure load graphs generated by the software were given. Iteration outputs, which are the failure load values, were given in Table 4-53 and they were compared to the actual failure loads obtained at the end of field PL tests. Ratio of iterated failure load to actual one ranges from 19 to 750. This shows that iterated failure load values were overestimated since the inputs were based on compressive loading.

vi. In order to find the actual model parameters and represent the PL test applied under field conditions, PL numerical modeling study was performed by changing iteration input parameters of “Parallel bond normal strength” and “Parallel bond elasticity modulus”. Final values for these parameters were summarized in Table 4-54. Parallel bond normal strength ranges from 0.006MPa to 0.270MPa and parallel bond elasticity modulus changes between 0.005GPa to 0.870GPa. These values can help future researchers while modeling their problem (excavation, slope etc.) in PFC for calibration of their models in tension for the specified rock types.

vii. The behavior of rock specimens were also observed in these UCS and PL iterations by using the video files created by PFC. Since UCS test relies on inducing shear stress by a compressive force application and PL test relies on the principle of inducing tensile stress into the body by the application of a compressive force, rock specimens behaved differently under different loading conditions. While, in UCS modeling, cracking starts to develop throughout the specimen, in PL modeling it starts to develop on the contact points of conical platens and the specimens and cracks grow towards the center of the specimen until the specimen fails. Median cracks, which are observed in brittle materials, developed during PL tests that were modeled by using the input parameters of UCS tests.

However, crushing based failure, which is specific for softer materials, was observed during the PL models representing the actual field PL tests.

viii. Results of the UCS and PL iterations for elasticity modulus between parallel bonds (pb_Ec) and mean normal strength between parallel bonds (pb_sn) were compared in Table 4-55. Although the material is the same, each test yields different pb_Ec and pb_sn values for its own calibration. This shows that UCS test calibration values, which are based on compressing, are different from PL test calibration values, which are based on tensioning. Ratios of elasticity modulus between parallel bonds of UCS to that of PL range from 10 to 103 and ratios of mean normal strength between parallel bonds of UCS to that of PL range from 18 to 5,247.

ix. Finally, conversion factors from PL to UCS for numerical models were determined. In the first phase, conversion factors were determined by using I_{S50} values which were calculated by using UCS calibrated failure loads. These conversion factors were not realistic values as the said failure loads were overestimated. In the second phase, conversion factors were determined by using I_{S50} values which were calculated by using iterated failure loads. These conversion factors are almost the same as the ones obtained as a result of the real tests and this shows that iteration processes were successfully completed for PL models.

Recommendations for conversion factor determination are listed below:

i. More PL and UCS tests should be performed.
ii. Drillhole intervals based on which PL and UCS tests are matched should be well arranged before testing.

Recommendations for numerical modeling part are as follows:

i. New bond models in new version of PFC can be tried to overcome the drawback of the software: overestimation of tensile strength of rocks.

ii. Specimen’s elasticity modulus was used for particle elasticity modulus during iterations. Iterations can be performed by determining particle elasticity modulus with more detailed studies.

iii. Particle friction coefficients, which were used for the iterations, were calculated by using the results of triaxial tests. Alternatively some constant values can be selected for this parameter.

iv. Effect of bedding in core specimens can be further analyzed during testing.

REFERENCES

Al-Jassar, S. H. and Hawkins, A. B., 1979. Geotechnical Properties of the Carboniferous Limestone of the Bristol Area the Influence of Petrography and Chemistry. 4th ISRM Congress, September 2–8, Montreux, Switzerland, pp. 3–13.

Anon, 1972. The Preparation of Maps and Plans in terms of Engineering Geology. Quarterly Journal of Engineering Geology. 5, 293-382.

ASTM D5731-08, 2008. Standard Test Method for Determination of the Point Load Strength Index of Rock and Application to Rock Strength Classifications, ASTM International, West Conshohocken, PA, 2008.

Bearman, R. A., 1999. The Use of the Point Load Test For the Rapid Estimation of Mode I Fracture Toughness. Int. J. Rock. Mech. Min. Sci., 36, 257–263.

Bieniawski, Z. T., 1975. Point Load Test in Geotechnical Practice. Eng. Geol. 9 (1), 1–11.

Bieniawski, Z. T., 1989. Engineering Rock Mass Classifications. Wiley, New York, 264 p.

Broch, E., 1983. Estimation of Strength Anisotropy Using the Point Load Test. Int. J. Rock Mech. Min. Sci. Geomech. Abstr. 20(4), 181–187.

Broch, E. and Franklin, J. A., 1972. Point-Load Strength Test. Int. J. Rock Mech. Min. Sci. 9 (6), 669–697.

BSI, 1981. Code of Practice for Site Investigation. BS 5930. British Standards Institution, 147 pages.

Cai, W., 2013. Discrete Element Modeling of Constant Strain Rate and Creep Tests on a Graded Asphalt Mixture" University of Nottingham, Doctor of Philosophy Thesis.

Cho, N., Martin, C. D. and Sego, D. C., 2007. A Clumped Particle Model for Rock. International Journal of Rock Mechanics and Mining Sciences. 44, 7, pp. 997-1010.

Cundall P. A. and Strack O. D. L., 1979. A Discrete Numerical Model for Granular Assemblies, Geotechnique, vol. 29, pp. 47-65.

DEÜ, 2001. Dokuz Eylül Üniversitesi Ankara Beypazarı Doğal Soda Sahası Yeraltı İşletme Projesi, DEU-MAG-20011. 156 sayfa.

Fookes, P. G., Gourley, C. S. and Ohikere, C., 1988. Rock Weathering in Engineering Time. Quarterly Journal of Engineering Geology, 21, 33-57pp.

Gong, Q. M., Zhao, J. and Jiao, Y. Y., 2005. Numerical Modeling of the Effects of Joint Orientation on Rock Fragmentation by TBM cutters. Tunnel. Underground Space Technol. 20 (2), 183–191.

Greminger, M., 1982. Experimental Studies of the Influence of Rock Anisotropy on Size and Shape Effects in Point-Load Testing. Int. J. Rock Mech. Min. Sci. 19, 241–246.

Guidicini, G., Nieble, C. M. and Cornides, A. X., 1973. Analysis of Point Load Test as a Method for Preliminary Geotechnical Classification of Rocks. Bulletin of International Association of Engineering Geology, 7, 37-52 pp.

Gunsallus, K. L. and Kulhawy, F. H., 1984. A Comparative Evaluation of Rock Strength Measures. Int. J. Rock Mech. Min. Sci. and Geomech. Abstr., 24(5): 233–248.

Güner, D., 2014. Experimental and Numerical Analysis of Effect of Curing Time on Mechanical Properties of Thin Spray-on Liners.

Hawkins, A. B., 1986. Rock Descriptions. In: Hawkins AB (ed) Site Investigation Practice: Assessing BS 5930, Geological Society, pp 59–66.

Helvacı, C., İnci, U., Yılmaz, H. and Yağmurlu, F., 1989. Geology and Neogene Trona Deposits of the Beypazarı Region, Turkey. Turkish Journal of Engineering and Environmental Sciences, 13(2). 245-256.

Innaurato, N., Oggeri, C., Oreste, P. P. and Vinai, R., 2007. Experimental and Numerical Studies on Rock Breaking With TBM Tools Under High Stress Confinement. Rock Mech. Rock Eng. 40 (5), 429–451.

ISRM, 1972. Suggested Methods for Determining the Point Load Strength Index of Rock Materials. ISRM Comm. on Standard. of Lab. Tests. 1, 8–13.

ISRM, 1985. ISRM Suggested Methods. Suggested Method for Determining Point-Load Strength. Int. J. Rock Mech. Min. Sci. 22, 53–60.

Kahraman, S., 2001. Evaluation of Simple Methods for Assessing the Uniaxial Compressive Strength of Rock. Int. J. Rock Mech. Min. Sci. 38, 981–994.

Kahraman, S., 2014. The Determination of Uniaxial Compressive Strength from Point Load Strength for Pyroclastic Rocks. Engineering Geology, 170, 33-42.

Kahraman, S. and Günaydın, O., 2009. The Effect of Rock Classes on the Relation Between Uniaxial Compressive Strength and Point Load Index. Bull Eng Geol Environ (2009) 68:345–353.

Kazerani, T. and Zhao, J., 2010. Micromechanical Parameters in Bonded Particle Method for Modeling of Brittle Material Failure. International Journal for Numerical and Analytical Methods in Geomechanics Volume 34, Issue 18, pp 1877–1895.

Kias, C. M., 2013. Investigation of Unstable Failure in Underground Coal Mining Using the Discrete Element Method, Colorado School of Mines Doctor of Philosophy Thesis (Mining and Earth Systems Engineering).

McFeat-Smith, I. and Tarkoy, P. J., 1979. Assessment of Tunnel Boring Performance. Tunnels and Tunneling, 33–37.

Meredith, P. G., 1990. Fracture and Failure in Brittle Polycrystals: An Overview. In D. J. Barber & P. G. Meredith (Eds.), Deformation Processes in Minerals, Ceramics and Rocks. London: Unwin Hyman.

Mishra, D. A. and Basu, A., 2013. Estimation of Uniaxial Compressive Strength of Rock Materials by Index Tests Using Regression Analysis and Fuzzy Inference System. Eng. Geol. http://dx.doi.org/10.1016/j.enggeo.2013.04.004.

Norbury, D. R., 1986. The Point Load Test. Site Investigation Practice Assessing BS 5930, Special Publication No 2, 325-329pp.

Pettifer, G. S. and Fookes, P. G., 1994. A Revision of the Graphical Method for Assessing the Excavatability of Rock. Quarterly Journal of Engineering Geology 27, 45. 164.

PFC2D, ItascaTM, 2008. Particle Flow Code in 2 Dimensions User's Guide, PFC2D Version 4.0.

Potyondy, D. O., 2014. The Bonded-Particle Model as a Tool for Rock Mechanics Research and Application: Current Trends and Future Directions. Itasca Consulting Group, Inc., Minneapolis, MN, USA.

Potyondy, D. O., 2015. The Bonded-Particle Model as a Tool for Rock Mechanics Research and Application: Current Trends and Future Directions. Geosystem Engineering, 18:1, 1-28.

Potyondy, D. O. and Cundall, P. A. 2004. A Bonded-Particle Model for Rock. International Journal of Rock Mechanics & Mining Sciences 41 (2004) 1329–1364.

Read, J. R. L., Thornten, P. N. and Regan, W. M., 1980. A Rational Approach to the Point Load Test. Proceedings of the 3rd Australian–New Zealand Geomechanics Conference. vol. 2 New Zealand Institution of Engineers, Wellington, pp. 35–39.

Rodrigues, J. D. and Jeremias, F. T., 1990. Assessment of Rock Durability Through Index Properties. Proc. 6th. Int. Congress IAEG, Amsterdam, Balkema-Rotterdam, Vol. 4, pp. 3055 3060.

Rusnak, J. and Mark, C., 2000. Using the Point Load Test to Determine the Uniaxial Compressive Strength of Coal Measure Rock. In: Peng, S.S., Mark, C. (Eds.), Proceedings of the 19th International Conference on Ground Control in Mining, August 8–10, Morgantown, West Virginia, pp. 362–371.

Singh, T. N., Kainthola, A. and Venkatesh, A., 2012. Correlation Between Point Load Index and Uniaxial Compressive Strength for Different Rock Types. Rock Mech. Rock. Eng., 45, 259–264.

Vallejo, L. E., Welsh, R. A. and Robinson, M. K., 1989. Correlation Between Unconfined Compressive and Point Load Strength for Appalachian rocks. In: Khair, A. W. (Ed.), Proceedings of the 30th US Symposium on Rock Mechanics. Balkema, Rotterdam, pp. 461–468.

Wijk, G., 1980. The Point Load Test for the Tensile Strength of Rock. Geotechnical Testing; Journal, 3, 49-54pp.

Yoon, J. S., 2007. Application of Experimental Design and Optimization to PFC Model Calibration in Uniaxial Compression Simulation. Int. J. Rock Mech. Min. Sci., 44, 871–879.

Yoon, J. S., Zang, A. and Stephansson, O., 2012. Simulating Fracture and Friction of Aue Granite Under Confined Asymmetric Compressive Test Using Clumped Particle Model. Int. J. Rock Mech. Mining Sci. 49, 68–83.